NASA CR-134523

FINAL REPORT

FUNDAMENTAL STUDY OF TRANSPIRATION COOLING

By

J.C.Y. Koh

J.L. Dutton

B.A. Benson

Prepared for

National Aeronautics and Space Administration

August 1973

Contract NAS 3-12012

BOEING AEROSPACE COMPANY

Kent, Washington

NASA CR-134523

FINAL REPORT
FUNDAMENTAL STUDY OF TRANSPIRATION COOLING

By

J. C. Y. Koh

J. L. Dutton

B. A. Benson

Prepared for

National Aeronautics and Space Administration

August 1973

Contract NAS 3-12012

Technical Management
NASA-Lewis Research Center
Cleveland, Ohio
Anthony Fortini, Program Manager

BOEING AEROSPACE COMPANY

Kent, Washington

FOREWORD

This document constitutes the final report for the NASA contract NAS 3-12012, "Fundamental Study of Transpiration Cooling" initiated in July 1968. The authors are indebted to A. Fortini, the NASA-Lewis technical manager, for assistance and technical advice essential to the successful completion of this contract.

ABSTRACT

Isothermal and non-isothermal pressure drop data and heat transfer data generated on porous 304L stainless steel "Rigimesh", sintered spherical stainless steel powder, and sintered spherical OFHC copper powder are reported and correlated. Pressure drop data was collected over a temperature range from 500°R to 2000°R and heat transfer data collected over a heat flux range from 5 to 15 BTU/in^2-sec. It was found that flow data could be correlated independently of transpirant temperature and type (i.e., H_2, N_2). Heat transfer data was correlated on the basis of $Nu/Pr^{1/3}$ vs. Re. Also, it was found that no simple relation between heat transfer coefficient and specimen porosity was obtainable.

TABLE OF CONTENTS

		Page
	ABSTRACT	iii
	SUMMARY	viii
1.0	INTRODUCTION	1
2.0	EXPERIMENTAL APPARATUS AND TEST PROCEDURES	3
	2.1 Specimen Description	3
	2.2 Isothermal Test Hardware	10
	2.3 Heat Transfer Test Hardware	17
3.0	GENERAL DISCUSSION OF TEST RESULTS	25
4.0	DATA ANALYSIS	29
	4.1 Pressure Drop	29
	4.2 Heat Transfer	35
5.0	CONCLUSIONS AND RECOMMENDATIONS	44
	5.1 Conclusions	44
	5.2 Recommendations	45
6.0	REFERENCES	46
	NOMENCLATURE	48
	CONVERSION FACTORS	51
	FIGURES	52
	TABLES	81
	APPENDIX A - PRESSURE DROP DATA	83
	APPENDIX B - HEAT TRANSFER DATA	117

LIST OF FIGURES

Figure No.		Page
1.	Rigimesh Specimen Mounted for Test	53
2.	Powder Specimen Mounted for Test	54
3.	Schematic of Isothermal Test Set-up	55
4.	Schematic of Hydrogen Heater	56
5.	Schematic of Heat Transfer Test Hardware	57
6.	Thermocouple Locations	58
7.	Furnace Operational Schematic	59
8.	Test Set-up Schematic	60
9.	Photo of Xenon Lamp	61
10.	Energy Distribution at High Power	62
11.	Energy Distribution at Low Power	63
11A.	Energy Distribution with Light Pipe	64
12.	Light Pipe Photo	65
13.	Gas Temperature Measurement Probe	66
14.	Pressure Drop Characteristics for Flow Through Sintered 304L Stainless Steel Wire Mesh (Rigimesh)	67
15.	Pressure Drop Characteristics for Flow Through Sintered Spherical 304L Stainless Steel Powders	68
16.	Pressure Drop Characteristics for Flow Through Sintered Spherical OFHC Copper Powders	69
17.	Pressure Drop Characteristics for Flow Through a Packed Bed of Spherical Particles, Cylinders or Cubes	70
18.	Nusselt, Prandtl vs. Reynolds Number Correlation for Rigimesh Material R-10-3/8 (.116 Porosity)	71
19.	Nusselt, Prandtl vs. Reynolds Number Correlation for Rigimesh Material R-20-1/2 (.187 Porosity)	72
20.	Nusselt, Prandtl vs. Reynolds Number Correlation for Rigimesh Material R-40-3/8 (Porosity .369); R-40-1/2 (Porosity .401)	73

LIST OF FIGURES (Cont.)

Figure No.		Page
21.	Stanton, Prandtl, Reynolds vs. Reynolds Number Correlation for Rigimesh Material R-10-3/8 (.116 Porosity)	74
22.	Stanton, Prandtly, Reynolds vs. Reynolds Number Correlation for Rigimesh Material R-20-1/2 (.187 Porosity)	75
23.	Stanton, Prandtl, Reynolds vs. Reynolds Number Correlation for Rigimesh Material R-40-3/8 (.369 Porosity); R-40-1/2 (.401 Porosity)	76
24.	Nusselt, Prandtl vs. Reynolds Number Correlation for Sintered Stainless Steel Powders	77
25.	Stanton, Prandtl, Reynolds vs. Reynolds Number Correlation for Sintered Stainless Steel Powders	78
26.	Nusselt, Prandtl vs. Reynolds Number Correlation for a Packed Bed of Particles	79
27.	Stanton, Prandtl, Reynolds vs. Reynolds Number Correlation for a Packed Bed of Particles	80

LIST OF TABLES

Table No.		Page
1	Test Specimen Description	82
Appendix A		
A1 through A10	Low Temperature Isothermal Test Data	83 — 107
A11 through A19	Elevated Temperature Isothermal Test Data	108 — 116
Appendix B		
B1 through B13	Heat Transfer Test Data	117 — 166

SUMMARY

The rational approach to the design of a transpiration cooled structure is dependent upon an understanding of fluid transport and heat transfer phenomena in porous metal materials. The research reported in this document was specifically designed to provide a fundamental understanding of these phenomena under conditions of high heat flux and large transpirant mass flow rates.

The research program was divided into three separate but interdependent efforts. First, the porous materials selected for this study were characterized in detail to yield a complete quantitative description of the internal microstructure. The materials selected were stainless steel "Rigimesh" wire form, stainless steel sintered powder, and OFHC copper sintered powder. Samples of Rigimesh in 10%, 20%, and 40% porosity were studied. The stainless and copper powders were 10%, 20% and 30% porous. Three thicknesses (1/4", 3/8", 1/2") of each material type were evaluated. Also, a 1" thick piece of each material type and porosity level was tested to determine the thermal conductivity and electrical resistivity of the specimen. The characterization results and the thermal conductivity data and analysis are reported in references 1, 2, 3 and reference 6 respectively.

The second effort was a comprehensive test program undertaken to generate flow and heat transfer data on each of the three porous metal types as well as each porosity and thickness variation. Transpirant mass flow rate, temperature, temperature gradient and pressure drop data were

generated for both isothermal and applied heat flux conditions. Test temperature levels varied from 500°R to 2000°R with applied heat flux levels as high as 15 BTU/in^2-sec. The pressure range over which data was collected was from 15 psia to 2000 psia with differential pressures from 0 to 1000 psid. The transpirant was gaseous hydrogen for the major portion of the test program; however, nitrogen was used on some tests to evaluate the effects of a different test medium. Complete, tabulated, test data is reported in Appendix A and B of this document.

Analysis and interpretation of the test data constitute the third major effort of this research program. Data is correlated on the basis of isothermal and non-isothermal pressure drop data and also on the basis of the heat transfer characteristics of the porous metals. The analytical effort and data interpretation constitute a large portion of the body of this document. The pressure drop correlations and the heat transfer correlations are presented separately in Sections 4.2.4 and 4.2.5 respectively.

1.0 INTRODUCTION

Historically, transpiration cooling has been of interest because of its capability to maintain the structural integrity of permanent surfaces exposed to a wide range of thermal environments. Logical application areas are: the throat region of solid propellant or regeneratively cooled rocket engines, high performance turbine blade cooling, and for the entire combustion chamber and nozzle regions of advanced technology liquid chemical and gas core nuclear rockets. In addition, transpiration cooling offers a unique solution to the problem of maintaining a fixed aerodynamic nose cone shape on a re-entry vehicle.

Considerable analytical and experimental work has been done in the last twenty years in an effort to provide the requisite technology base to allow the design of "working" transpiration cooling systems. However, insufficient information exists regarding the heat transfer and transpirant pressure drop at the high heat flux levels for which transpiration cooling would logically be applied. Therefore, it has been the purpose of this research to study the fluid flow and heat transfer phenomena in porous metals to provide the detailed information required for the successful design of transpiration cooled systems.

The research effort presented in this report is a combination of experimental and analytical work. Experimentally, data on thermal conductivity, electrical resistivity, pressure drop, and heat transfer in porous metals has been generated under conditions indicative of proposed transpiration cooled systems. The data in each of these test categories has been analyzed and correlated in a form useful for design application.

1.0 Cont.

The porous metals under study in this research include stainless steel "Rigimesh" wire forms, sintered stainless steel spherical powders, and sintered O.F.H.C. copper spherical powders. Bulk porosities of the porous metals ranged from 0.1 to 0.4 and thickness from 1/4" to 1/2" for flow tests, with 1" specimens for conductivity measurements. The selected metals were characterized in detail to yield a comprehensive definition of the internal geometry and dimensions. Table 1 is a listing of the materials tested. A more detailed coverage is given in Section 2.1 and in references 1, 2 and 3.

Thermal conductivity and electrical resistivity of the porous metals were measured by Dynatech Corporation (references 2 and 6) and the results were correlated and reported in reference 7.

Pressure drop and heat transfer characteristics of porous metals were measured and correlated. The facility and the method of measurements are described in Section 2. The data analyses and correlations are discussed in Section 4. Finally, in Section 5, conclusions drawn from this effort, and recommendations for additional work are presented.

2.0 EXPERIMENTAL APPARATUS AND TEST PROCEDURES

The test conditions used in this program can be divided into two categories. These are: (1) tests conducted under isothermal conditions at temperature levels ranging from ambient to 2000°R, and (2) heat transfer tests with incident radiant heat flux levels ranging from 5 to 15 BTU/sec-in^2 (720 to 2160 BTU/sec-ft^2).

To satisfy the specialized requirements of the two test categories unique test equipment was developed. The resulting isothermal and heat transfer test facilities constitute two separate test set-ups with some common components.

The porous test specimens, their mounting development, and actual test coupons are common to both test set-ups. The mounting techniques developed were different for the Rigimesh wire-form material and the sintered spherical powder metals. A description of these designs and the description of the two test facilities and their capabilities are outlined below.

2.1.0 Specimen Description

Three porous metal types were chosen for investigation in this program. They were (1) 304L stainless steel "Rigimesh" wire form, (2) 304L stainless powder form, and (3) OFHC (oxygen free high conductivity) copper powder form. These metals were produced to program specifications and fully characterized prior to testing. The characterization determined the following physical parameters: general contaminate level, bulk porosity, degree of interconnected porosity, uniformity of microstructure, mean hydraulic pore diameter, and chemical composition of

2.1.0 Cont.

the parent wrought metal. The characterization data and the details of the experimental procedure are given in reference 1 for the Rigimesh material and in references 2 and 3 for the powders.

2.1.1 Rigimesh Specimens

A brief outline of the characterization data is given here. The Rigimesh metal was produced by the Pall Corporation, and Rigimesh is a trade name. The metal specifications were written to satisfy the program requirements, but do not constitute a major deviation from the standard Rigimesh specifications. The program required a wire form porous metal, having a uniform open porosity in three porosity levels (10, 20, and 40%). Each porosity level was to be produced in four thicknesses (1/4", 3/8", 1/2" and 1"). The original wire cloth was 24 x 110 mesh of a plain dutch weave with the warp wire at 0.010" diameter and the fill wire at 0.015" diameter. The materials were produced in squares 2 1/2" on a side in each porosity and thickness. In some cases several squares were produced in a given porosity or thickness in order to obtain an "in tolerance" part.

The characterization of these Rigimesh materials showed the following results: the degree of interconnected porosity for the 10%, 20%, and 40% Rigimesh was 86.8%, 94.2% and 99.2% respectively. This is an average value based on three specimens in each porosity and is the result of mercury penetration measurements. The mean pore diameter for the 10%, 20%, and 40% material is approximately 20 μ, 65 μ, and 100 μ respectively, where μ indicates linear distance in microns.

2.1.1 Cont.

The 1/4", 3/8", and 1/2" thick materials were used for fabricating flow test specimens while the 1" material was used for thermal conductivity measurements. The thermal conductivity determination was made on each of the three porosity levels and the results are detailed in references 6 and 7. Briefly, it was determined that thermal conductivity of porous metals (including the spherical and non-spherical powders, foamed and felt metallic porous metal) can be computed from the information of solid metals conductivity or solid metals electrical resistivity. For sintered powder and Rigimesh, the dimensionless thermal conductivity is given by

$$\frac{\lambda}{\lambda_o} = \frac{1 - \xi}{1 + 10\xi^2}$$

where λ is the porous metal conductivity

λ_o is the solid metal conductivity

ξ is the porosity

The reader is referred to reference 7 for more detailed explanations and for the electrical resistivity correlations.

Figure 1 shows a typical Rigimesh specimen mounted for testing. The sample mount design shown in the figure is the result of an extensive design analysis. The design is an effort to satisfy the conflicting structural and heat transfer requirements imposed by the test objectives. The elevated temperature isothermal tests were conducted at 2000°R for the stainless parts and 1700°R for the copper specimens. The pressure drop across the porous specimen at the elevated temperature was a test variable, with a maximum value of 1000 psid. The coupling of high pressure drop and elevated temperature put rigid structural restraints

2.1.1 Cont.

on the specimen mount design. The structural requirements of the mount design are in opposition to the isothermal requirement. During both heat transfer and isothermal tests there exist conduction paths through the test hardware which allow heat transfer from the porous specimen to the surroundings. Such conduction heat losses cause temperature gradients in the specimen which disturbs the one-dimensionality of the temperature and flow field. The need to minimize conduction losses is apparent.

The requisite structural strength and thermal isolation was achieved by the mount design shown in Figure 1. The mount is machined from a 1/2" thick disk of 304L stainless steel, 2 1/2" in diameter. The mount has a slightly tapered hole 3/4" in diameter located on the disk center line. The taper total angle is 3°. The Rigimesh specimen is machined to a tapered cylinder to match the mount hole. The specimen/mount assemblies were then joined by electron beam welding. The weld yields a metal to metal fusion joint over the entire specimen/mount interface. This method of joining the specimen and specimen holder gives a high strength assembly with minimum possibility of gas flow along the specimen/mount interface. The electron beam power settings and the specimen positioning parameters were determined with comparative ease by trial and error with dummy specimens. The electron beam weld on the Rigimesh specimens produced a drop-through "flash" on the underside of the specimen. The flash was removed down to the specimen surface by electric discharge machining with a 3/4" diameter graphite bar as the electrode.

2.1.1 Cont.

Thermal isolation of the test specimen is accomplished by interrupting the conduction path between the specimen and the support structure heat sink. The mount material is removed in a cylindrical configuration around the specimen. Only a thin flange and four stiffening webs remain in contact with the porous specimen. This increased the effective thermal resistance between the porous specimen and the heat sink.

After fabrication of the Rigimesh test assemblies the parts were cleaned by exposure to a hot trichlorethylene degreasing bath and subsequent "bake-out" in a "hard" vacuum. The parts were held at 1800°F in the vacuum furnace for a period of 2 hours.

2.1.2 Porous Powder Specimens

The porous powder specimens were provided to Boeing as "government furnished material". The materials were produced by Nuclear Metals Division of Whittaker Corporation through NASA contract NAS 3-13309. Complete details of the manufacture and characterization of the porous powders is given in references 2 and 3; a brief description is given here.

The starting powders, OFHC copper, and 304L stainless steel were produced from bar stock meeting the chemical composition requirements of ASTM B-133 and Mil-S-4043 respectively. The patented "rotating bar" technique was used to produce the spherical powders from the raw stock. This process is described in references 2 and 4. The powders so produced were then screened until only the 105 to 125 micron particles remained.

2.1.2 Cont.

The powder was then sintered by hot isostatic compaction to yield 1" diameter bars of 10%, 20%, and 30% porosity. The specimens for test and characterization were machined from the 1" diameter bars. Metal smearing that occurred due to machining was removed by an acid etch process. The specimens were then sealed in polyethylene bags to prevent oxidation and delivered to Boeing for verification of vendor characterization and for mounting in the specimen holders.

The characterization measurements yielded the following results: the percent of interconnected porosity for the 10%, 20%, and 30% porous powders is 92.2%, 97.9% and 98.1% respectively for the stainless material and 100% for all the copper materials. The mean hydraulic pore diameter for the 10%, 20%, and 30% porosity levels is 7.4 μ, 19.1 μ, and 25.6 μ for the stainless and 7.4 μ, 14.4 μ, and 20.3 μ for the copper specimens. The data is based upon mercury penetration measurement and is presented in detail along with other data in reference 3. The summary of the results of the porous powder conductivity measurements is given in Section 2.1.1. The detailed results are presented in references 2 and 7.

The porous powder specimens are subject to the same requirements for mounting as outlined above, and therefore the mounts are of a design similar to the Rigimesh mounts. Figure 2 shows a typical powder specimen mounted and ready for test. Unlike the Rigimesh specimens, the powders proved very difficult to electron beam weld to their holders. After many attempts to develop sound welds between solid and porous OFHC copper and solid and porous 304L stainless steel, it was decided that sufficient

2.1.2 Cont.

weld quality and reliability could not be achieved. The primary problem encountered with the weld joints centered around the low strength of the porous material. The residual stress field in the weld joint produced by the weld process caused radial and circumferential cracks in the porous material directly adjacent to the heated zone. This problem was evident in all specimen types but was more severe in the copper material and in the high porosity specimens. Because of these problems the specimen mount design was modified to eliminate the electron beam welding process. Successful specimen mounting was achieved by brazing the sample materials to their mounts. The braze alloy was pre-loaded into two small grooves in the holder and the porous specimen and holder assembly was heated in a vacuum furnace to produce the braze joint. The porous powder specimens were sealed on their outside circumferential surfaces to prevent braze alloy penetration during the oven heat cycle. This was accomplished by electroplating a thin layer of material on the circumferential surface of the specimens. The electroplate layer was 0.008" to 0.010" thick and was copper for the copper specimens and nickel for the stainless specimens. The braze alloy used was 62% Cu + 35% Au + 3% Ni for the stainless steel specimens with a melt temperature of 2300°R. The copper specimens were brazed with 65% Au + 32% Ni + 3% Cu with a melt temperature of 2160°R.

The porous powder test assembly was cleaned by flushing with distilled water and x-ray inspected prior to testing to check for any possible braze infiltration.

2.1.2 Cont.

It should be noted that two problems were recognized with the mounting process outlined above. First, the electroform process to seal the outer circumferential surface of the powder parts yields a seal thickness that is somewhat variable and has a relatively rough exterior. This then, requires a machine "clean-up" of the parts to give the tight tolerance to the specimen diameter required for the brazing operation. Also, the electroform process occurs in a suitable electrolyte which penetrates the entire volume of the porous specimen. Consequently, great care must be taken not to contaminate the material with particulates or residual electrolyte. Electrolyte removal was accomplished by specimen cleaning in distilled water at or near the normal boiling point. The second problem area is the braze operation itself. Here again, painstaking attention to detail must be exercised to ensure the porous specimen does not become infiltrated with the braze filler. This can occur two ways; either the liquid braze filler can penetrate microscopic cracks in the electroform seal surface or the liquid can overflow the boundaries and enter the specimen through the front or back surface. Some slight degree of braze infiltration was evident in a few specimen x-rays. This was primarily due to penetration of imperfections in the seal layer. Due to the dimensions of the affected area, as seen in the x-ray, it was felt that the program test results would not be significantly affected.

2.2.0 Isothermal Test Hardware

The isothermal test system is shown schematically in Figure 3. It consists of three basic components: the hydrogen supply and control network, the hydrogen heater, and the system instrumentation. A description of each element is given below.

2.2.1 Hydrogen Supply and Control System

The hydrogen supply system utilizes a bottle farm made up of 28 bottles of 1.3 ft^3 (water volume) each. Initially the bottles were 3500 psi charge pressure which gave a total hydrogen capacity of 8700 SCF. The farm was upgraded during the test program to 6000 psig bottles of 1.15 ft^3 each giving a total hydrogen capacity of 13,150 SCF. A regulator at the manifold end of the bottle farm gives a controlled supply pressure of 2000 psig during a test run. The hydrogen flow rate is controlled by manually regulating the pressure drop across the porous specimen. This is accomplished by two remotely driven dome motor type needle valves located upstream and downstream of the test specimen. The upstream and downstream pressure on the specimen is independently variable over the supply range of 0 to 2000 psig. The specimen is mounted within a stainless steel pressure vessel which is water cooled and equipped with sufficient ports to satisfy the instrumentation requirements. The hydrogen is piped away from the test piece and is vented to atmosphere 20' above the roof of the test building. Test control of the hydrogen flow is maintained from a remote location where the test operator can monitor and regulate the pressure drop and flow rate at will.

The 13,150 SCF of hydrogen on hand allows a test duration of 5 to 6 minutes at the highest flow rates and up to 1 1/2 hours at the lowest rates. Operator safety is maintained by separation of the operator and the hydrogen flow system. Also, the flow system was pressure tested and equipped with pressure relief devices prior to the initial hydrogen flow tests.

2.2.2 Hydrogen Heater

The isothermal test requirements define the operating criteria of the hydrogen heater. These criteria proved very difficult to satisfy with a single heater design. The heater must be capable of generating a 2000°R outlet gas temperature over a mass flow range of 150:1 with a gas density variation of 4:1. This means that a heater of fixed configuration would experience a gas velocity variation of 600:1 and consequently a very large variation in heater pressure drop and power dissipated.

A hydrogen heater capable of meeting these strenuous requirements was developed after the application of conventional heater designs proved unsuccessful. Figure 4 gives the layout of the hydrogen heater as finally configured. The unit is driven by an electrical resistance heated core of molybednum wire, helically wound in a dense array supported by beryllia insulators. The insulators are strips of beryllia mounted in slots on a molybdenum bar at six evenly spaced radial locations, like longitudinal fins on a tube. Evenly spaced holes in the edge of the strips hold the molybdenum wire coils in place. There are three discrete circuits or legs to the heater, all wound through the same insulators in alternating holes. The resistance wire is 1/16" in diameter and the heater contains 45' of wire. The resistance heater assembly is 1 1/2" in diameter and approximately 18" long. Concentric with the heater core is a cylindrical heat exchanger device. This device is constructed from a 60' long 1/4" diameter stainless steel tube of 0.020" wall thickness. The stainless tube was wound over a bar to form a cylinder 2.0" in diameter in the same manner as a coil spring. The seam between adjacent coils of tube was welded along the

2.2.2 Cont.

entire coil length to form a sealed cylinder. When installed in the pressure vessel the heat exchanger and resistance core are arranged so that the incoming hydrogen flows through the heat exchanger before passing over the resistance heater core. Also, the system is equipped with a valve, external to the pressure vessel, which allows a bypass flow of hydrogen directly from the supply to the resistance core. Energy transfer in this arrangement is accomplished by direct convection transfer between the flowing gas and the wire core and indirectly by radiation transfer between the core and the coiled tube heat exchanger. This arrangement yields a heater with a very wide operating range.

For tests where the mass flow is very small, essentially all the heat transfer takes place in the tube coil where convection coefficients are relatively high and the core velocity is extremely low. On the other hand, for the high flow rate tests the heat exchanger is partially bypassed to avoid excessive pressure drop, and velocity in the core is sufficient to accomplish the required heat transfer. The resistance core temperature ranged between 2500°F and 3900°R (lengthwise average) depending on test conditions, while the stainless tube coil ranged from 1700°R to 2500°R. Power consumption by the heater ranged from 5 KW to 120 KW during the test program. During tests with the densest specimens at the lowest specimen pressure drop, excess hydrogen flow through the heater was required to stay below heater operational limits. On these occasions, the excess hydrogen was cooled and carried away by the exhaust system.

2.2.2 Cont.

The experience of this program demonstrated the need for an extremely clean transpirant flow so as not to contaminate the porous specimens and change their flow characteristics. After some initial problems involving boron-nitride as a heater construction material, the above described design and choice of materials proved successful.

2.2.3 Isothermal Test Instrumentation

The significant measurements made during the isothermal tests were those required to yield three categories of information. These are: the transpirant flow rate, the temperature level, and the pressure at various locations. The test set-up schematic, Figure 3, shows the relationship between the different measurement devices. The hydrogen mass flow was measured by "short radius" ASME orifice plates of six different diameters. The orifice diameters used are 0.009", 0.014", 0.020", 0.048", 0.052", and 0.085". This diameter range is required to measure the whole mass flow range experienced in the tests. The two largest diameter orifice plates were used upstream of the specimen, directly following the control regulator. These plates measure the high end of the flow range and were not allowed to approach choked conditions. The other plates, mounted downstream of the specimen, were for the low range of hydrogen mass flow and ran choked, with their downstream pressure held at atmosphere. The upstream and downstream orifice plates were plumbed in parallel with the valves separating each orifice. This arrangement allows quick orifice size selection by simply opening or closing the proper valves. The orifice plates were calibrated by Boeing Metrology Labs in nitrogen, and in hydrogen at the test site by the test personnel. The supply pressure on the upstream side of the selected orifice plate and the differential across

2.2.3 Cont.

the plate were measured with strain gage transducers calibrated "end to end" on site. The differential pressure ranged between 10 psid and 300 psid, consequently two transducers were requirdd. A 0 to 50 psid and a 0 to 300 psid transducer were connected in parallel across the orifice and the desired range could be selected by the test operator by remote valve selection. The overall error in the mass flow measurement system is less than ±3% based upon the accuracy of the individual components and upon the comparison data between orifices at fixed mass flows.

The pressure data was collected as shown in the schematic (Figure 3). The upstream, downstream, and differential pressure at the specimen were measured independently for greatest accuracy. The upstream transducer was 0-2000 psia, the downstream was 0-1000 psia and the differential transducer was ±1000 psid. The transducers were calibrated "end to end" on site against a ±1/4% standard and the calibration was repeated at regular intervals during the program or whenever the system was dismantled. The pressure measurements are in error by less than 1 1/2% over their useful range.

Temperature measurements were made with chromel-alumel thermocouples referenced to a 150°F standard. The gas temperature was measured directly upstream of the test specimen with a shielded thermocouple and again downstream of the specimen just beyond the specimen exit surface. The specimen material temperature was measured in three locations at the downstream surface. The three locations were at the center, the edge and at mid radius on the specimen. The multiple

2.2.3 Cont.

indication gives a measure of the radial gradient in the specimen which in turn is an indication of the conduction heat loss in the specimen. All the thermocouples in the system were grounded junction, sheath type, with stainless steel sheath; their relative location is shown in Figure 6. The thermocouple junctions were held in contact with the specimen surface by a high spring force. The gas thermocouples were free standing and shielded to minimize errors in measurement. Errors in the temperature measurement are virtually impossible to assess under test conditions; however, the thermocouple materials used throughout the test system were within ISA specifications and the reference junction was calibrated to be within ±0.25°F of the 150°F standard. The static instrumentation errors in the temperature measurement system are therefore believed to be within ±1% of reading but not better than ±2°F at the low end of the range.

The data acquisition system used was a 200 channel "Dymec" digital system. The data was collected on printed paper tape at the rate of 10 channels per second. There were 20 channels used, counting the actual data and the control information. The data was lumped in consecutive channels so as to limit the time interval over which the data was collected. This tends to limit the distortion in the data due to any transient effects.

2.3.0 Heat Transfer Test Hardware

The general layout of the heat transfer test system is shown schematically in Figure 5. Comparison with Figure 3 shows that the heat transfer test set-up is somewhat more elaborate than the isothermal

2.3.0 Cont.

set-up. This is the result of a move of the test site from the remote test location for the isothermal tests, to a site of general test and office use. Due to the hazardous nature of the test, additional safety precautions were required at the new test site. The layout schematic shows these safety features. The arc-image furnace and the test chamber were placed in a steel "explosion proof" room with the hydrogen supply located outside the room in an open court. The test operations site was within a large room containing the steel room. A sensitive hydrogen detector was placed in the exhaust vent to the steel room. The detector was interlocked to the hydrogen controls and the electrical supply for the arc-image furnace. Complete system shutdown would occur if a hydrogen concentration above the set-point was detected by the sensor.

The major test system components relavent to the objectives of the heat transfer test are the hydrogen supply, arc-image furnace and light pipe, and the test chamber and instrumentation. Each of these components is described below.

2.3.1 Hydrogen Supply System

The hydrogen supply system for this test is essentially the same as the isothermal test set-up. However, modifications were made to provide for remote shutoff of the 28 bottle farm and increased purge capability was added to meet facility safety requirements. Because of the reduced mass flow in the heat transfer tests the hydrogen supply capacity will allow continuous flow for up to two hours. The hydrogen

2.3.1 Cont.

exhaust system was different in the heat transfer tests, in that the exhaust stack was equipped with a back-pressure device. This device maintains a positive back pressure of 35 psia on the exhaust line through the action of a "floating" weight valve. This device precludes back diffusion of air into the vertical exhaust stack and the possibility of explosion.

2.3.2 Arc-Image Furnace

A comprehensive description of the development and calibration of the arc-image furnace is given in reference 5. The design and development of this thermal radiation device was a response to the test requirements of this program. The thermal radiation generator is a high radiance arc lamp coupled with a water cooled aluminized collector. Figure 7 shows the furnace operational schematic and Figure 8 is a schematic of the furnace as set up for actual test.

A photo of this lamp is shown in Figure 9. A special feature of the lamp is its small (6 millimeter) arc gap. The small gap provides the high radiance and source geometry required to yield the desired irradiance at the target with the 22 inch collector. The arc gap dimensions are controlled by a high velocity jet of xenon gas flowing between the electrode and cathode. This jet "pinches" the arc and maintains the arc dimensional stability. The unique lamp was designed and built by the Tamarack Scientific Company and is designated model MTF-50. Its nominal power rating is 50 KW for 50 hours of operation.

2.3.2 Cont.

Figures 10 and 11 show the energy distribution from the lamp and collector at the target (3/4" diameter), at high and low power settings. These measurements were made by use of a calibrated radiometer. As the figure demonstrate, the energy distribution is radially non-uniform. The maximum to minimum power levels within the 3/4" diameter target circle define the uniformity ratio. The ideal uniformity ratio would, of course, be 1.0. However, as seen in the figures the ratio is greater than 3. This degree of non-uniform energy distribution was not acceptable for the heat transfer tests, which are intended to be one dimensional.

The non-uniformity of incident energy at the target was greatly reduced by the application of a "light pipe". The light pipe used in the arc-image furnace was developed jointly by Boeing and Tamarack with technical design assistance from NASA-Lewis. The specific design configuration chosen was the result of an evolutionary development, involving several iterations to complete. The light pipe configuration used is shown in Figure 12. It consists of a water cooled structure, through the center of which is a tapered hole. The sides of the hole form a hexagonal reflecting surface. The side spacing at the entrance hexagon is 1.35 inches across the flats and the exit spacing is 0.75 inches across the flats.

The light pipe improves the uniformity of the energy distribution by accepting the available energy at the entrance, and reflecting it repeatedly through the pipe. This uniformly redistributes the energy at the pipe exit. The reflecting surfaces are high efficiency reflectors. However, due to the multiple bounces of the majority of the rays, the

2.3.2 Cont.

overall pipe efficiency is 80%. The arc-image furnace coupled with the light pipe yields a maximum flux level of 17.27 BTU/in^2-sec. (2490 BTU/ft^2-sec) with a uniformity ratio of 1.07 at the target plane. A typical heat flux scan with the light pipe is shown in Figure 11A. In this test program the irradiated specimen and the energy source must be separated by a quartz window because of the hydrogen transpirant used. This quartz window was 1" thick and reduced the effective flux level to just over 15 BTU/in^2-sec. (2160 BTU/ft^2-sec).

2.3.3 Heat Transfer Test Instrumentation

The instrumentation set-up for the heat transfer tests is very similar to the arrangement used for the isothermal test. The hydrogen flow rate was measured with the same orifice plates used in the isothermal set-up. The mass flow was measured upstream of the porous specimen with sub-critical flow through the plates. Pressure data was collected upstream, across, and downstream of the test article. The pressure levels were from 50 to 1000 psia differential. Due to the wide range, two transducers were used in the upstream as well as the differential location. Upstream the transducers were either 0 to 300 psia or 0 to 1000 psia, while the differentials were 0 to 200 psid or 0 to 1000 psid. All pressure transducers were calibrated "end to end" at the test location.

Test temperature at the orifice location and the upstream gas and specimen temperature were measured with chromel/alumel thermocouples referenced at 150°F. The thermocouples were sheath type 1/16" in diameter with a stainless steel sheath and grounded junctions. The

2.3.3 Cont.

downstream (hot side) specimen and gas temperature measurements required special instrumentation developed specifically for this test application. The hot-side temperature measurements are extremely difficult to make because of the very high level of incoming thermal radiation. The specimen and light pipe are arranged so that the specimen heated surface is within 0.025" of the end of the light pipe. Consequently, the only access to the specimen surface is through the center of the light pipe. The radiant flux level within the light pipe center is sufficient to generate extremely high temperatures in exposed materials which are uncooled. Also, temperature measurement devices placed in the flux field in the center of the pipe will cause shadows and disturb the uniform flux distribution on the specimen.

A development effort was required to explore and evolve methods to measure the hot side surface temperature and the exit gas temperature with sufficient reliability and accuracy to generate useful test results. After testing and evaluating many alternate thermocouple designs and considering infrared and other measurement schemes, the final measurement configuration was decided upon.

Tests with multiple thermocouples located on various test specimens showed that there exists only very small radial temperature gradients in the porous specimens. Therefore, a surface temperature measurement made at the specimen edge will yield nominally, the same data as a measurement made at the center. The material surface temperatures were measured by spot welding a small (.005" diameter wire) thermocouple

2.3.3 Cont.

junction at each specimen edge. Tests also showed that there is a significant variation in the gas temperature between the specimen center and edge. This is due to circulation and mixing of cooler gases from the test chamber volume. The test chamber is water cooled and the hydrogen is dumped into the chamber volume at the exit of the specimen. A small amount of entrainment of the cooler hydrogen occurs due to the light pipe position. Therefore, the gas temperature at the specimen edge is reduced and the measurement must be made at the specimen center line and very near the exit surface. Also, because the specimen material exhibits a significant reflectivity a certain amount of thermal radiation will be "bounced" off the specimen surface. The gas temperature measurement device must be shielded from this energy source so as not to influence the measurement.

Figure 12 shows the probe developed to measure the hot side gas temperature at the specimen center. The probe is basically two tubes, one copper and the other stainless steel. The stainless tube has a coolant flow of gaseous nitrogen which flows down the tube interior and returns via a smaller tube within the stainless tube. The nitrogen turns the corner at the termination of the stainless tube, this end being at the sample end of the light pipe. The copper tube runs parallel with the stainless tube in such a way that it is in the shadow of the cooled stainless tube at the entrance to the light pipe.

2.3.3 Cont.

This arrangement reduces the heat load on the copper tube by protecting it with the cooled stainless tube. The two tubes are joined together by a full radius braze joint along the entire length of the exposed assembly. Therefore, the copper tube can conduct its heat energy into the stainless tube. The copper tube terminates 1/4" from the heated specimen surface. The copper and stainless tubes pass through a pressure seal in the vessel wall and the stainless tube is plumbed to a nitrogen supply while the copper tube is vented to atmosphere. A small (0.025" diameter) sheathed thermocouple is located within the copper tube, and held on the center line by small spacers. The downstream end of the pressure vessel is held at a positive pressure between 25 and 40 psia. A sample of the heated hydrogen flows through the copper tube and past the thermocouple junction yielding the desired temperature data. The pressure drop available for this flow is largely spent at the thermocouple junction and near vicinity. Therefore, the velocity at the junction is quite high and the thermocouple set-up has a high recovery factor.

The outer copper tube acts as the conduit for the hot gas sample and as a radiation shield for the thermocouple junction. Radiation errors are minimized by locating the thermocouple junction 3/8" inside the termination of the copper tube. This effectively reduces the view factor between any reflecting surface and the thermocouple junction. Also, because of the relatively high flow rate of hydrogen within the copper tube, the tube is held near the hydrogen temperature and therefore radiation transfer between the thermocouple and the tube is negligible.

2.3.3 Cont.

The instrumentation errors associated with the heat transfer test are of the same magnitude as the isothermal test, error level. Mass flow measurements are within ±3%, the pressure measurements are within ±1 1/2%, and the temperature errors are ±1% of reading or ±2°F, whichever is greater. This applies to all the temperature measurements except the hot side gas temperature and the hot side material temperature. These two measurements are difficult to quantitatively assess. On the basis of test results with multiple thermocouples used simultaneously and through many hours of test experience on this program, it is felt that the temperature measurements on the hot side of the specimen are within ±2 1/2% of reading or ±10°F whichever is greater.

Data acquisition equipment used in the heat transfer tests was the 200 channel "Dymec" digital system, and two Hewlett Packard, 7100B, strip chart recorders. The "Dymec" system prints the data on paper tape and was the principal data acquisition system. The two, two-channel recorders gave four channels on which to monitor test parameters. A continuous real time display of the specimen pressure drop, the orifice pressure drop, and the hot side gas and specimen temperature were visible on the recorders. These displays were useful in indicating both the absolute level of each parameter and the timewise gradient. The attainment of steady state conditions from one test point to another was clearly visible on the recorders.

3.0 GENERAL DISCUSSION OF TEST RESULTS

This test program has demonstrated the sensitivity of the test data to specimen microstructure. Flow through the porous specimen is qualitatively similar to flow through a series of interconnected orifice passages. Also, for the largest portion of the flow range the flow across any given pseudo orifice is subcritical. Therefore, a small variation in equivalent pseudo orifice diameter (actually, mean pore diameter) will result in a much larger variation in the pressure drop. For non-choked flow, this pressure drop vs. pore diameter is a fourth power law as seen by the following orifice equation. For frictionless, subsonic flow through an orifice the mass flow rate is given as

$$\dot{M} = CA(\Delta p \rho)^{1/2}$$ where $\dot{M}$ = mass flow rate

Δp = orifice pressure drop

A = flow area (pore area)

d = pore diameter

C = constant

At a constant mass flow rate and noting that $A \propto d^2$ then

$$\Delta p \propto d^4$$

For choked flow at a constant mass flow rate the pressure drop is a complex function of the pore diameter and absolute pressure level. However, as the pressure ratio across a given pore increases the pressure drop versus pore diameter approaches a second power law. The effect of a change in the mean pore diameter between specimens of the same nominal porosity would be felt in both the heat transfer and the flow tests. This effect would show as an inconsistency between specimens for which the specifications were to be the same. In addition, correlations of the flow characteristics vs. porosity between specimens would be scattered in relation to the pore size variation.

3.0 Cont.

A second problem associated with the specimen microstructure is the variation in local permeability from location to location within a given specimen. Unless these variations are gross, this effect will not be evident in the pressure drop data. This is because the pressure drop and flow rate data are not spacially local measurements, but are integrated averages over the entire specimen cross section. The heat transfer data, on the other hand, is sensitive to spacial distributions of mass flow for two reasons. First, if a non-uniform coolant distribution is exhibited by the specimen, there will exist a non-uniform temperature distribution as well. The magnitude of the temperature variations, due to variations in specimen permeability, is increased because the gas density is sensitive to specimen temperature. If approximate local equilibrium is assumed, then the coolant temperature is near the specimen temperature. Also, the pressure drop across any given element of the specimen is the same from location to location. Therefore, a less dense coolant is flowing through the hotter portion of the specimen. Consequently, the temperature of this portion of the specimen is elevated still further.

Secondly, there exists on the specimen a location where the temperature has the same value as the area weighted average temperature. However, there is no assurance that the location of the thermocouples will coincide with this spot. In fact, it is quite unlikely that the two locations will coincide since the temperature distribution is not known, a priori.

3.0 Cont.

During the initial isothermal flow tests with the porous powder materials, it was observed that the data could not be correlated on the basis of thickness for a given porosity level. It was expected that the mass flow rate for a given porosity and pressure drop would be inversely related to the thickness. Despite the great care taken in the preparation of the raw specimen material, as described in references 2 and 3, there is evidently non-uniform microstructure between specimens in the powder group. It is felt that this may be the result of local compaction of the individual specimen during machining operations required to mount the test material in the specimen holder. Further evidence of the microstructure non-uniformity was demonstrated with a simple soap solution test. The specimen was placed in a test fixture which allows a slight flow of clean nitrogen to flow through the piece. A meniscus of soap solution is placed upon the horizontal specimen exit surface and the nitrogen allowed to flow. The bubble pattern and formation rate show clearly the degree of non-uniformity in the mass flow rate per unit surface area. This type of test showed some non-uniformity in all specimens. However, the non-uniformity was lowest in the Rigimesh materials and highest in the copper powders. Also, the non-uniformity was consistently less in the high porosity specimens.

This specimen behavior accounts to a large extent for the scatter present in the heat transfer data. In the case of the copper powder, the non-uniformity is of such a degree that the heat transfer coefficients are not presented. However, the raw data for all specimens tested has been included in Appendix B.

3.0 Cont.

It was observed that the material temperature at the back face (unheated side) of the porous specimen was only slightly elevated during the heat transfer tests. This phenomenon was observed throughout the test series. During the heat transfer test series the axial temperature variation was measured. This was accomplished by placing thermocouples at various axial locations along the specimen perimeter. Portions of the specimen support were removed to allow the attachment of the thermocouples. The results of these measurements demonstrated that the temperature gradient within the porous metal was considerably steeper than expected. Generally, it was concluded that the heat transfer between the porous structure and the coolant takes place in the first 1/8" below the heated surface.

4.0 DATA ANALYSIS

The data presentation and analysis are given in two parts. The data were correlated on the basis of pressure drop vs. mass flow rate for both isothermal and non-isothermal cases. Also, heat transfer coefficients between the material and the coolant are determined.

4.1 Pressure Drop

The pressure drop through the three varieties of porous metals was measured under both isothermal and non-isothermal conditions. The isothermal data was collected over a temperature range from 500°R to 2000°R. The non-isothermal tests were conducted at heat flux levels between 5 and 15 BTU/in^2-sec. with coolant temperatures varying from slightly above room temperature to over 2000°R. Complete listing of the test data is given in Appendix A.

4.1.1 Basic Flow Equations

All the pressure drop data are correlated in a form derived from the following modified Darcy equation:

$$-\frac{dp}{dx} = \alpha\mu\frac{\dot{m}}{g} + \frac{\beta\dot{m}^2}{\rho g} \qquad (1)$$

Using the ideal gas equation of state $\rho = \frac{p}{RT}$, equation (1) can be integrated to give:

$$-\bar{\rho}\,\Delta p = \frac{\alpha\mu\dot{m}L\bar{\rho}}{g} + \frac{\beta\dot{m}^2 L}{g} \qquad (2)$$

where $\bar{\rho} = \frac{\bar{p}}{RT} = \frac{p_{up} + p_{dn}}{2\,RT}$

$$\Delta p = p_{up} - p_{dn}$$

4.1.1 Cont.

Equation (2) may be rewritten in terms of the more familiar parameters, friction factor (f), and Reynolds number (Re), as follows:

$$fRe^2 = 2\alpha \frac{d}{S} Re + \frac{2\beta}{S} Re^2 \qquad (3)$$

where

$$f = \frac{\rho \Delta p \; g}{\frac{L}{2} (\dot{m})^2 \; S} \qquad (4)$$

$$Re = \frac{\dot{m} \; d}{\mu} \qquad (5)$$

4.1.2 Characteristic Lengths

The specimen characteristic lengths used in the Reynolds number and friction factor are the hydraulic diameter, d, and the reciprocal of the internal surface area per unit volume, S. The data on d and S is given in references 1 and 3. For this correlation, the numerical values of d and S, as taken from the mercury penetration measurements, were plotted as a function of porosity, ε. Smooth curves were then faired through the data. The equations written for these curves are as follows:

Rigimesh

$$d = 4.2 \times 10^{-3} \varepsilon^{1.68} \text{ (ft.)}$$

$$S = 1050 \; \varepsilon^{-.58} \text{ (ft}^{-1}\text{)}$$

Sintered Stainless Steel Powders

$$d = 7.22 \times 10^{-4} \varepsilon^{1.16} \text{ (ft.)}$$

$$S = 5540 \; \varepsilon^{-.16} \text{ (ft}^{-1}\text{)}$$

Sintered OFHC Copper Powders

$$d = 4.95 \times 10^{-4} \varepsilon^{1.16} \text{ (ft.)}$$

$$S = 8080 \; \varepsilon^{-.16} \text{ (ft}^{-1}\text{)}$$

4.1.2 Cont.

The isothermal flow data presented in references 8 and 9 is also correlated here for comparison. The surface area per unit volume for the packed bed of spheres or cylinders in reference 8 is calculated by the following equations. Assuming point contact:

$$S = \frac{6}{(d)_p} (1 - \varepsilon) \quad \text{spherical particles} \tag{6}$$

$$S = \frac{2(1 - \varepsilon)}{d_c} \left[\frac{d}{H} + 2 \right] \quad \text{cylinders} \tag{7}$$

where $(d)_p$ - diameter of particle

d_c = diameter of cylinder

H = height of cylinders

The hydraulic diameter is then calculated from

$$d = \frac{4\varepsilon}{S} \tag{8}$$

For the packed bed of spheres, cylinders, and cubes in reference 9, the surface area per unit volume listed in that reference is used and the hydraulic diameter is calculated by use of equation (8).

4.1.3 Correlation Equation for Pressure Drop

When the isothermal test data are plotted in a log-log format, it is found that fRe^2 can be represented by a set of parallel lines. For non-isothermal tests, the same correlation is valid provided that the property values ρ and μ are evaluated at the log mean temperature defined as:

$$T_{LM} = \frac{T_1 - T_2}{\ln T_1 - \ln T_2} \tag{9}$$

where T_1 and T_2 are the gas temperature at the inlet and outlet surfaces, respectively.

4.1.3 Cont.

As shown in equation (19) (see Section 4.2.2) the log mean temperature is the true average temperature of the gas when the temperature is an exponential function of (x), the distance through the specimen. It was found that the coefficients α and β of equation (3) are functions of material structure and porosity. For each material structure, the correlation can be simply represented by:

$$fRe^2 = C_1 \frac{Re}{[\xi(1-\xi)]^n} \left[1 + C_2 \frac{Re}{[\xi(1-\xi)]^n} \right] \qquad (10)$$

For the materials in this study and the data on packed beds of spheres, cylinders, and cubes (references 8 and 9), the constants C_1, C_2, and n are given in the following table.

Porous Structures	n	C_1	C_2	Range of Porosities	Range of Re_{dn}	Sources
Woven and Sintered Wire Mesh (Rigimesh)	3.9	1.99	7.39×10^{-5}	.087-.40	.7-870	Present data
Sintered 304L Stainless Spherical Powder	3.8	3.42	8.88×10^{-5}	.1-.31	.5-150	"
Sintered OFHC Copper Powder	2.8	10.7	7.55×10^{-4}	.1-.31	.35-96	"
Packed Bed of Spherical Particles, Cylinders or Cubes	2	22.8	1.17×10^{-3}	.359-.478	30-1100	Ref. 8, 9

The correlation is applicable for all gases. This is because test data collected with different flow media such as nitrogen and hydrogen were properly accounted for and correlated through the gas properties (molecular weight and viscosity).

4.1.3 Cont.

A comparison of test data and correlations is shown in Figures 14 to 17. Clearly, the correlation is satisfactory.

It may be pointed out that the correlation given by Ergun (reference 10) was also derived from equation (1). However, the functional relationship between α, β and the porosity ε given by Ergun does not fit the present data or the data of references 8, 9 and 11. This may be due to different porosity ranges. Ergun employed the data from a porosity range of 0.4 to 0.65, while the correlation given in equation (5) is for a porosity range from 0.1 to 0.478.

In principle, the constants C_1, C_2 and n are functions of the microstructures only. Since these constants are different for the stainless steel sintered spherical powder and the OFHC copper sintered powder, the microstructures of these two porous metals are apparently different. This microstructure variation (or local non-uniformity) is discussed under Section 3.0.

4.1.4 Error Analysis of Pressure Drop Data

The error analysis is performed for the Reynolds number Re and the product of friction factor and Reynolds number squared as follows:

4.1.4.1 Error in Reynolds Number

$$Re = \frac{\dot{m}d}{\mu}$$

$$\left|\frac{dRe}{Re}\right| \leq \left|\frac{d\dot{m}}{\dot{m}}\right| + \left|\frac{d(d)}{d}\right| + \left|\frac{d\mu}{\mu}\right|$$

For a fixed specimen and temperature, the hydraulic diameter and gas viscosity μ are constant. Therefore, the error in Reynolds number is

4.1.4.1 Cont.

directly proportional to the error in the maxx flux ($\dot{m}$) measurement. It is estimated that the error in the mass flux measurement is ±3%. Thus, the Reynolds number calculation is accurate to within ±3% assuming that there is no error in d and μ

$$fRe^2 = \frac{2\bar{\rho}\Delta P d^2 g}{LS^2}$$

$$\left|\frac{d\ fRe^2}{fRe^2}\right| \leq \left|\frac{d\bar{\rho}}{\bar{\rho}}\right| + \left|\frac{d\Delta p}{\Delta p}\right| + 2\left|\frac{d(d)}{(d)}\right| + \left|\frac{dS}{S}\right| + 2\left|\frac{d\mu}{\mu}\right|$$

Thus, for a given specimen and temperature, the maximum error of fRe^2 is equal to the sum of the errors of $\bar{\rho}$ and Δp. As discussed in the section (2.2.3) on instrumentation, it is estimated that the error in $\bar{\rho}$ and Δp is ±1.5%. Therefore, for a given specimen and temperature, the maximum error in fRe^2 is nominally ±3%.

In Figures 14 to 17 it is evident that the data points are scattered as much as 20% from the best correlation represented by the solid lines. This is due to a combination of the error in, $\dot{m}$, $\bar{\rho}\Delta p$, μ, d, S, ε as well as the approximate nature of the correlation itself.

4.1.4.2 Application of Results

For given porous metal, the porosity, ε, hydraulic diameter, d, internal surface area, S, and thickness, L, are presumedly known or can be found. The pressure drop as a function of mass flux m can be calculated by the following equation which is another form of equation (10):

$$p_1^2 - p_2^2 = \frac{RTLS\mu^2}{g\ d^2}\left[C_1 \frac{\dot{m}d}{\mu[\varepsilon(1-\varepsilon)]^n} + C_1C_2 \frac{\dot{m}^2d^2}{\mu^2[\varepsilon(1-\varepsilon)]^{2n}}\right] \quad (11)$$

4.1.4.2 Cont.

Thus, for a fixed downstream pressure p_2, the upstream or reservoir pressure p_1 required to provide a mass flux $\dot{m}$ at a given temperature T can be computed by equation (11). Notice that if the gas temperature through the porous materials is not a constant, a log mean temperature T_{LM} defined by equation (9) must be used in place of T in equation (11). Also, under this condition, T_{LM} is to be used for evaluating the viscosity of gas μ.

4.2 Heat Transfer

4.2.1 Determination of Heat Transfer Coefficient

The heat transfer coefficient between the porous material and the coolant is determined by the following equations derived in reference 12:

$$\frac{T_{fw} - T_f}{T_{mw} - T_f} = \frac{1}{B}\left[\frac{1 - \theta_{mo}e^{\gamma_2}}{e^{\gamma_1} - e^{\gamma_2}}\gamma_1 e^{\gamma_1} - \frac{1 - \theta_{mo}e^{\gamma_1}}{e^{\gamma_1} - e^{\gamma_2}}\gamma_2 e^{\gamma_2}\right] \tag{12}$$

where

$$B = \frac{\dot{m}Cp1}{k} \tag{13}$$

$$\gamma_1 = \frac{A}{2}\left[-1 + \sqrt{1 + \frac{4B}{A}}\right] \tag{14}$$

$$\gamma_2 = \frac{A}{2}\left[-1 - \sqrt{1 + \frac{4B}{A}}\right]$$

$$A = \frac{h\,L}{\dot{m}Cp} = \frac{\acute{h}SL}{\dot{m}Cp} \tag{15}$$

For a given specimen under a specified test condition, the temperatures, T_{fw}, T_f, T_{mw}, and the property values Cp, and k, as well as the thickness L are known. Therefore, the heat transfer coeffieicnt h' can be determined from equation (12).

For some conditions, equation (12) can be greatly simplified by considering the following:

4.2.1 Cont.

(a) γ_1 is always positive

(b) γ_2 is always negative

(c) $e^{\gamma_1} > e^{\gamma_2}$

Therefore, when $|\gamma_2|$ is relatively large the following approximations become nearly exact.

$$e^{\gamma_1} - e^{\gamma_2} \doteq e^{\gamma_1}$$

$$1 - (\theta_{mo}) e^{\gamma_2} \doteq 1$$

$$\gamma_2 e^{\gamma_2} \doteq 0$$

then equation (12) can be written as

$$\gamma_1 = B \left[\frac{T_{fw} - T_f}{T_{mw} - T_f} \right] \tag{16}$$

For all the heat transfer data evaluated in this report, the absolute value of is relatively large and therefore equation (16) can be substituted for equation (12).

The heat transfer parameter A may be expressed in terms of γ_1 and B as follows:

$$A = \frac{\gamma_1^2}{B - \gamma_1} \tag{17}$$

Thus, for any data point for which T_f , T_{fw} , T_{mw} and m are known, the parameter B can be calculated from equation (13) and the value of γ_1 and A may be computed from equations (16) and (17), consecutively.

4.2.2 Reference Temperature

The properties of the gas and porous material are functions of temperature. Since the temperature of both the coolant and the porous materials varies along the flow direction, a reference temperature must

4.2.2 Cont.

be used for the evaluation of property values. If it is assumed that the temperature of the gas and the porous material can be approximately expressed by a single-termed exponential function, the mean temperature along the flow path as shown in the following equations is the log mean temperature between the inlet and the outlet surfaces:

$$T = \frac{1}{L} \int_0^L T dx \tag{18}$$

$$\text{let } T = ae^{bx} \tag{19}$$

At $x = 0$, $T = To = a$

At $x = L$, $T = T_L = ae^{bL} = T_o\, e^{bL}$

and $bL = \ln T - \ln T_o$

Substituting equation (18) into (17) and performing the integration, one gets

$$T = \frac{1}{L}\left[\frac{a}{b} e^{bx}\right]_o^L = \frac{1}{bL}\left[ae^{bL} - a\right] = \frac{T_L - T_o}{\ln T_1 - \ln T_o} = T_{LM}$$

where

$$T_{LM} = \text{log mean temperature} = \frac{T_L - T_o}{\ln T_1 - \ln T_o} \tag{20}$$

When T_o and T_L are very close, i.e., $T_L = T_o + \delta T$, the log mean temperature T_{LM} can be reduced to the form shown in the following equation:

$$T_{LM} = \frac{\delta T}{\ln\left(1 + \frac{\delta T}{T_o}\right)} = \frac{\delta T}{\frac{\delta T}{T_o} - \frac{1}{2}\left(\frac{\delta T}{T_o}\right)^2} = \frac{T_o}{1 - \frac{1}{2}\left(\frac{\delta T}{T_o}\right)} \tag{21}$$

For $\delta T = 0$

$T_{LM} = T_o$

Thus, for isothermal condition, the log mean temperature is the prevailing temperature, as it should be.

4.2.3 Presentation of Heat Transfer Results

The dimensionless parameters in heat transfer are Nusselt number, Stanton number, Prandtl number, and Reynolds number. They are defined as follows:

$$\left.\begin{aligned} Nu &= \frac{h\,d}{k} \\ St &= \frac{h}{SmC_p} \\ Pr &= \frac{C_p}{K} \\ Re &= \frac{md}{} \end{aligned}\right\} \qquad (22)$$

The property values of the gas, including thermal conductivity k, heat capacity at constant pressure C_p, and the viscosity μ are evaluated at the log mean temperature T_{LM}.

Some of the results of the tests are presented graphically in the form of $\frac{Nu}{Pr^{1/3}}$ vs. Re and $St\ Pr^{2/3}\ Re^2$ vs. Re. $\frac{Nu}{Pr^{1/3}}$ vs. Re was used because, in the case of incompressible flow over a body, $\frac{Nu}{Pr^{1/3}}$ is found to be a function of Reynolds number. $St\ Pr^{2/3}\ Re^2$ was used because it corresponds to the parameter fRe^2 in momentum transfer. When the plot of $St\ Pr^{2/3}\ Re^2$ vs. Re is compared with the plot of fRe^2 vs. Re, one can see whether or not there is a similarity between momentum and energy transfer for flow through porous materials.

4.2.3.1 Stainless Steel Rigimesh Porous Materials

Figures 18, 19 and 20 show the parameter $\frac{Nu}{Pr^{1/3}}$ as a function of Re for the stainless steel Rigimesh at porosity levels of .116, .187 and .369 to .401. The nominal incident heat flux levels were 7.5 and 15 BTU/in^2-sec, for this data. It appears that the dimensionless heat transfer coefficient is independent of the heat flux level. The heat transfer results of Denton (reference 15) and Coppage and London (reference 16) are shown as dotted lines in Figure 20 for comparison. Their results are 25% to 40% lower than the present data. This could be due to the difference in porous structures, since their results are for the case of a packed bed of spheres.

Figures 21, 22 and 23 show St $Pr^{2/3}$ Re^2 as a function of Re for the same three specimens. Notice from Figures 18 through 23, the slope of the data line increases as the porosity decreases. This same phenomenon was also found in reference 16. However, this trend does not appear in the pressure data. Therefore, it is concluded that there is no similarity between heat and momentum transfer in the porous materials. This same conclusion was also found in references 8, 9 and 16. It is for this reason that the heat transfer data cannot be combined in a single correlation, as has been done for the pressure drop data.

4.2.3.2 Stainless Steel Sinterered Powder

Figure 24 shows $\frac{Nu}{Pr^{1/3}}$ as a function of Reynolds number for the sintered stainless steel powder in two porosity levels. Figure 25 shows the same data in the form of St $Pr^{2/3}$ Re^2 vs. Re. Again, Figures 24 and 25 show the increase in slope as the porosity decreases.

4.2.3.3 Packed Bed of Particles

Figure 26 shows $\frac{Nu}{Pr^{1/3}}$ as a function of Reynolds number for a packed bed of spheres, cylinders, and cubes from references 8 and 9. Figure 27 shows the same data in the format $St\ Pr^{2/3}\ Re^{2}$ vs. Re. Considering the difficulty of the experiment and the variety of geometry of the particles, the correlation is satisfactory.

4.2.4 Error Sensitivity Analyses for the Heat Transfer Measurement

From equation (17),

$$\ln A = 2 \ln \gamma_1 = \ln (B-\gamma_1)$$

$$\frac{dA}{A} = 2 \left|\frac{d\gamma_1}{\gamma_1}\right| + \left|\frac{d(B-\gamma_1)}{B-\gamma_1}\right| = \left|2 + \frac{\gamma_1}{B-\gamma_1}\right| \left|\frac{d\gamma_1}{\gamma_1}\right| \qquad (23)$$

From equation (16)

$$\ln \gamma_1 = \ln B + \ln (T_{fw} - T_f) - \ln (T_{mw} - T_f)$$

$$\frac{d\gamma_1}{\gamma_1} \leq \left|\frac{dB}{B}\right| + \left|\frac{dT_{fw}}{T_{fw} - T_f}\right| + \left|\frac{dT_{mw}}{T_{mw} - T_f}\right| \qquad (24)$$

Substituting equation (24) into equation (23),

$$\frac{dA}{A} \leq \left|2 + \frac{\gamma_1}{B-\gamma_1}\right| \left[\left|\frac{dB}{B}\right| + \left|\frac{d\,T_f}{T_{fw} - T_f}\right| + \left|\frac{d\,T_{mw}}{T_{mw} - T_f}\right|\right] \qquad (25)$$

if $\left|\frac{dB}{B}\right| \leq .02$, $\left|\frac{dT_{fw}}{T_{fw} - T_{fw}}\right| \leq .05$, $\left|\frac{d\,T_{mw}}{T_{mw} - T_{fw}}\right| \leq .05$

$$\left|\frac{dA}{A}\right| \leq .12 \left[2 + \frac{1}{B-1}\right]$$

where the numerical values are taken from the accuracy assigned the measured parameters involved.

Test data show that B and γ_1, in general, are of the same order of magnitude and the term $\frac{\gamma_1}{B-\gamma_1}$ could be from 1 to 10. This indicates

4.2.4 Cont.

that the maximum uncertainty of the parameter A could be from 36% to 150%. This inherent error sensitivity, together with the non-uniformity of flow through certain test specimens is responsible for the scattering of the heat transfer data.

4.2.5 Correlation of Heat Transfer Data

Approximate equations were fitted into the heat transfer data presented in Figures 18 to 27. The results are shown below:

$$\frac{Nu}{Pr^{1/3}} = .01\ Re^{2.5} \quad (\text{Rigimesh}, \xi = .116) \tag{26}$$

$$\frac{Nu}{Pr^{1/3}} = .163\ Re - 0.22 \quad (\text{Rigimesh}, \xi = .187) \tag{27}$$

$$\frac{Nu}{Pr^{1/3}} = 4 + 0.11\ Re \quad (\text{Rigimesh}, \xi = .369 \text{ to } .401) \tag{28}$$

$$\frac{Nu}{Pr^{1/3}} = .1 + .16\ Re \quad (\text{Sintered stainless steel powder}, \xi = .2118) \tag{29}$$

$$\frac{Nu}{Pr^{1/3}} = .228 + .0358\ Re \quad (\text{Sintered stainless steel powder}, \xi = .3186) \tag{30}$$

4.2.6 Application of Heat Transfer Data

The information on heat transfer coefficients between the porous materials and their gaseous coolant may be used to design a transpiration cooled system. For given environmental conditions and vehicle configuration, such as a nose cone or nozzle throat, the heat flux is specified or can be estimated. The allowable surface temperature is also specified from the structural considerations. The problem is usually to determine the coolant mass flux $\dot{m}$ such that the metal temperature will not exceed the allowable value. This calculation may be performed by the following steps:

1. Estimate a mass flux $\dot{m}$

4.2.6 Cont.

2. Compute the coolant temperature T_{fw} at the exit surface by the energy balance equation:

$$T_{fw} = T_{f_{oo}} + \frac{\psi q_o}{\dot{m} C_p} \tag{31}$$

where

ψ = blocking function due to mass injection (see reference 17).

3. For a given porous material, estimate the hydraulic diameter d and the surface area per unit volume of the porous structures. Compute the Reynolds number and determine the dimensionless heat transfer coefficient Nu from the appropriate equation or graph. Compute A, B, γ_1 and γ_2 from equations (13) to (15).

4. Test data show that the thermal boundary layer of the coolant at the inlet surface is negligibly small and the gas temperature at the inlet surface can be taken as the coolant temperature immediately upstream of the surface. Thus, the dimensionless porous material temperature at the inlet surface can be found by the following equation (reference 12):

$$\theta_{mo} = \frac{\gamma_1 - \gamma_2}{\gamma_1 e^{\gamma_2} - \gamma_2 e^{\gamma_1}} \tag{32}$$

5. A check is now made to see if the estimated $\dot{m}$ is the correct one by use of the following expression for the dimensionless temperature of the coolant at the exit surface (equation 12).

$$\frac{T_{fw} - T_f}{T_{mw} - T_f} = \frac{1}{B}\left[\frac{1-\theta_{mo}e^{\gamma_2}}{e^{\gamma_1} - e^{\gamma_2}}\gamma_1 e^{\gamma_1} - \frac{1-\theta_{mo}e^{\gamma_1}}{e^{\gamma_1} - e^{\gamma_2}}\gamma_2 e^{\gamma_2}\right] \tag{33}$$

Since all the quantities in equation (33) are either given or calculated, equation (33) can be used to check the correctness of the estimated m. If equation (33) is not satisfied, a new estimate of m must be used and the calculations repeated until a correct m is found.

4.2.6 Cont.

In cases where the coolant and the material temperatures are very close at the inlet surface, step 3 can be bypassed and equation (33) is simplified by putting $\theta_{mo} = 0$.

Once the mass flux is found, the pressure drop across the porous material can be found by the method outlined in Section 2.

5.0 CONCLUSIONS AND RECOMMENDATIONS

5.1 Conclusions

Pressure drop and heat transfer for flow through three different porous metals having various porosity and thickness values have been measured and analyzed. Based on this study, the following conclusions are given:

(1) For a given porous metal structure and porosity, the dimensionless product of density and pressure drop, fRe^2, is a function of Reynolds number only, independent of the kind of gas. This functional relationship is applicable for isothermal flow at room temperature and at high temperature as well as for non-isothermal flow provided that the property values are evaluated at a log mean temperature between the coolant at the inlet and the outlet surfaces.

(2) The dimensionless product of density and pressure drop for the porous materials can be correlated in the form of

$$fRe^2 = C_1 \frac{Re}{[\xi(1-\xi)]^n} \left[1 + C_2 \frac{Re}{[\xi(1-\xi)]^n} \right]$$

C_1, C_2, and n are functions of the microstructures of the porous materials. This correlation is valid for sintered porous materials as well as for packed beds of various shaped particles.

(3) The heat transfer coefficient is plotted in the form of $\frac{Nu}{Pr^{1/3}}$ vs. Re and $St\, Re^2\, Pr^{2/3}$ vs. Re. No simple correlation has been found to represent the heat transfer coefficient independent of specimen porosity.

(4) There exists no simple direct relation between momentum transfer and heat transfer for flow through porous materials.

5.2 Recommendations

In the fRe^2 vs. Re plots, it was found that the slope of the curves increases as the Reynolds number increases. Therefore, the correlation is valid only for the Reynolds number range measured in the tests. Outside this range, extrapolation is uncertain, and additional test data is required. The quality of heat transfer data is less than desired due primarily to the non-uniformity of mass flux across the sample. To generate better heat transfer data, development work is needed to produce more uniform test specimen.

6.0 REFERENCES

1. R. E. Regan, "Characterization of Porous Matrices for Transpiration Cooled Structures", NASA CR-72699 (1970)
2. G. Friedman, "Fabrication, Characterization and Thermal Conductivity of Porous Copper and Stainless Steel Materials", NASA CR 72755 (1971)
3. R. E. Regan, "Characterization of Porous Powder Metal Matrices for Transpiration Cooled Structures", NASA CR-72994 (1971)
4. U.S. Patent No. 3,099,041
5. "Development of a High Irradiance Source," A. R. Lunde, a paper published in the Proceedings of the Sixth Space Simulation Conference, 1972, NASA-SP-298
6. R. R. Tye, "An Experimental Investigation of Thermal Conductivity and Electrical Resistivity of Three Porous 304L Stainless Steel "Rigimesh" Material to 1300°K," NASA-CR 72710 (1970)
7. J. C. Y. Koh, Anthony Fortini, "Thermal Conductivity and Electrical Resistivity of Porous Material", NASA CR-120854 (1971)
8. B. W. Gamson , G. Thodos and O. A. Hougen, "Heat, Mass and Momentum Transfer in the Flow of Gases through Granular Solids", A.I. Ch. E Trans. Volume 39, No. 1 P1-35 (1943)
9. M. B. Glaser and G. Thodos, "Heat and Momentum Transfer in the Flow of Gases through Packed Beds", A.I. Ch. E Journal Vol. 4, No. 1 P. 63-74 (1958)
10. E.R. G. Eckert and R. Drake, "Heat and Mass Transfer", McGraw-Hill Book Company, 2nd Ed., p. 252 (1959)
11. R. D. Turnacliff, "An Experimental Study of Local Convective Heat Transfer and Pressure Drop for Laminar and Turbulent Flow of Air Within a Uniformly Packed Bed of Spheres at Three Different Porosities", Ph.D. Thesis, University of Minnesota (1957)

6.0 Cont.

12. J. C. Y. Koh and E. P. del Casal, "Heat and Mass Flow through Porous Matrices for Transpiration Cooling", Proceedings of the 1965 Heat Transfer and Fluid Mechanics Institute, p. 261-281 (1965)

13. H. Littman, R. G. Barile, and A. H. Pulsifer, "Gas-Particle Heat Transfer Coefficients in Packed Beds at Low Reynolds Number", I&EC Fundamentals, Vol. 7, No. 4, November 1968, p. 554-561

14. J. DeAcetis and G. Thodos, "Mass and Heat Transfer in Flow of Gases through Spherical Packings", Industrial and Engineering Chemistry, Vol. 52, No. 12, December 1970, p. 1003-1006.

15. W. H. Denton, C. H. Robinson, and R. S. Tibbs, "The Heat Transfer and Pressure Loss in Fluid Flow through Randomly Packed Spheres", A.E.R.E. Report HPC-35-13, AT7:22, June 1944 (available through U.S. AEC Technical Information Division, ORE, Oak Ridge, Tennessee)

16. J. E. Coppage and A. L. London, "Heat Transfer and Flow Friction Characteristics of Porous Media", Chem. Engr. Progress, Vol. 52, No. 2 P57F-63F (1956)

17. L. W. Woodruff, "Transpiration Effects on Heat Transfer", The Boeing Co., D2-22202.

NOMENCLATURE

Unless specified otherwise, the symbols in this report are defined as follows:

A	heat transfer parameter
B	mass flux parameter
C_p	specific heat of coolant at constant pressure
d	characteristic diameter
f	friction factor
g	gravitational constant
h'	heat transfer coefficient per unit volume
k	thermal conductivity
L	thickness of porous material
$\dot{m}$	mass flux
Nu	Nusselt number
p	pressure
Pr	Prandtl number of fluid
q	heat flux
R	gas constant
S	internal surface area per unit volume
R_e	Reynolds number

St	Stanton number
T	temperature
X	distance measured from the fluid inlet surface along flow direction
α	viscous permeability parameter
β	inertia permeability parameter
η_1	defined in equation (14)
η_2	defined in equation (14)
θ	$\frac{T - T_{f\infty}}{T_{mw} - T_{\infty}}$
μ	viscosity of fluid
$\bar{\mu}$	micron (10^{-6} meter)
ξ	porosity = $\frac{\text{void volume}}{\text{total volume}}$
ρ	density of coolant

Subscripts

LM	log mean
f	fluid
fw	fluid at exit wall surface
f_∞	reservoir of far upstream

m	matrix
mo	matrix at inlet surface
mw	matrix at outlet surface
o	at inlet surface
w	at outlet surface

Conversion Factors

Parameter	U.S. Engineering	Conversion Factor	International System
q	$\frac{BTU}{ft^2\text{-}sec.}$	1.6342×10^{6}	$\frac{w}{m^2}$
h	$\frac{BTU}{ft^3\text{-}sec\text{-}^\circ R}$	6.7021×10^{2}	$\frac{w}{m^3\text{-}^\circ K}$
C_p	$\frac{BTU}{lbm\text{-}^\circ R}$	4.1868×10^{3}	$\frac{J}{kg\text{-}^\circ K}$
k	$\frac{BTU}{sec\text{-}^\circ R\text{-}ft}$	6.2265×10^{3}	$\frac{w}{m\text{-}^\circ K}$
m	$\frac{lbm}{ft^2\text{-}sec}$	4.8824×10^{-4}	$\frac{kg}{m^2\text{-}sec}$
μ	$\frac{lbm}{ft\text{-}sec}$	1.4882×10^{0}	$\frac{N\text{-}sec}{m^2}$
P	$\frac{lbf}{ft^2}$	4.7880×10	$\frac{N}{m^2}$
ρ	$\frac{lbm}{ft^3}$	1.6018×10	$\frac{kg}{m^3}$

NOTATION:

meter (m)	Newton (N)
killogram (kg)	Joule (J)
degree Kelvin (°K)	watt (w)

FIGURES

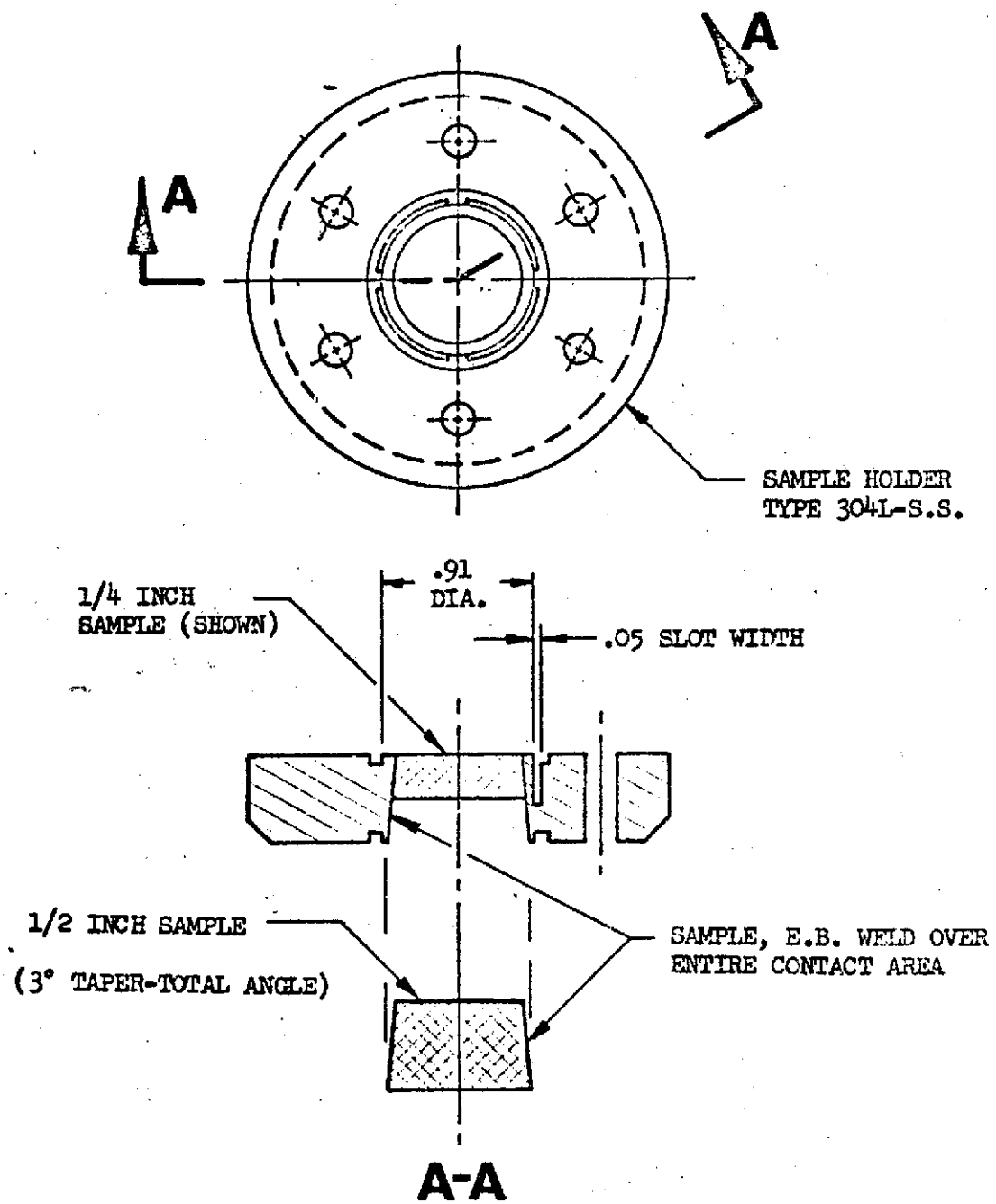

FIG. 1 RIGIMESH SPECIMEN, MOUNTED FOR TEST

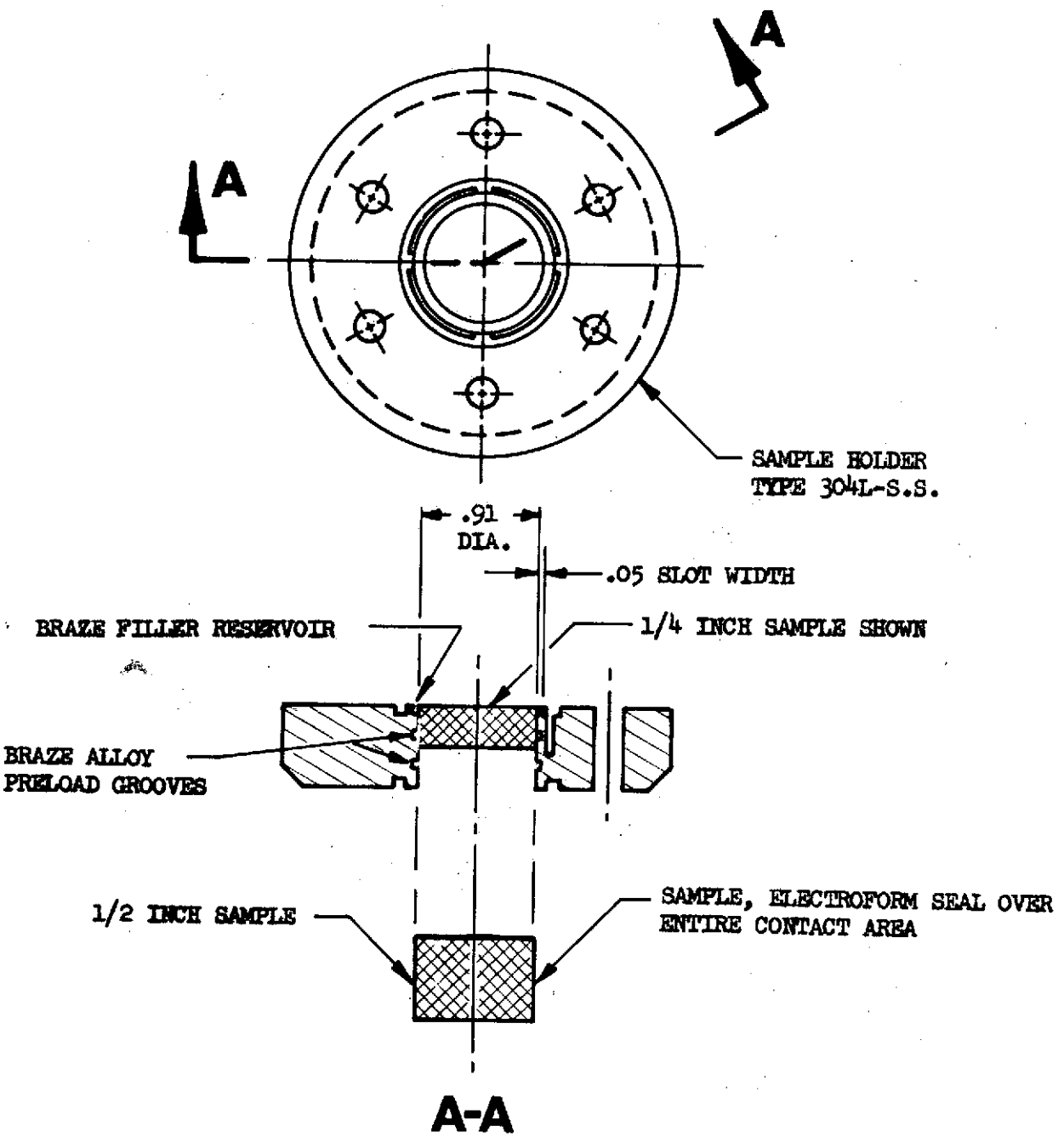

FIGURE 2. POWDER SPECIMEN, MOUNTED FOR TEST

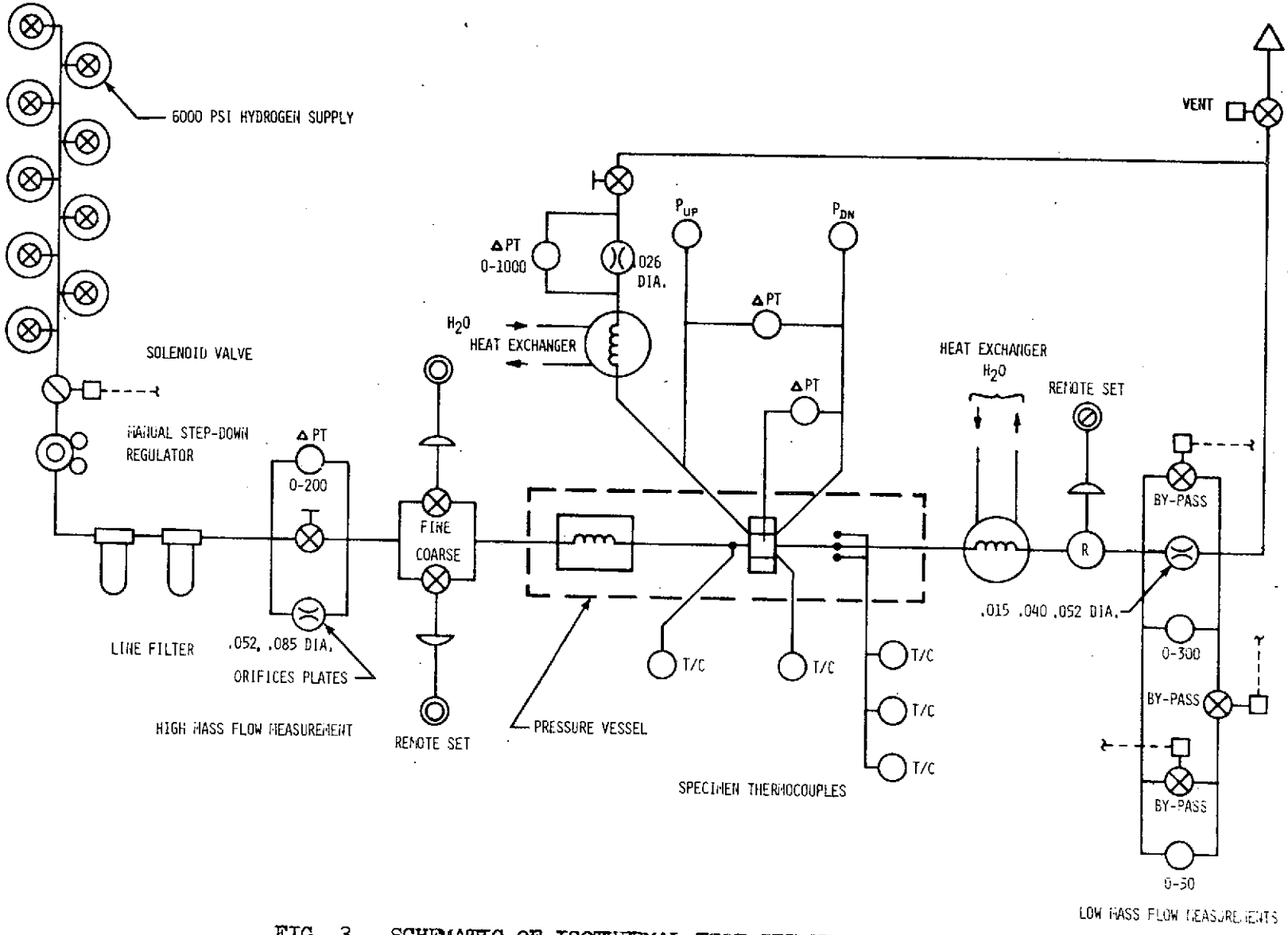

FIG. 3 SCHEMATIC OF ISOTHERMAL TEST SET-UP

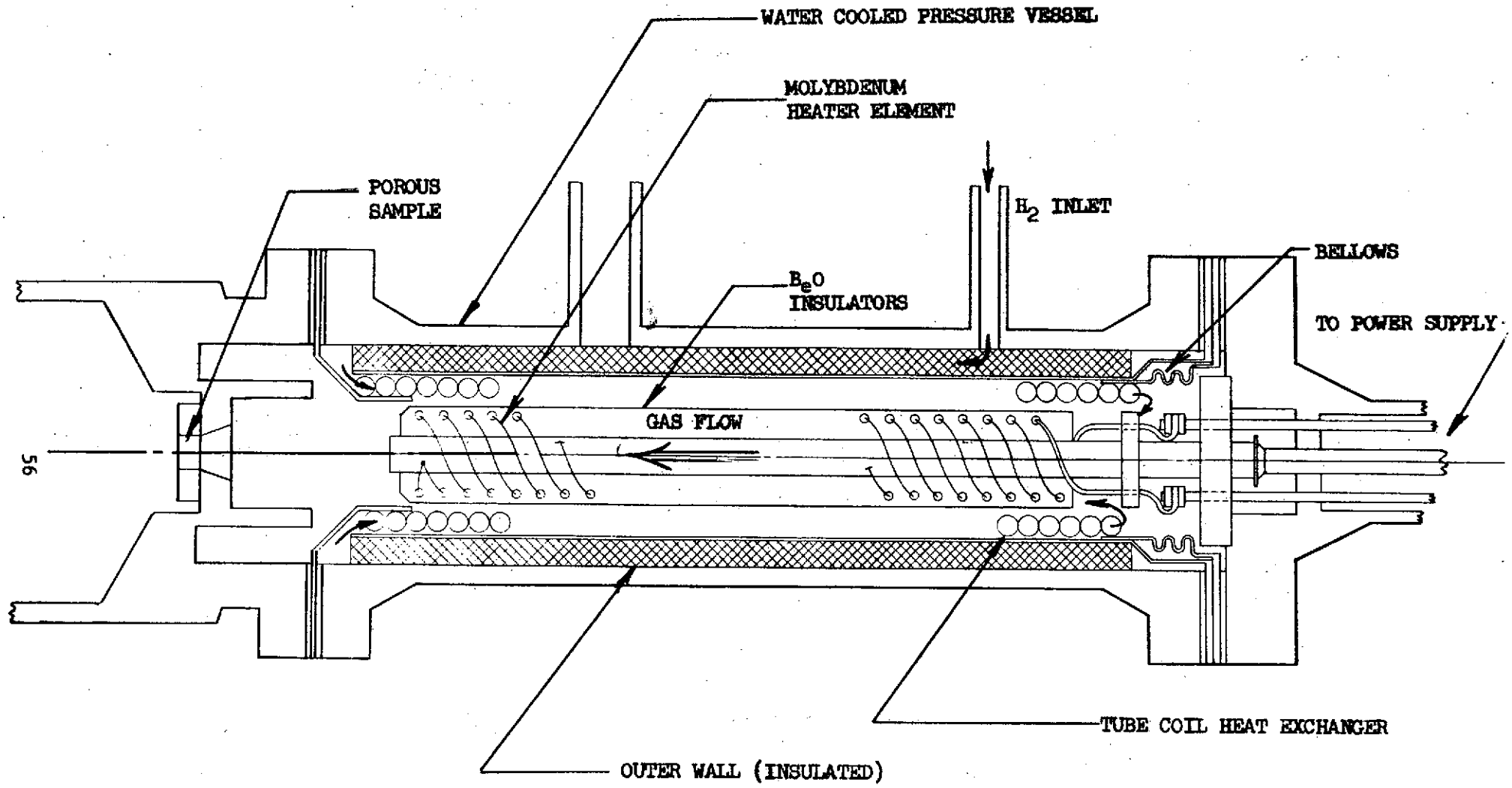

FIG. 4 ISOTHERMAL HYDROGEN HEATER

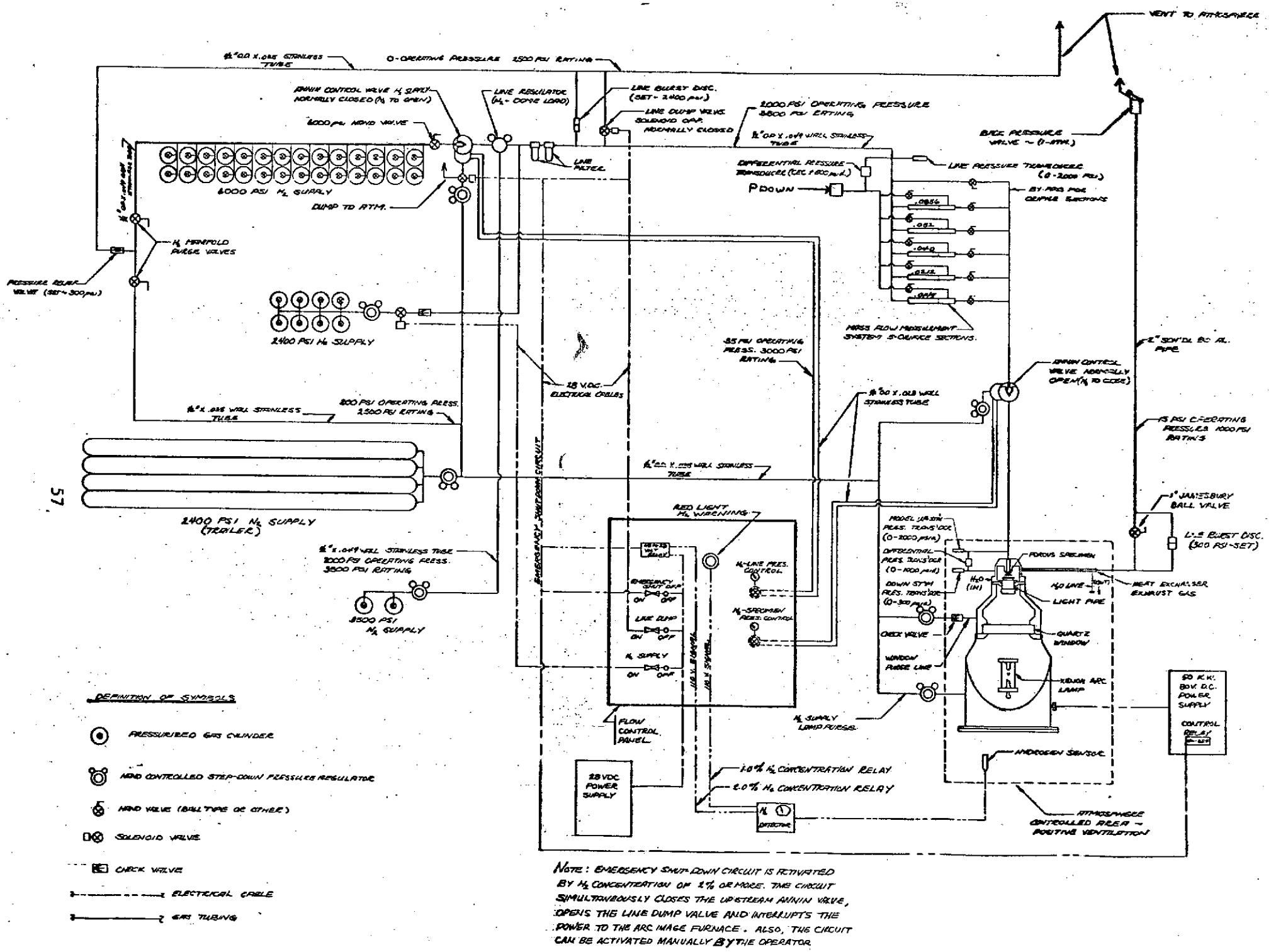

NOTE: EMERGENCY SHUT-DOWN CIRCUIT IS ACTIVATED BY H_2 CONCENTRATION OF 2% OR MORE. THE CIRCUIT SIMULTANEOUSLY CLOSES THE UPSTREAM ANINN VALVE, OPENS THE LINE DUMP VALVE AND INTERRUPTS THE POWER TO THE ARC IMAGE FURNACE. ALSO, THE CIRCUIT CAN BE ACTIVATED MANUALLY BY THE OPERATOR.

FIG. 5 SCHEMATIC OF HEAT TRANSFER TEST HARDWARE

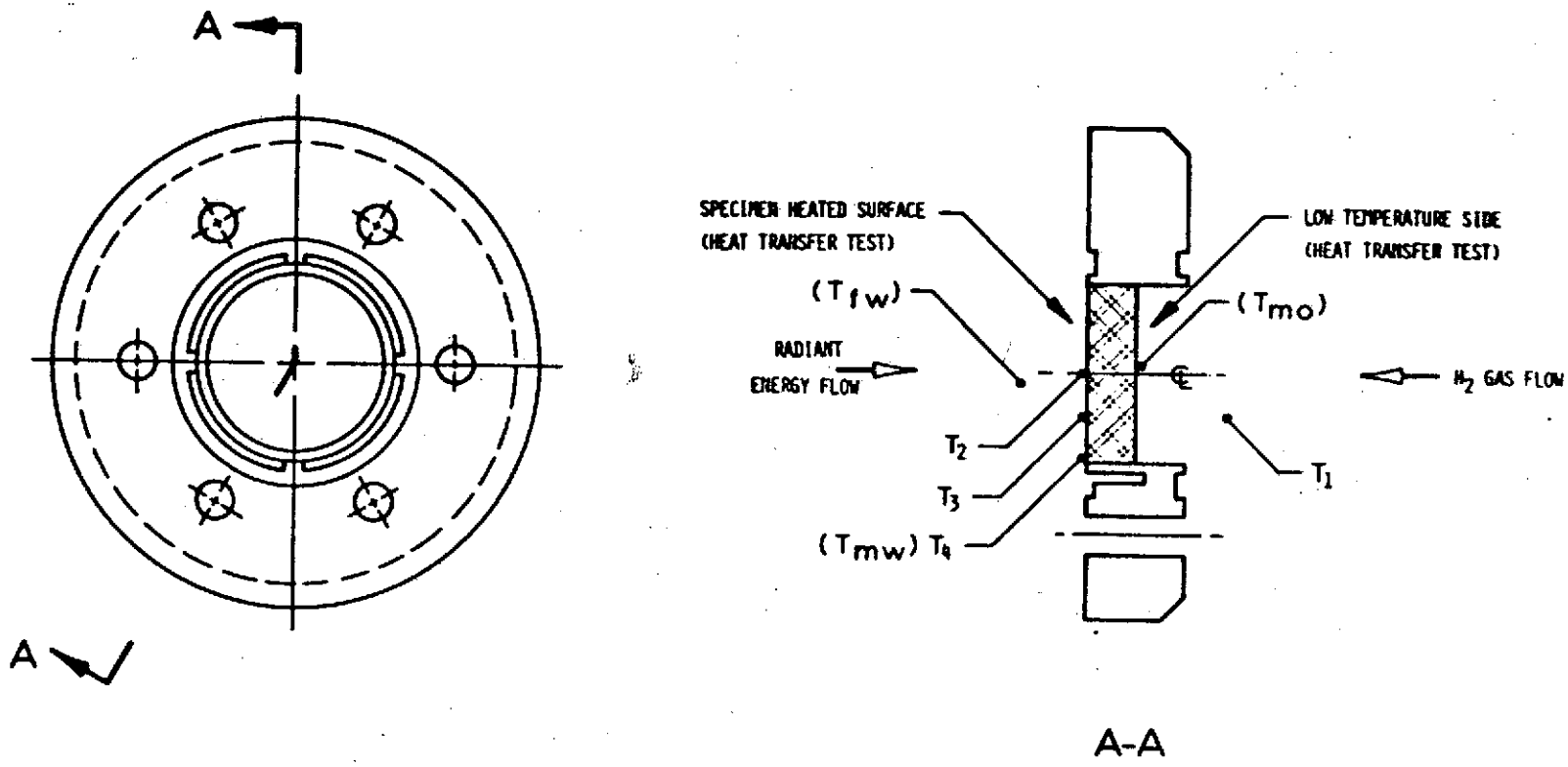

NOTATION
ISOTHERMAL TEST T_1, T_2, T_3, T_4
HEAT TRANSFER TEST $T_{foo}, T_{fw}, T_{mo}, T_{mw}$

FIG. 6 THERMOCOUPLE LOCATIONS

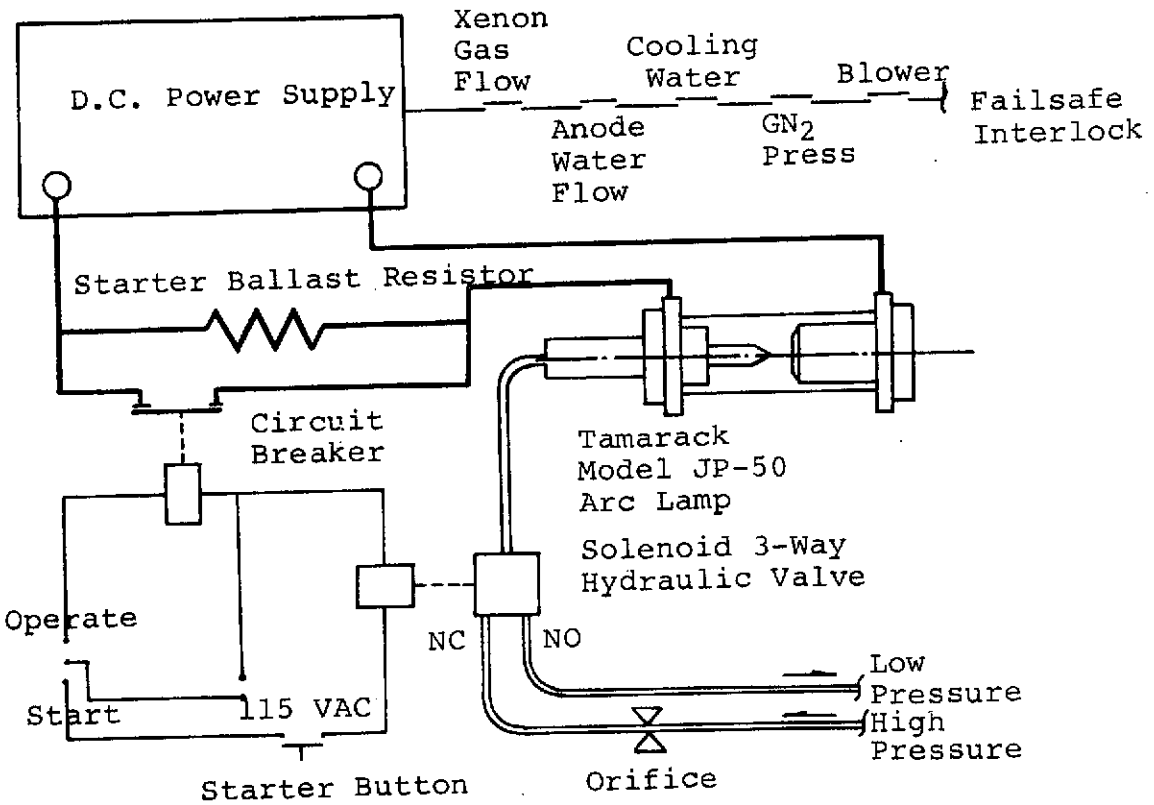

FIG. 7 FURNACE OPERATIONAL SCHEMATIC

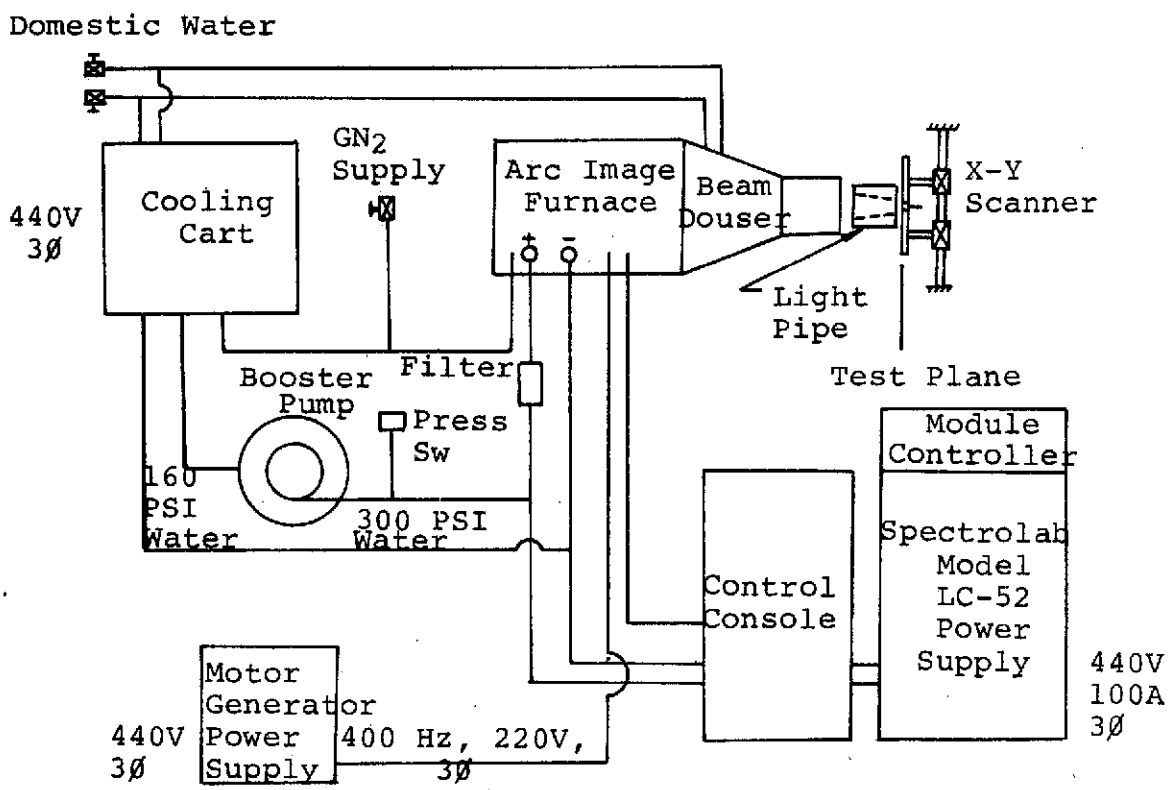

FIG. 8 TEST SET-UP SCHEMATIC

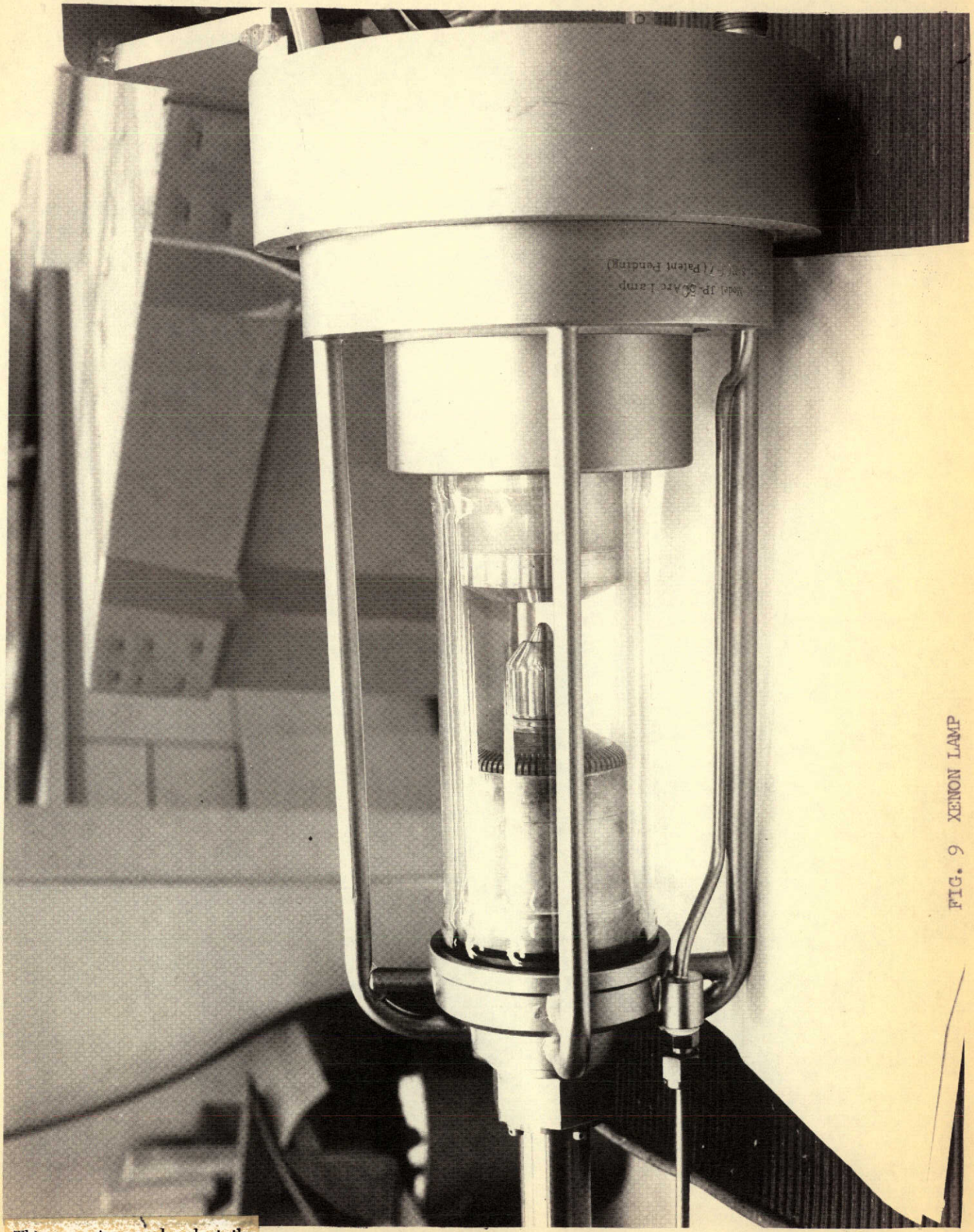

FIG. 9 XENON LAMP

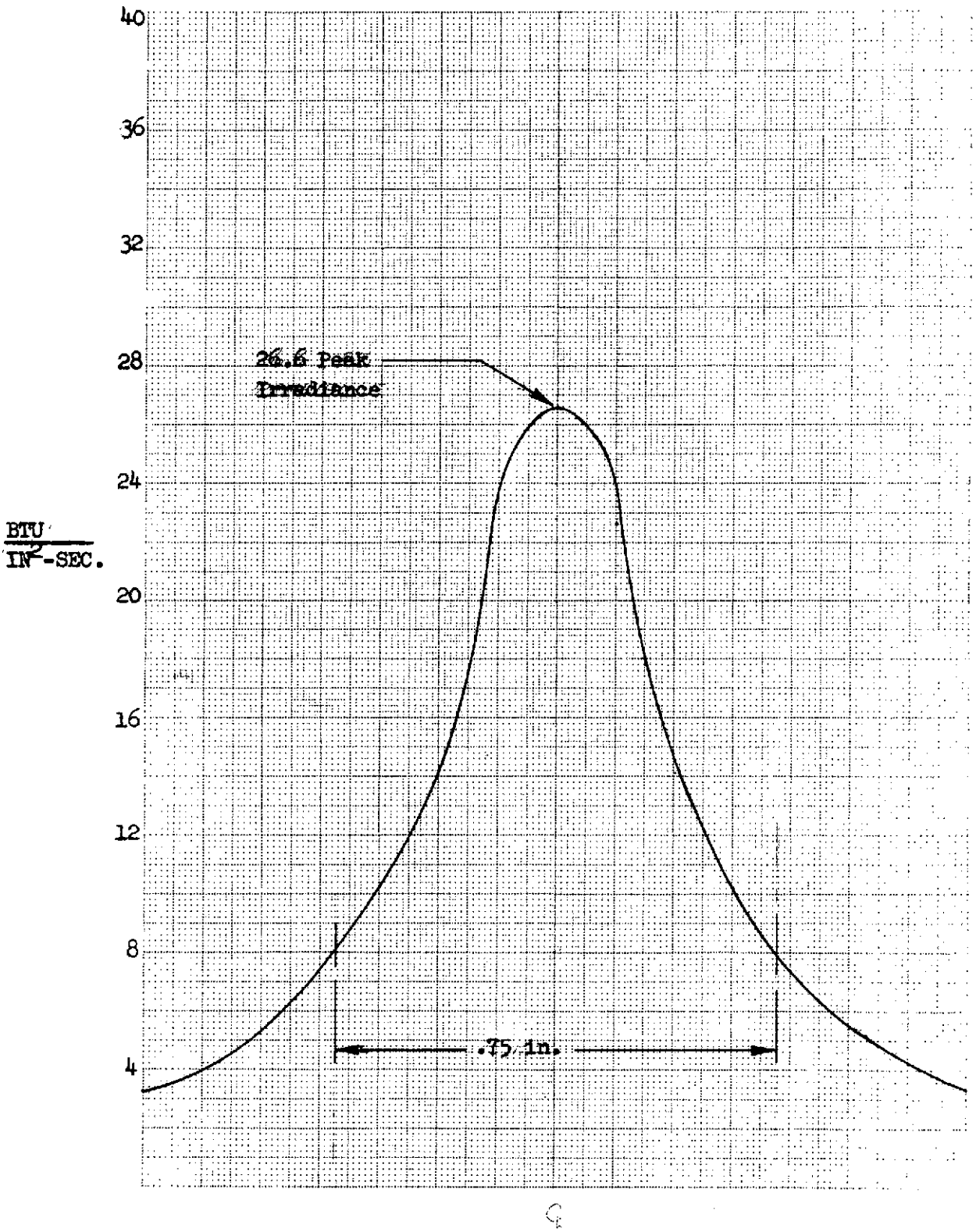

FIG. 10 TYPICAL HIGH POWER IRRADIANCE SCAN

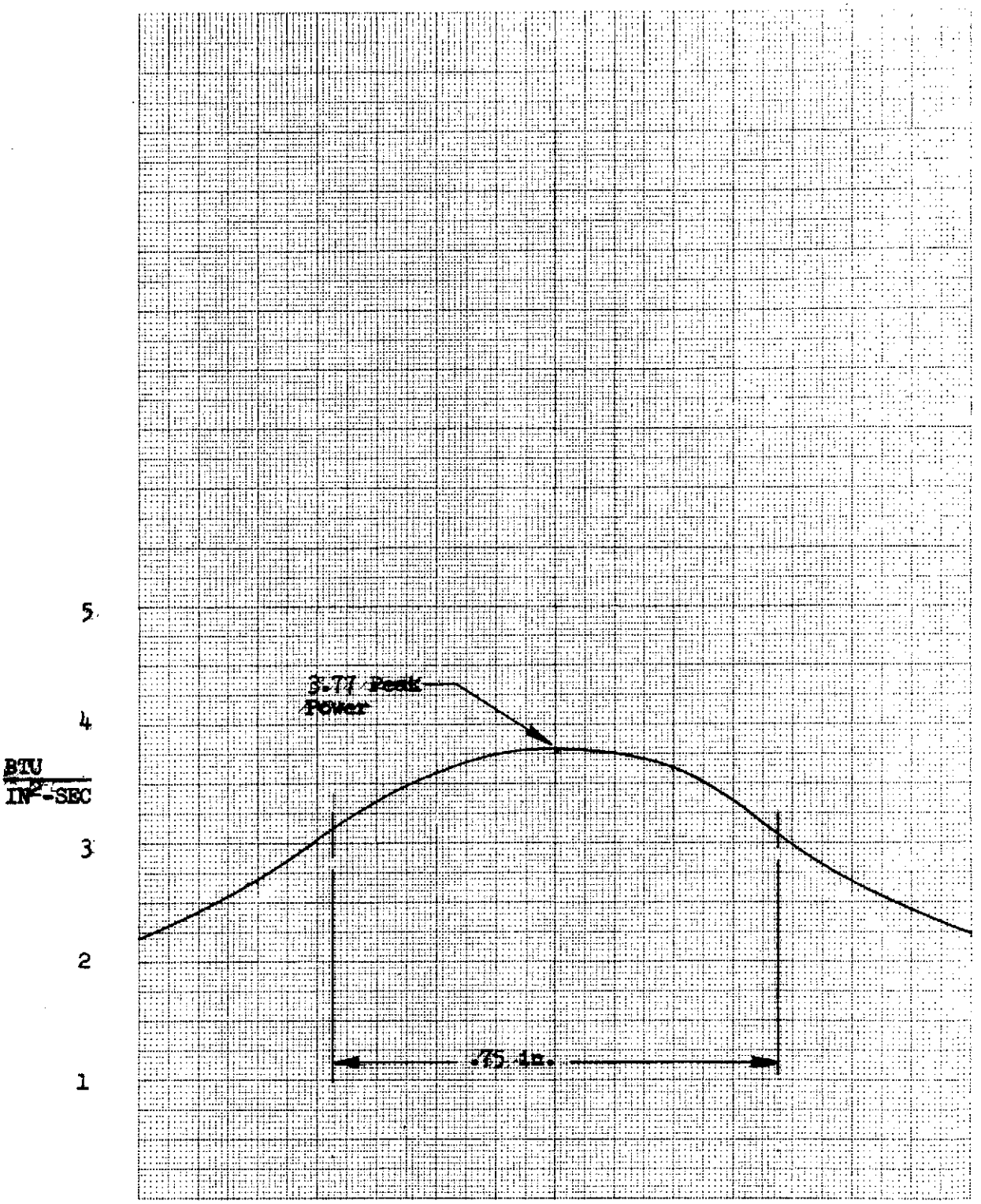

FIG. 11 TYPICAL LOW POWER IRRADIANCE SCAN

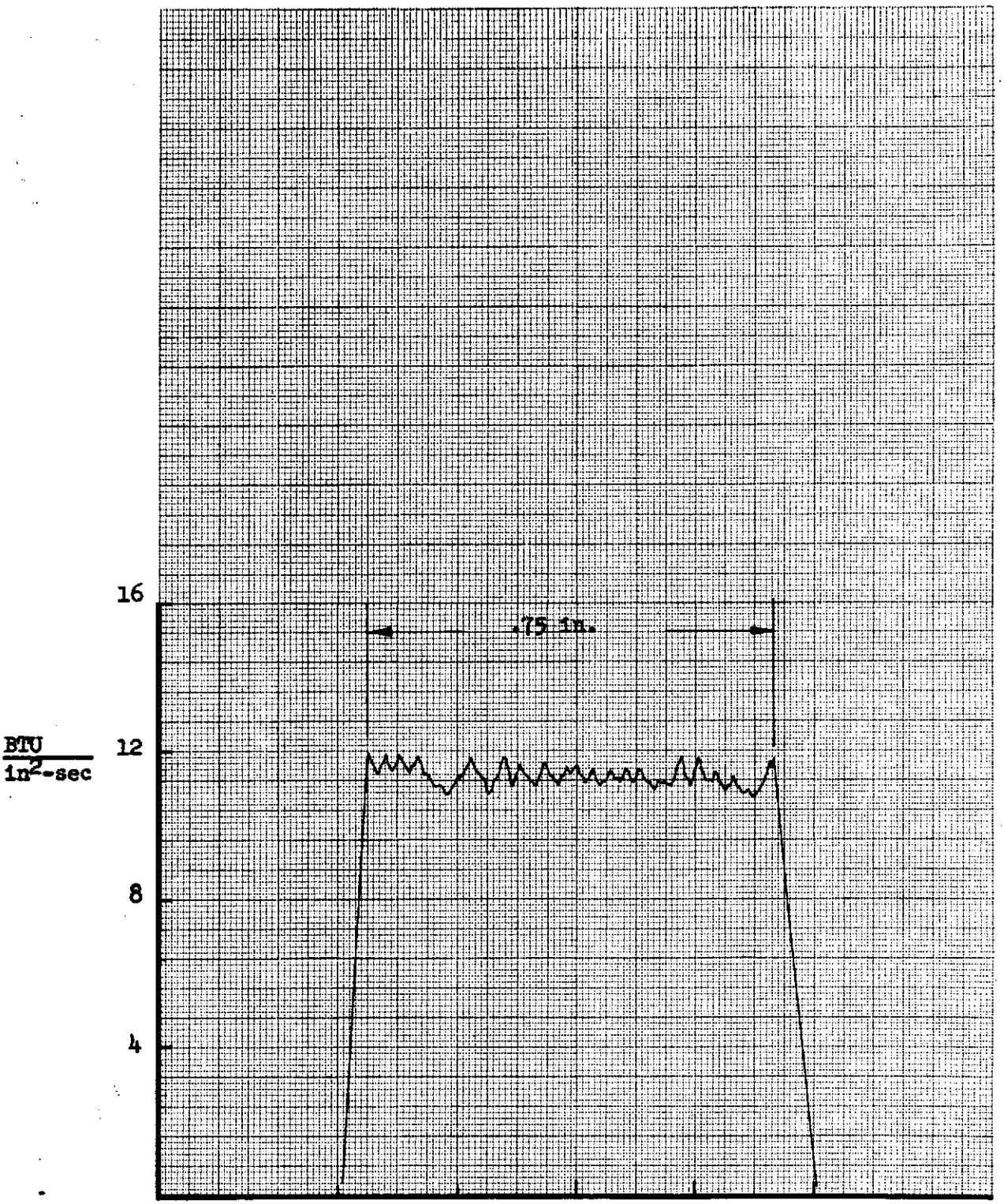

FIG. 11A. TYPICAL HIGH POWER SCAN WITH LIGHT PIPE

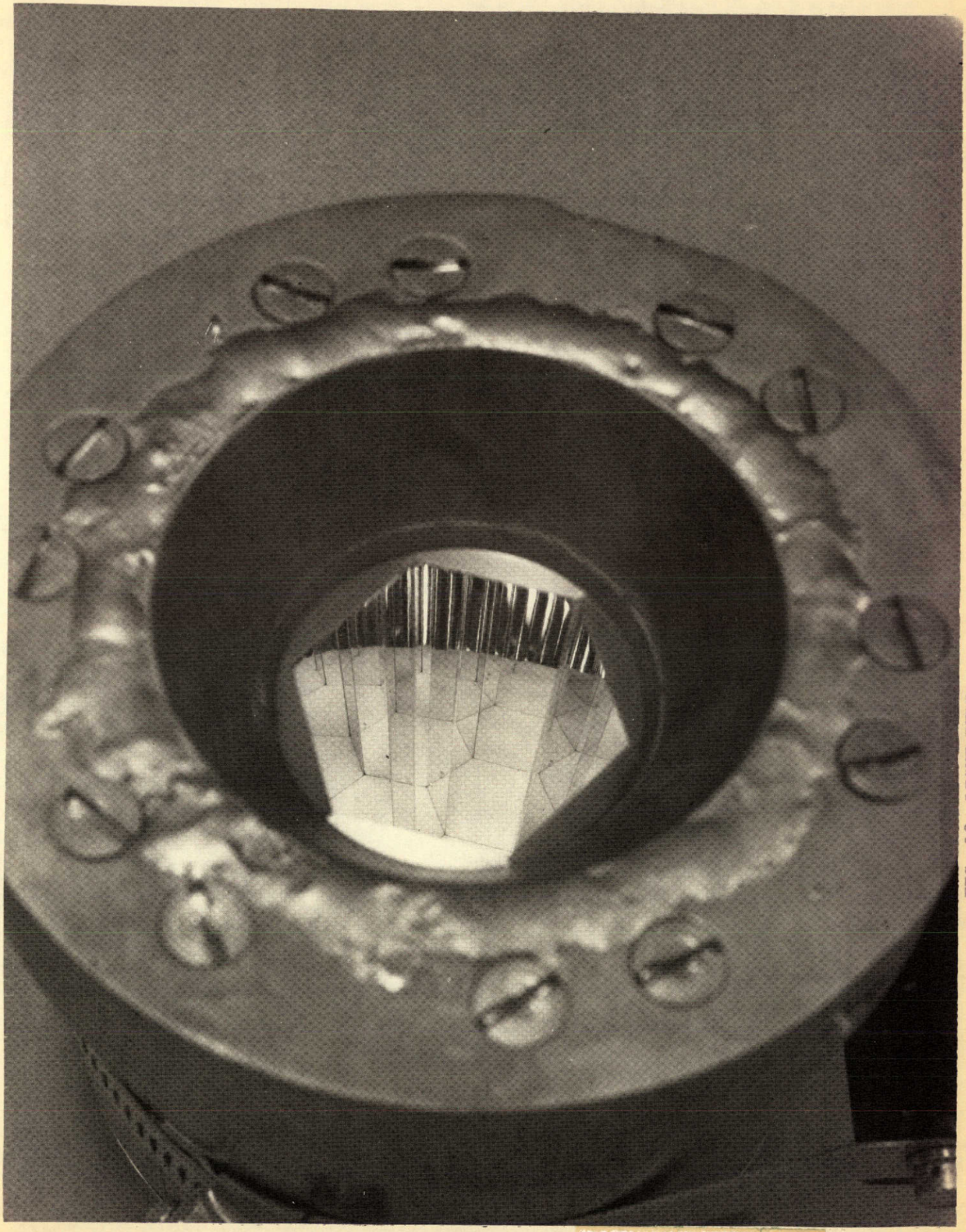

FIG. 12 LIGHT PIPE

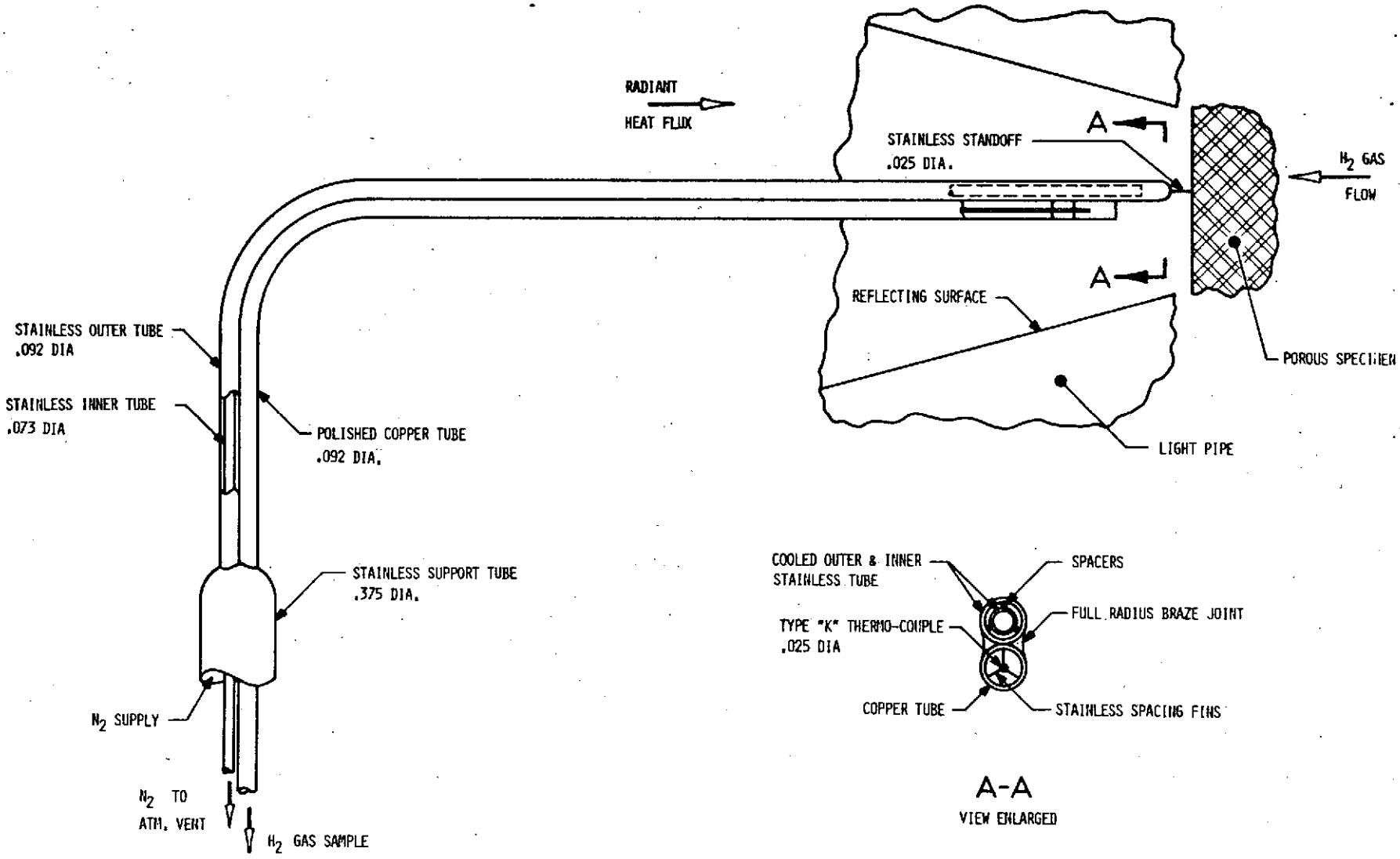

FIG. 13 GAS TEMPERATURE MEASUREMENT PROBE

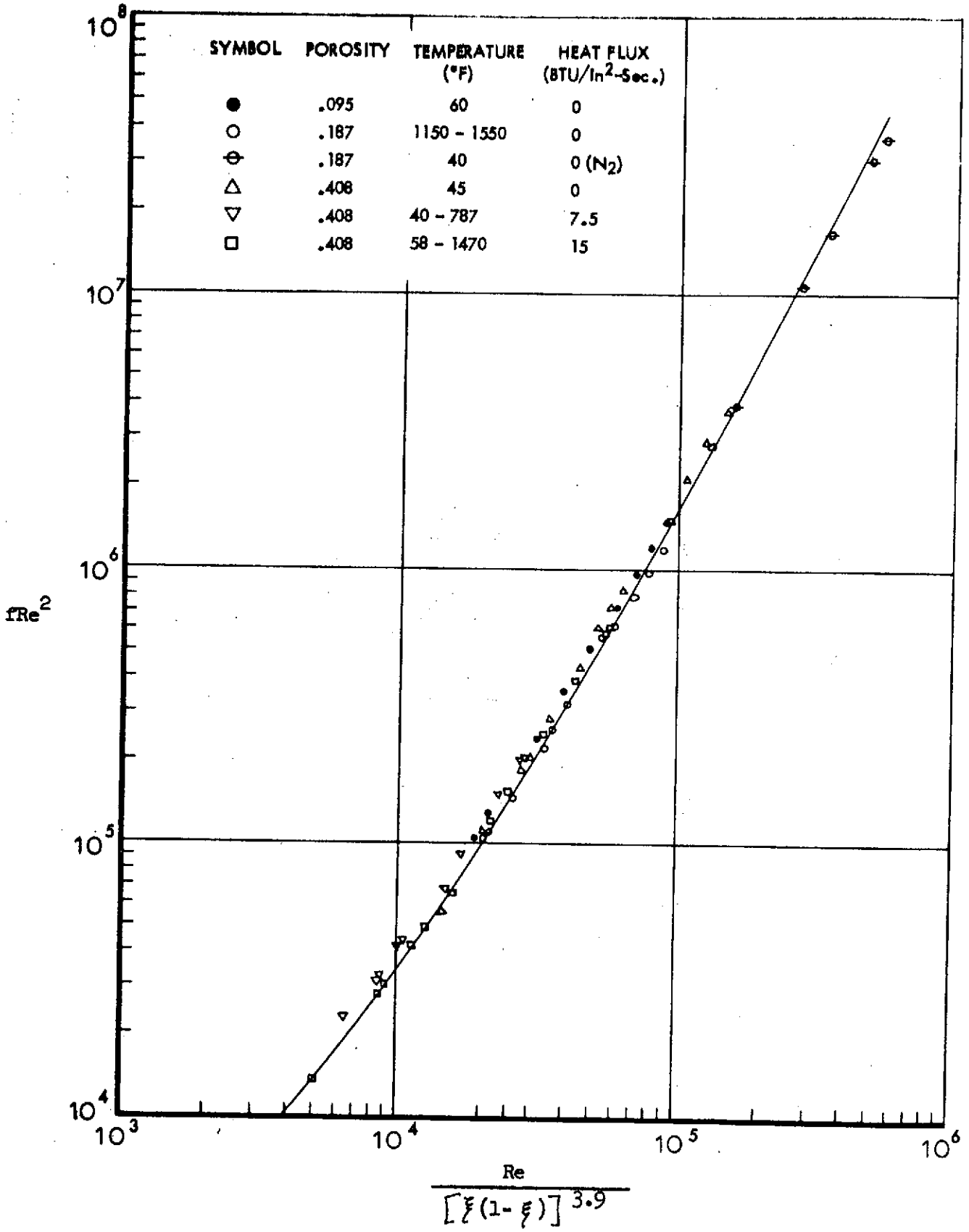

FIG. 14 PRESSURE DROP CHARACTERISTICS FOR FLOW THROUGH SINTERED 304L WIRE MESH (RIGIMESH)

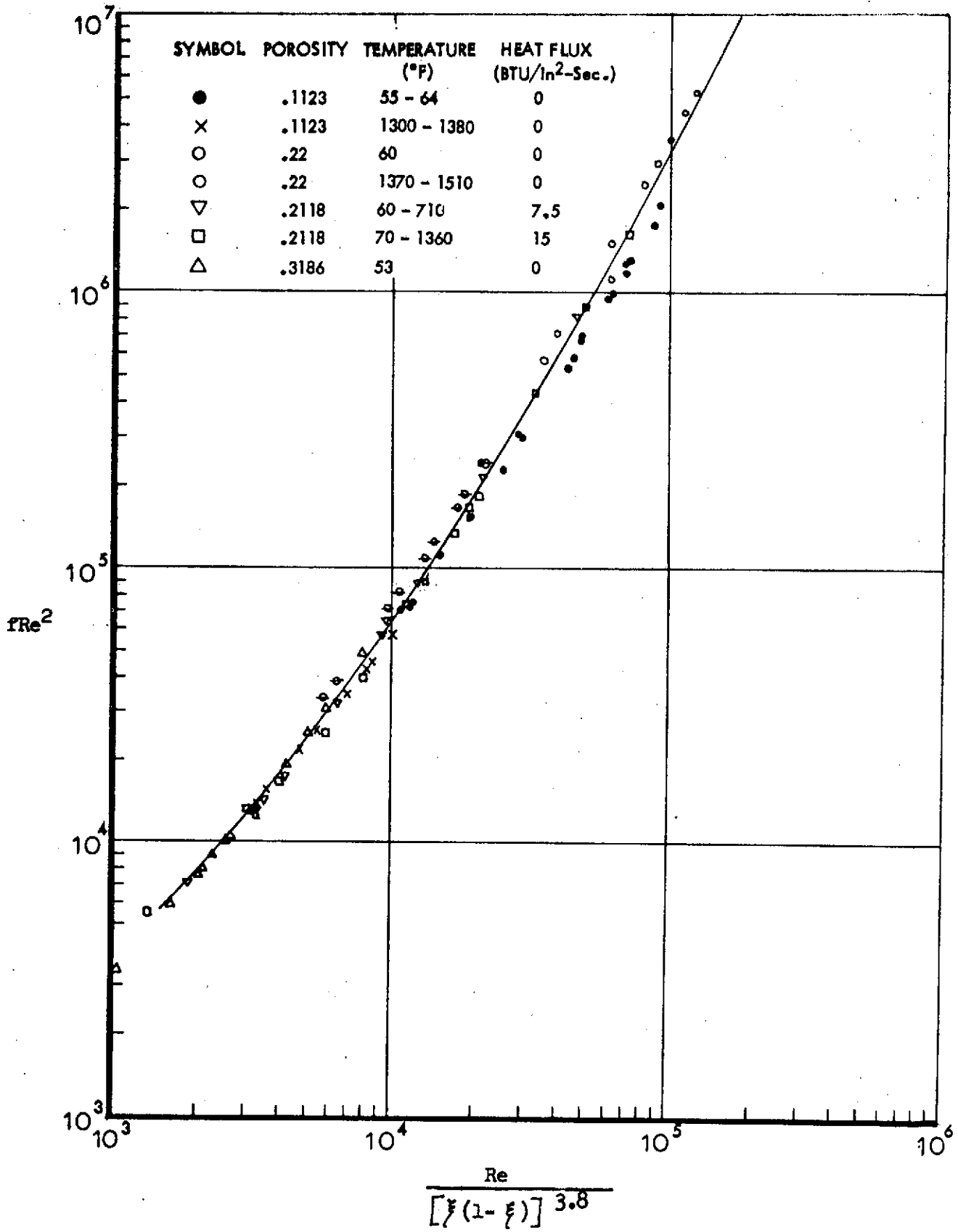

FIG. 15 PRESSURE DROP CHARACTERISTICS FOR FLOW THROUGH SINTERED 304L STAINLESS SPHERICAL POWDERS

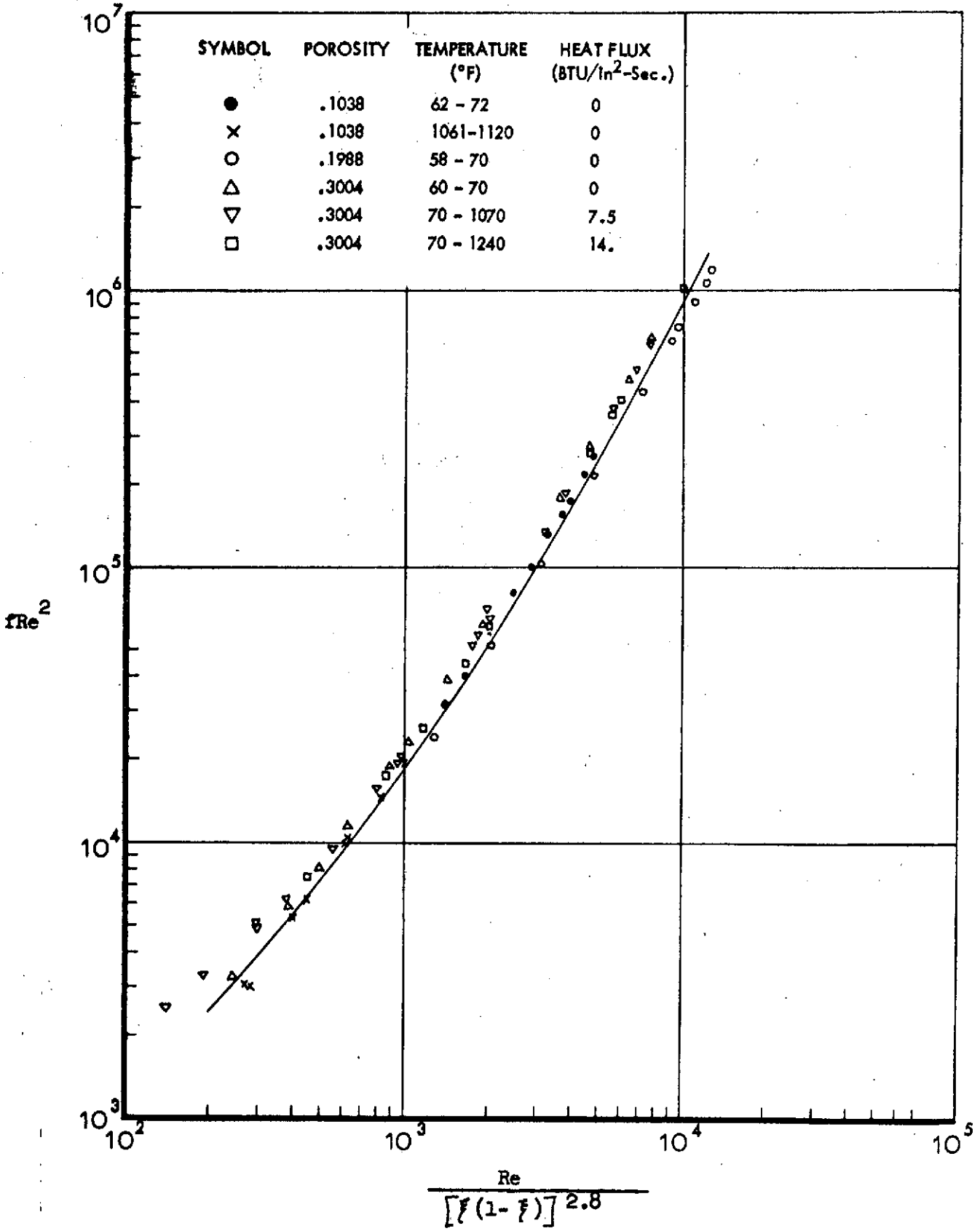

FIG. 16 PRESSURE DROP CHARACTERISTICS FOR FLOW THROUGH SINTERED OFHC COPPER SPHERICAL POWDERS

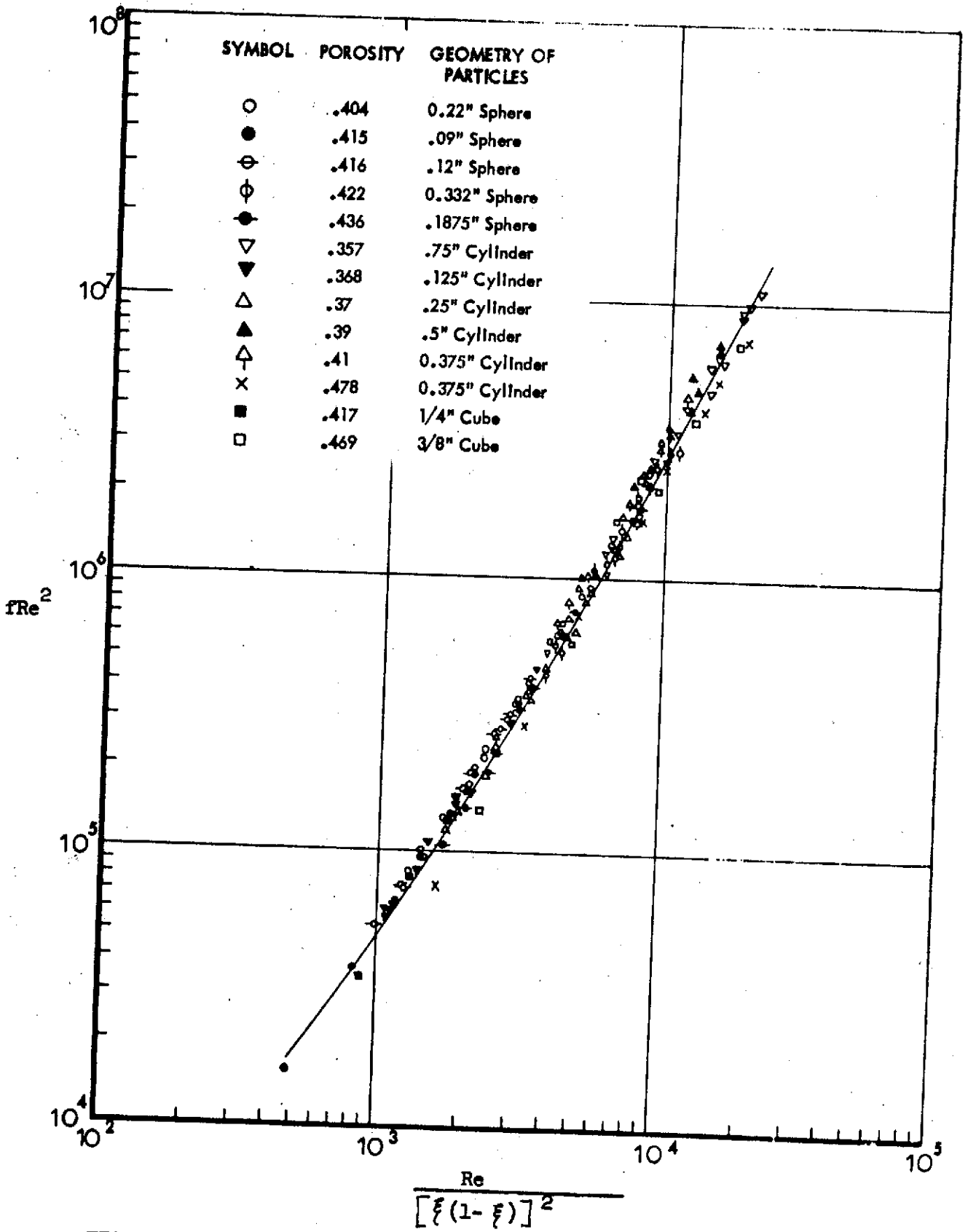

FIG. 17 PRESSURE DROP CHARACTERISTICS FOR FLOW THROUGH A PACKED BED OF SPHERICAL PARTICLES, CYLINDERS OR CUBES

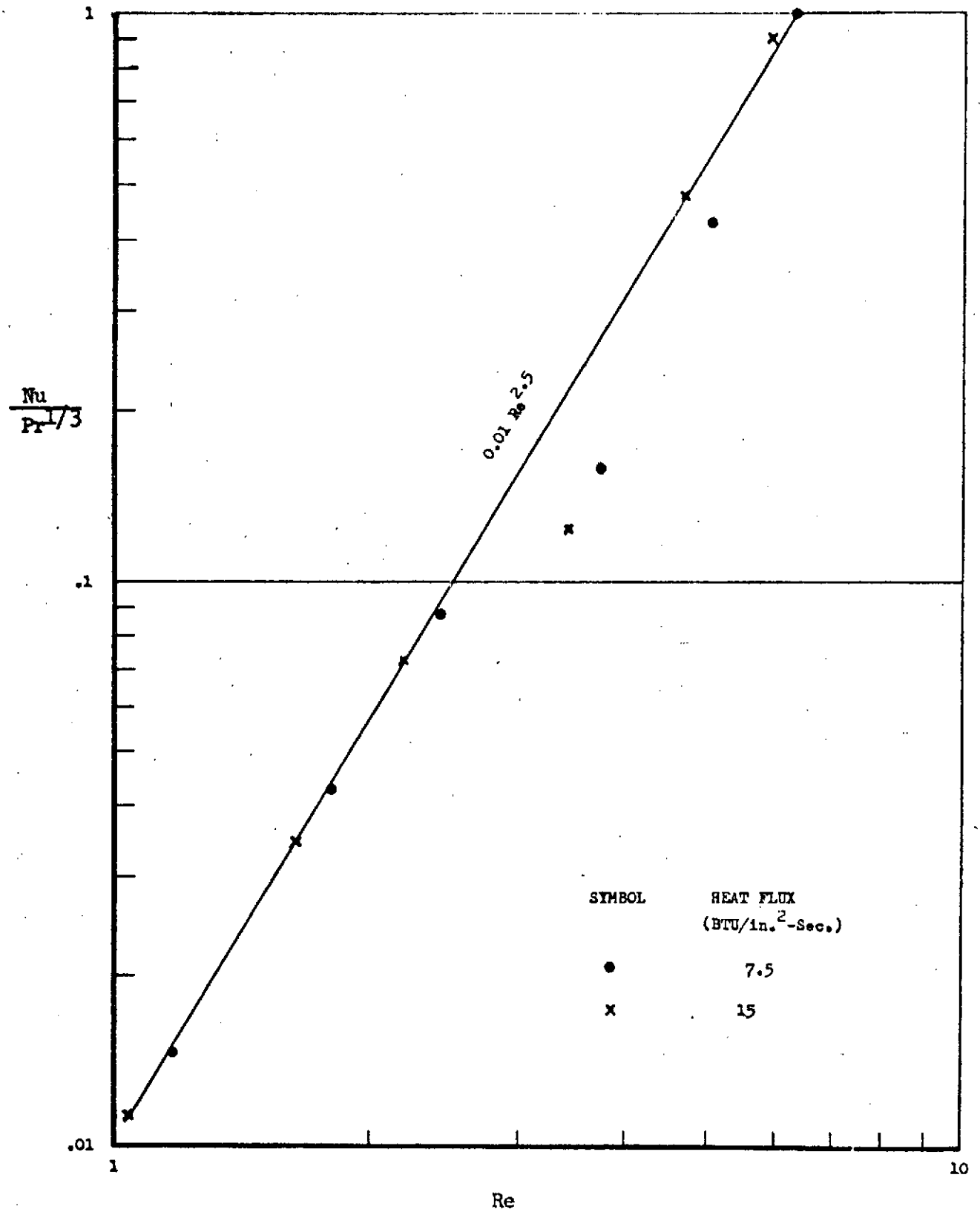

FIG. 18 NUSSELT, PRANDTL VS. REYNOLDS NUMBER CORRELATION FOR RIGIMESH MATERIAL R-10-3/8 (.116 POROSITY)

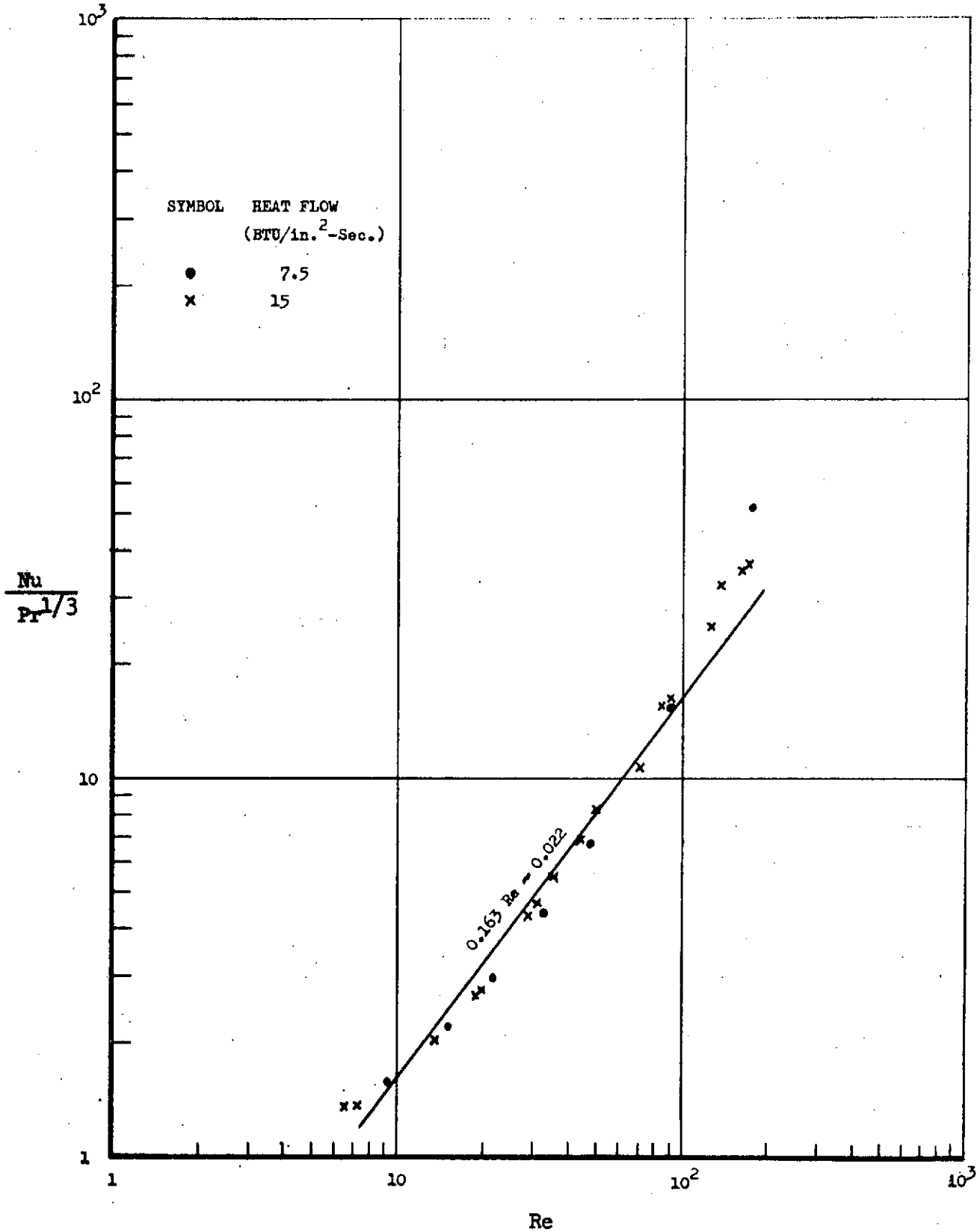

FIG. 19 NUSSELT, PRANDTL VS. REYNOLDS NUMBER CORRELATION FOR RIGIMESH MATERIAL R-20-1/2 (.187 POROSITY)

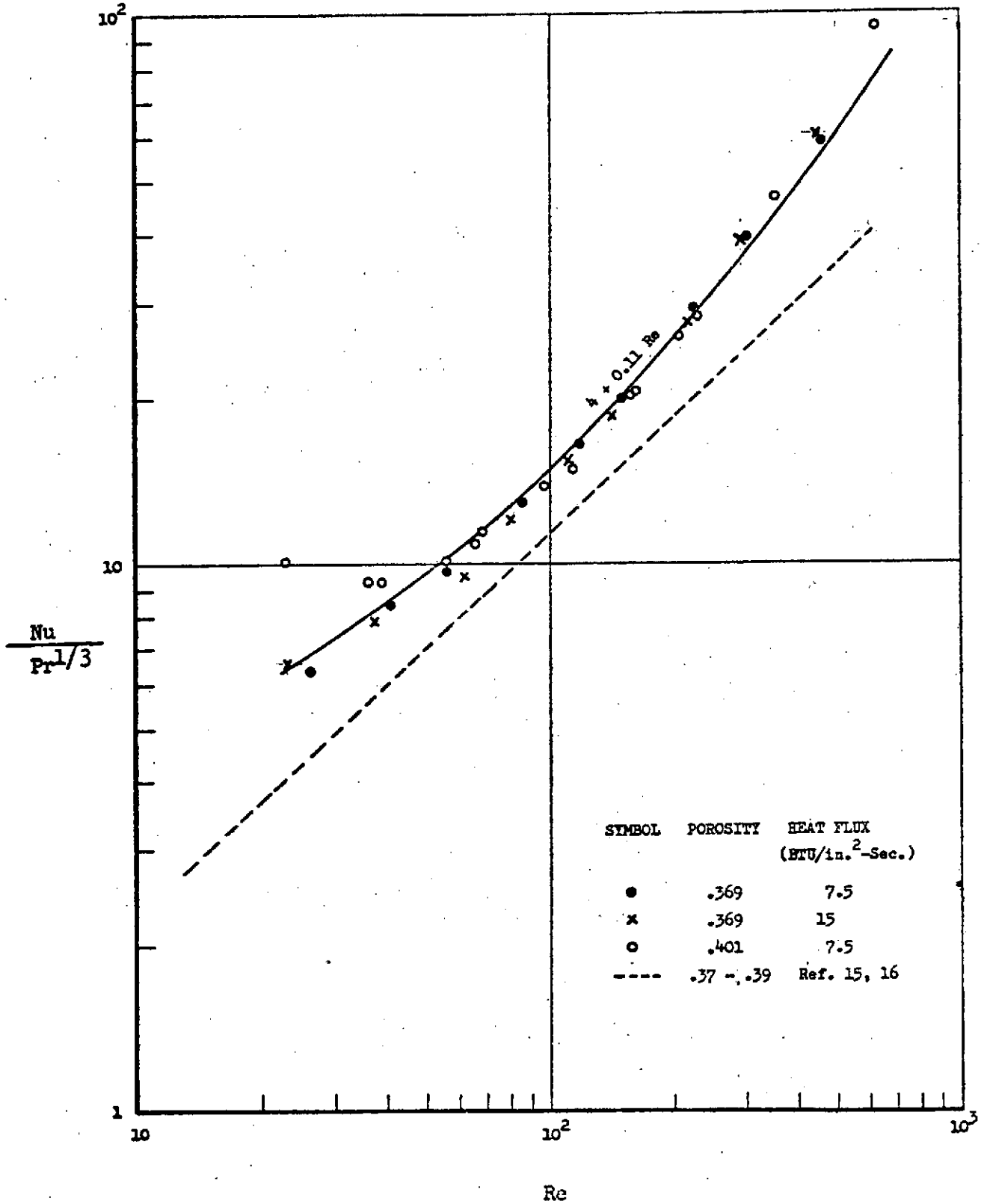

FIG. 20 NUSSELT, PRANDTL VS. REYNOLDS NUMBER CORRELATION FOR RIGIMESH MATERIAL R-40-3/8 (POROSITY .369); R-40-1/2 (POROSITY .401)

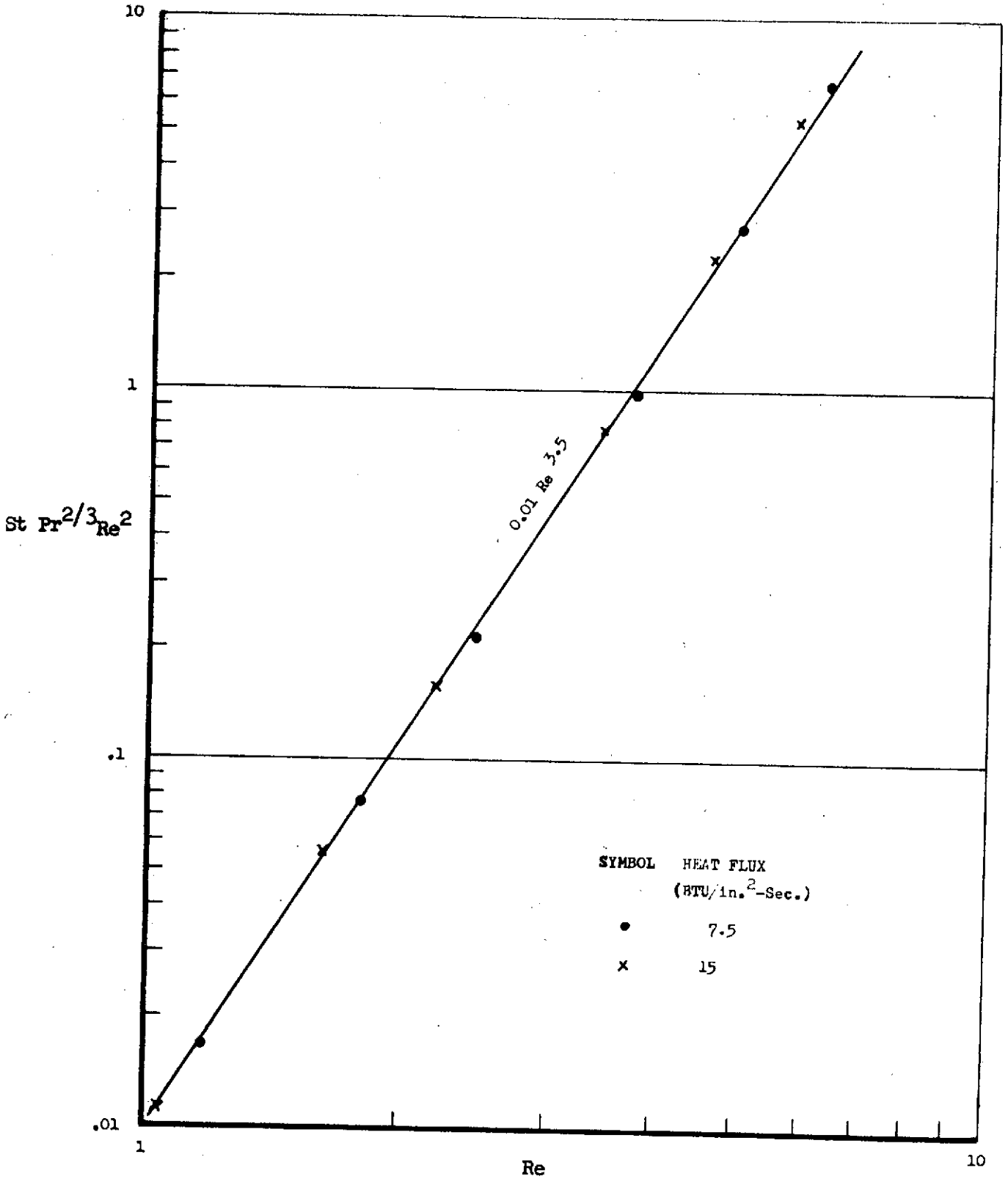

FIG. 21 STANTON, PRANDTL, REYNOLDS VS. REYNOLDS NUMBER CORRELATION FOR RIGIMESH MATERIAL R-10-3/8 (.116 POROSITY)

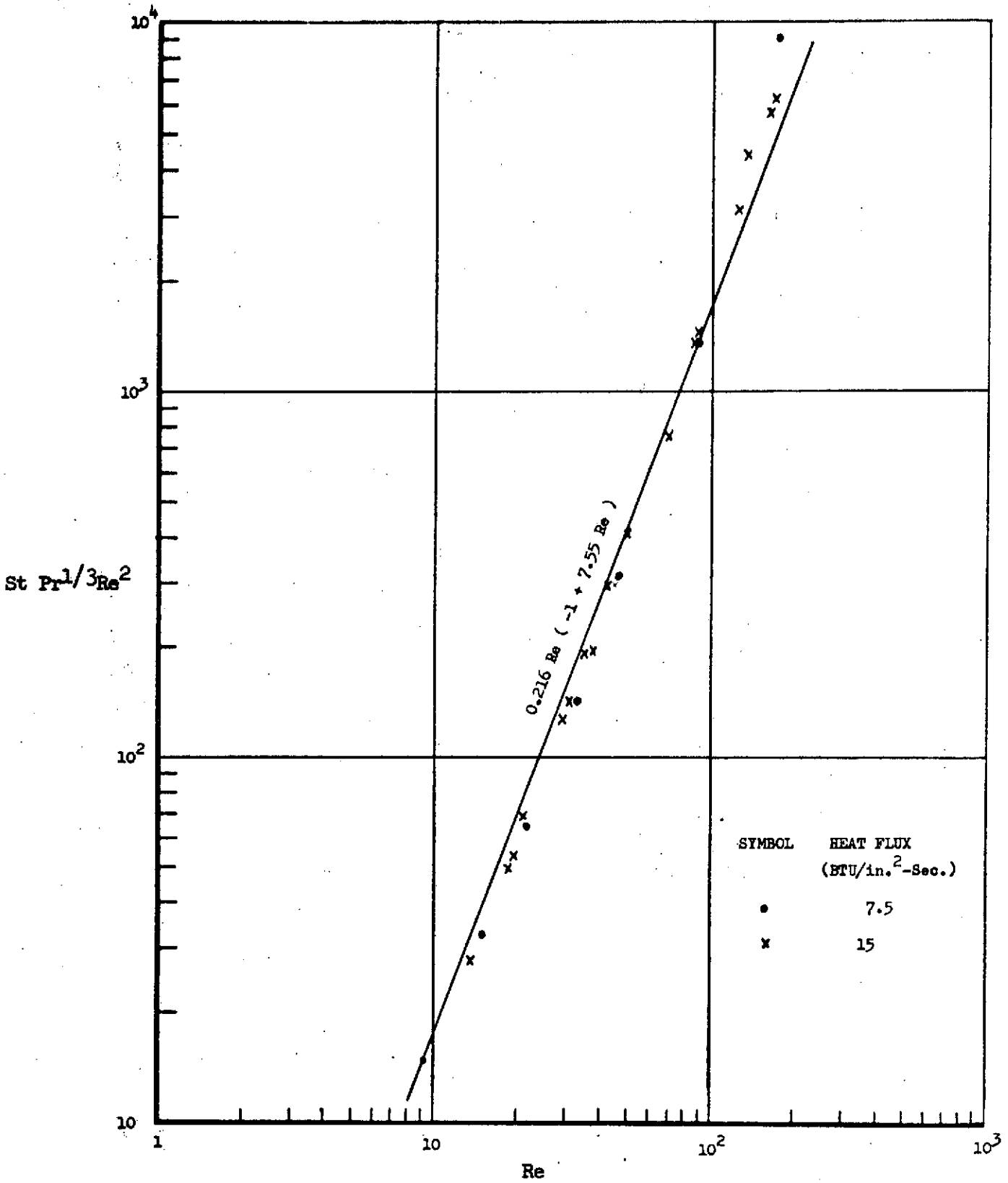

FIG. 22 STANTON, PRANDTL, REYNOLDS VS. REYNOLDS NUMBER CORRELATION FOR RIGIMESH MATERIAL R-20-1/2 (.187 POROSITY)

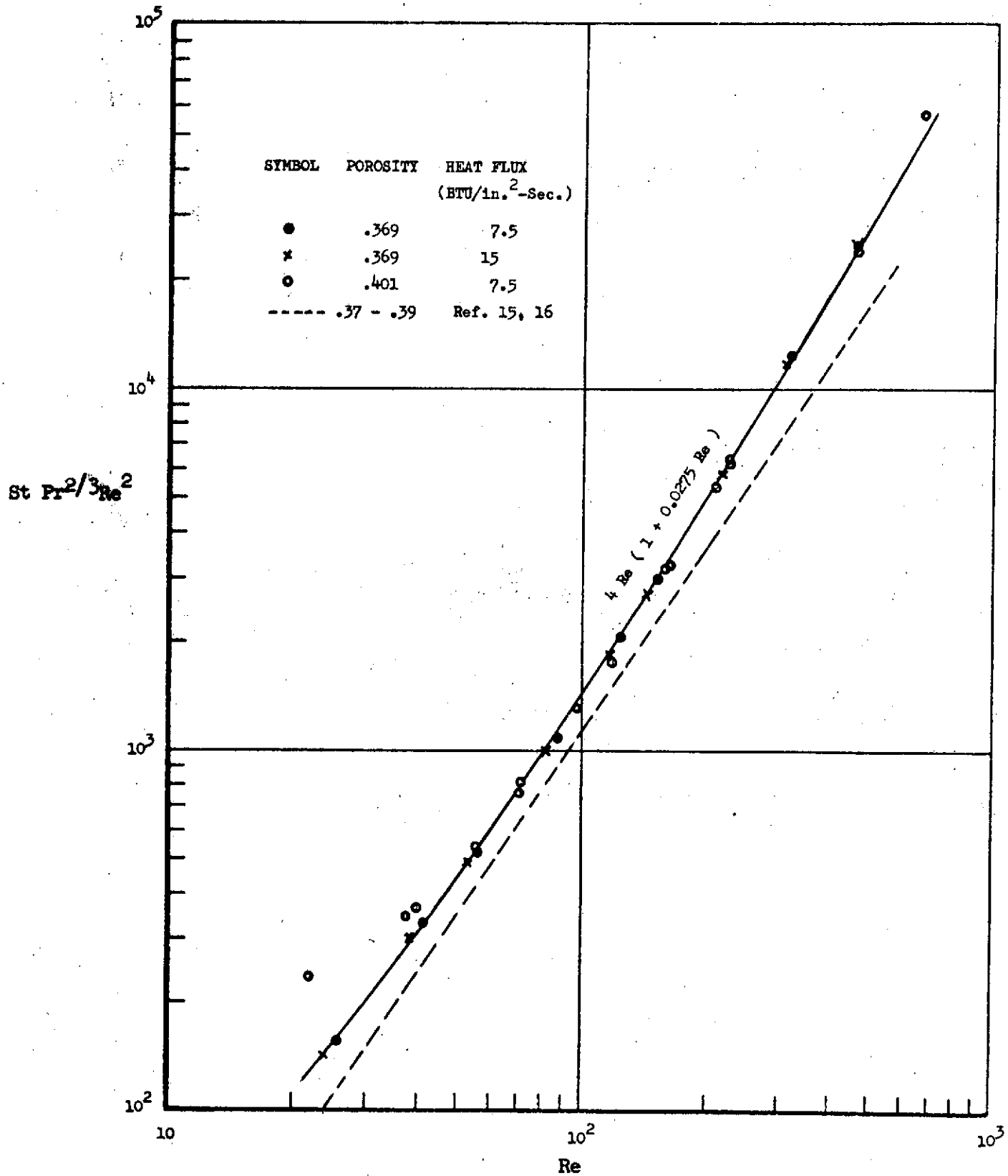

FIG. 23 STANTON, PRANDTL, REYNOLDS VS. REYNOLDS NUMBER CORRELATION FOR RIGIMESH MATERIAL R-40-3/8 (.369 POROSITY); R-40-1/2 (.401 POROSITY)

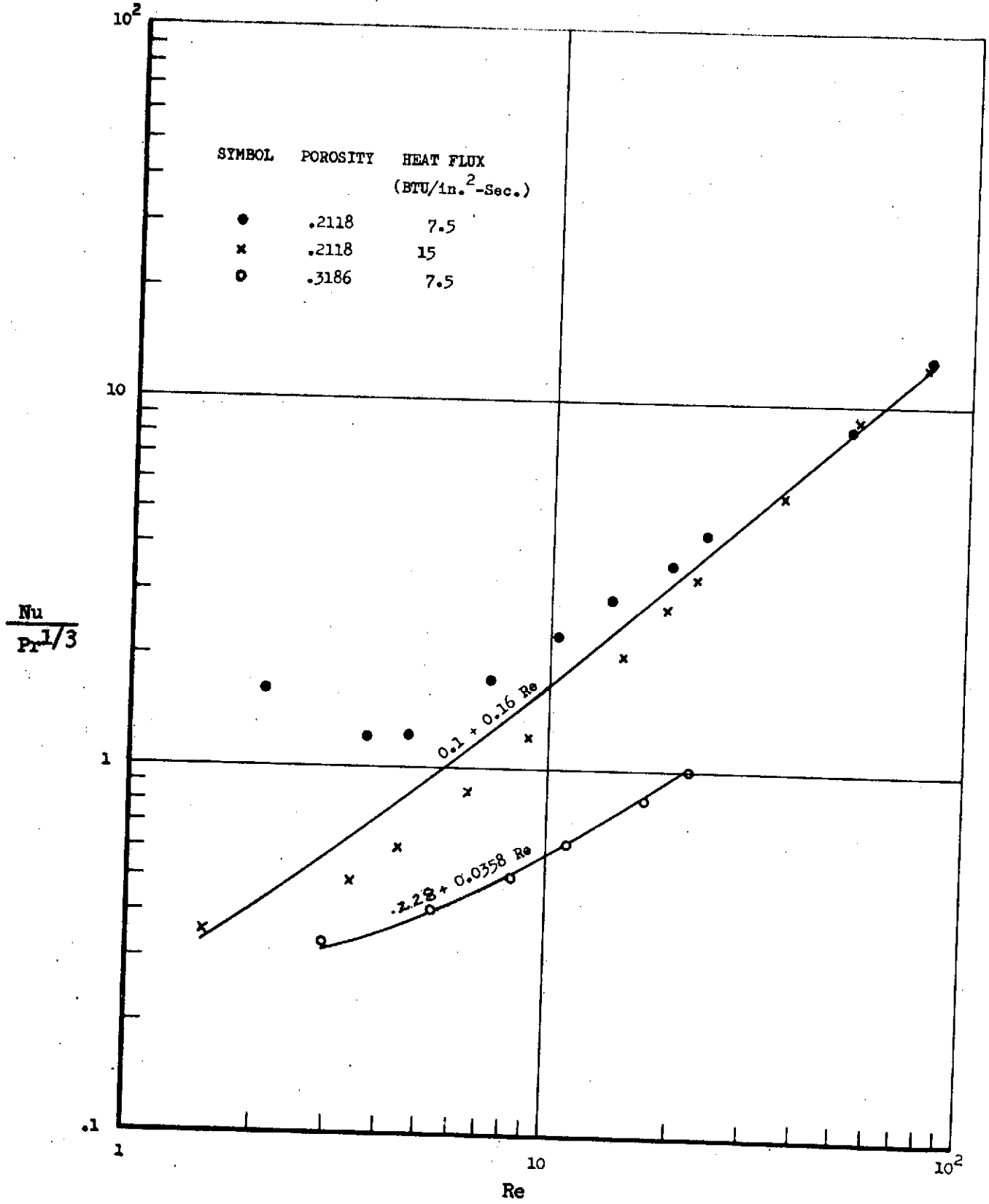

FIG. 24 NUSSELT, PRANDTL VS. REYNOLDS NUMBER CORRELATION FOR SINTERED STAINLESS STEEL POWDERS

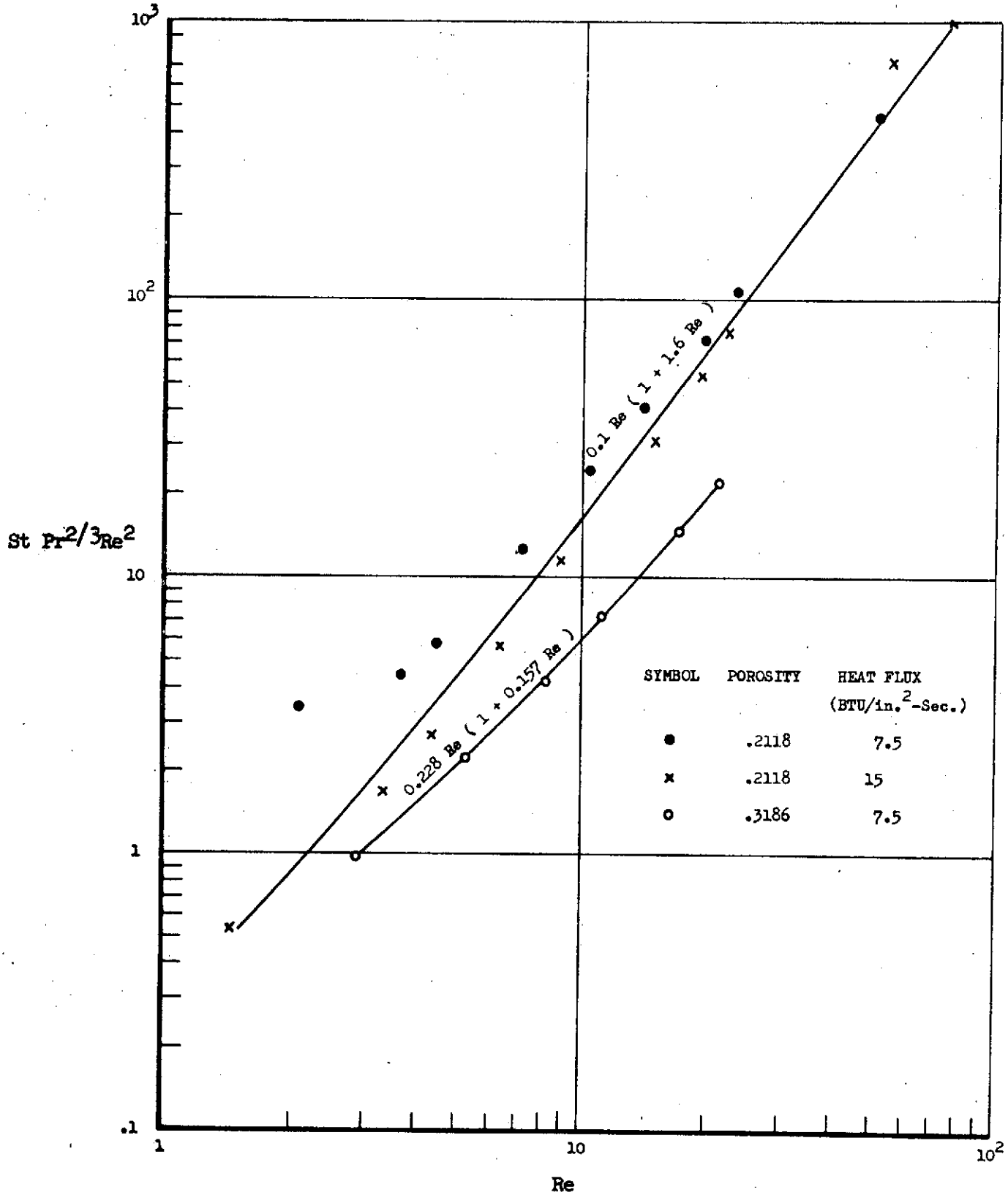

FIG. 25 STANTON, PRANDTL, REYNOLDS VS. REYNOLDS NUMBER CORRELATION FOR SINTERED STAINLESS STEEL POWDERS

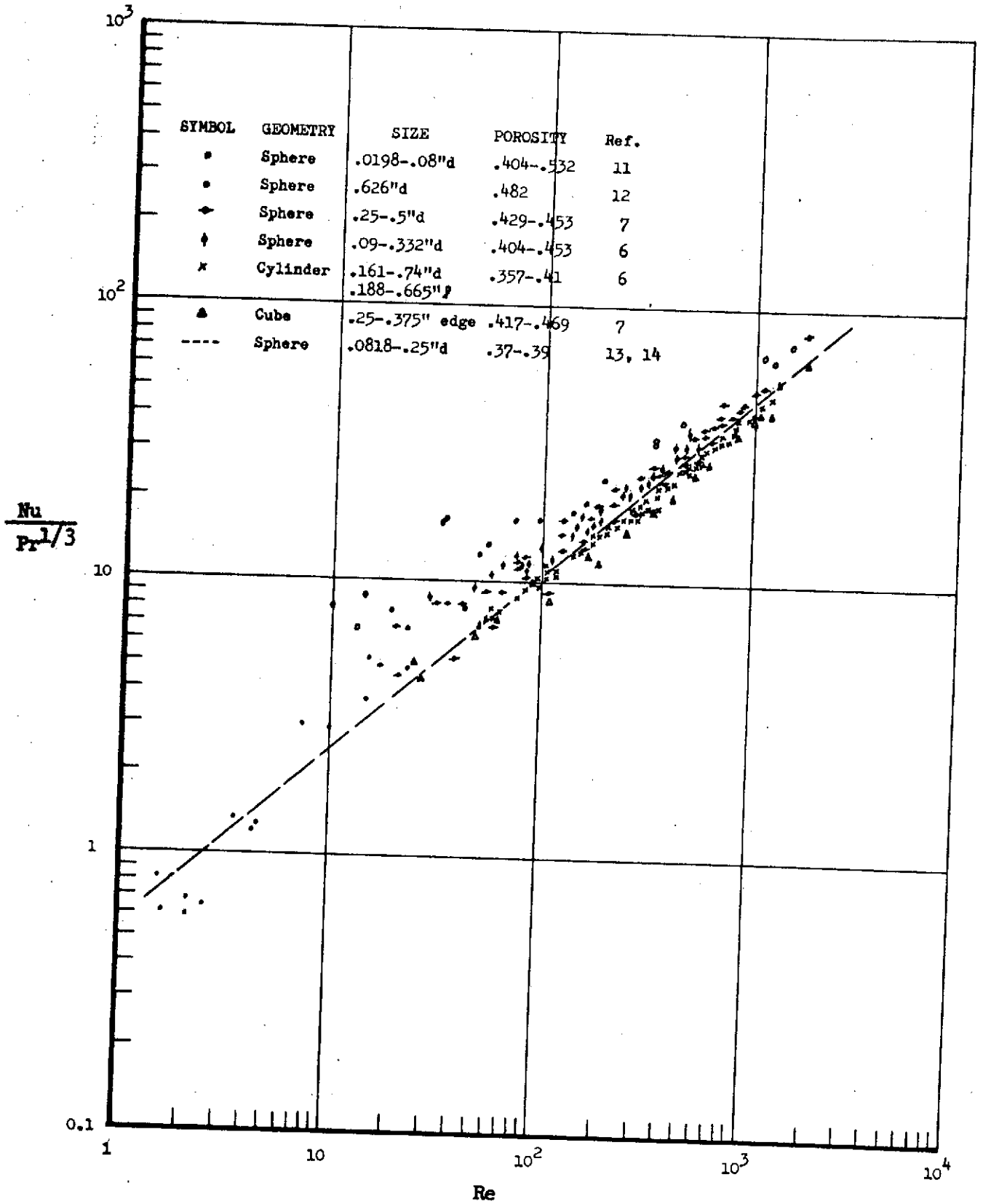

FIG. 26 NUSSELT, PRANDTL VS. REYNOLDS NUMBER CORRELATION FOR A PACKED BED OF PARTICLES

TABLES

TABLE I Test Specimens

Description	Porosity	Thickness (in.)	Mean Diameter (in.)	Hydraulic Diameter (ft.)	Surface Area per Unit Volume (ft^{-1})
R-10-1/4	.093	.216	.683	7.77×10^{-5}	4160
R-10-3/8	.095	.377	.754	8.05×10^{-5}	4110
R-10-1/2	.087	.455	.716	6.94×10^{-5}	4330
R-20-1/4	.194	.267	.675	2.67×10^{-4}	2720
R-20-3/8	.198	.383	.754	2.76×10^{-4}	2690
R-20-1/2	.187	.515	.707	2.51×10^{-4}	2780
R-40-1/4	.401	.244	.687	9.05×10^{-4}	1780
R-40-3/8	.399	.407	.738	8.97×10^{-4}	1790
R-40-1/2	.408	.492	.670	9.31×10^{-4}	1770
S-10-1/4	.1123	.25	.734	5.71×10^{-5}	7860
S-10-1/2	.0962	.500	.735	4.78×10^{-5}	8058
S-20-1/4	.206	.248	.734	1.15×10^{-4}	7136
S-20-3/8	.2118	.369	.730	1.19×10^{-4}	7102
S-20-1/2	.22	.495	.73	1.25×10^{-4}	7060
S-30-3/8	.3186	.375	.732	1.92×10^{-4}	6652
C-10-1/4	.1101	.247	.749	3.83×10^{-5}	11500
C-10-1/2	.1038	.484	.750	3.58×10^{-5}	11600
C-20-1/2	.1988	.501	.740	7.6×10^{-5}	10500
C-30-1/2	.3004	.494	.703	1.23×10^{-4}	9790

APPENDIX A

TABLE A-1 Low Temperature Isothermal Test Specimen R-10-1/4

ξ = .093 L = .216" A = 2.54×10^{-3} ft^2

S = 4160 ft^{-1} d = 7.77×10^{-5} n = 3.9

p_{up} (psi)	p_{dn} (psi)	p (psi)	T (R)	m (lb/ft^2-sec.)	Re	fRe^2	RE/
815	517	292	532	.403	5.24	1.42×10^6	8.07×10^4
926	512	406	539	.507	6.54	2.1×10^6	1.01×10^5
1094	507	578	539	.620	7.99	3.32×10^6	1.23×10^5
1295	507	778	540	.804	10.4	5.03×10^6	1.59×10^5
1513	503	1000	540	.969	12.5	7.22×10^6	1.92×10^5
1517	504	1002	540	.972	12.5	7.25×10^6	1.93×10^5
1388	507	870	540	.874	11.3	5.9×10^6	1.73×10^5
1131	491	630	540	.681	8.77	3.66×10^6	1.35×10^5
946	516	418	538	.516	6.66	2.19×10^6	1.03×10^5
711	495	204	538	.318	4.11	8.85×10^5	6.32×10^4
709	493	204	538	.316	4.09	8.82×10^5	6.29×10^4
753	480	272	526	.374	4.9	1.27×10^6	7.54×10^4
928	482	446	527	.528	6.9	2.37×10^6	1.06×10^5
1104	492	612	527	.665	8.7	3.7×10^6	1.34×10^5
1311	487	824	527	.831	10.9	5.6×10^6	1.67×10^5
1510	492	1018	527	.988	12.9	7.7×10^6	1.99×10^5

TABLE A-1 Continued

Specimen R-10-1/4

p_{up} (psi)	p_{dn} (psi)	p (psi)	T (R)	m (lb/ft^2-sec.)	Re	fRe^2	Re/
1320	478	840	523	.850	11.2	5.81×10^6	1.72×10^5
1101	490	610	518	.677	8.96	3.81×10^6	1.38×10^5
892	484	408	517	.508	6.72	2.22×10^6	1.04×10^5
696	479	220	514	.329	4.37	1.02×10^6	6.73×10^4

TABLE A-2 Low Temperature Isothermal Test Specimen R-10-1/2

ξ = .087 L = .455" A = 2.8×10^{-3} ft^2

S = 4330 ft^{-1} d = 6.94×10^{-5} ft n = 3.9

P_{up} (psi)	P_{dn} (psi)	p (psi)	T (R)	m (lb/ft^2-sec.)	Re	fRe^2	Re/
815	582	240	540	.229	2.65	4.42×10^5	5.16×10^4
684	463	228	537	.206	2.38	3.44×10^5	4.64×10^4
997	498	507	537	.375	4.33	9.98×10^5	8.44×10^4
1160	495	676	537	.467	5.39	1.47×10^6	1.05×10^5
1454	505	962	537	.621	7.18	2.48×10^6	1.4×10^5
1511	499	1024	537	.654	7.55	2.71×10^6	1.47×10^5
1320	493	835	537	.557	6.43	1.99×10^6	1.25×10^5
1172	490	691	537	.482	5.57	1.51×10^6	1.08×10^5
919	485	440	537	.344	3.97	8.16×10^5	7.74×10^4
881	492	395	537	.316	3.65	7.16×10^5	7.12×10^4
735	495	246	537	.225	2.6	3.98×10^5	5.07×10^4
709	503	212	537	.203	2.35	3.36×10^5	4.58×10^4
687	501	181	516	.179	2.12	3.1×10^5	4.14×10^4
925	503	415	516	.325	3.85	8.54×10^5	7.51×10^4
1092	495	588	516	.425	5.03	1.34×10^6	9.81×10^4
1316	501	807	516	.543	6.43	2.11×10^6	1.25×10^5

TABLE A-2 Continued — Specimen R-10-1/2

P_{up} (psi)	P_{dn} (psi)	p (psi)	T (R)	m (lb/ft^2-sec.)	Re	fRe^2	Re/
1526	503	1014	516	.657	7.78	2.96×10^6	1.52×10^5
1332	500	823	517	.557	6.59	2.16×10^6	1.28×10^5
1112	499	608	517	.439	5.20	1.41×10^6	1.01×10^5
905	506	391	517	.316	3.74	7.93×10^5	7.3×10^4
724	498	223	517	.207	2.45	3.92×10^5	4.78×10^4
316	31	290	532	.108	1.25	1.36×10^5	2.43×10^4
465	32	440	532	.170	1.98	2.95×10^5	3.86×10^4
566	32	542	531	.212	2.47	4.38×10^5	4.82×10^4
659	32	636	531	.252	2.93	5.94×10^5	5.71×10^4
851	32	832	531	.340	3.95	9.9×10^5	7.71×10^4
1024	33	1008	531	.418	4.86	1.44×10^6	9.48×10^4
739	31	720	531	.289	3.36	7.48×10^5	6.55×10^4
594	31	572	531	.224	2.61	4.94×10^5	5.09×10^4
398	28	375	531	.141	1.64	2.16×10^5	3.2×10^4
1038	31	1024	538	.428	4.94	1.43×10^6	9.64×10^4
770	29	752	538	.305	3.52	7.88×10^5	6.87×10^4

TABLE A-2 Continued — Specimen R-10-1/2

p_{up} (psi)	p_{dn} (psi)	p (psi)	T (R)	m ($\frac{lb}{ft^2-sec.}$)	Re	fRe^2	$R^{E/}$
630	29	610	540	.241	2.77	5.24×10^5	5.40×10^4
557	29	535	540	.21	2.41	4.09×10^5	4.70×10^4
352	28	327	539	.121	1.39	1.63×10^5	2.72×10^4

TABLE A-3 Low Temperature Isothermal Test Specimen R-20-1/4

ξ = .194 L = .267 A = 2.48×10^{-3} ft^2

S = 2720 ft^{-1} d = 2.67×10^{-4} ft n = 3.9

P_{up} (psi)	P_{dn} (psi)	p (psi)	T (R)	m ($\frac{lb}{ft^2-sec.}$)	Re	fRe^2	Re/
209	18.5	190	526	2.14	96.6	2.4×10^6	1.34×10^5
429	21	407	526	4.66	210	1.02×10^7	2.91×10^5
482	21.9	460	526	5.20	234	1.28×10^7	3.25×10^5
635	24.6	610	526	6.94	312	2.22×10^7	4.34×10^5
782	28.3	754	526	8.83	397	3.39×10^7	5.52×10^5
849	28.9	820	526	9.35	421	3.99×10^7	5.85×10^5
1044	33.3	1011	526	11.7	528	6.04×10^7	7.34×10^5
851	28.9	822	527	9.31	419	4×10^7	5.82×10^5
727	26.3	697	527	7.82	352	2.91×10^7	4.89×10^5
422	20.9	399	527	4.52	203	9.77×10^6	2.82×10^5
55	28	23	541	.364	16	9.74×10^4	2.22×10^4
63	29	31	542	.48	21.1	1.46×10^5	2.94×10^4
69	29	37	545	.504	22.3	1.87×10^5	3.09×10^4
112	29	80	546	1.04	246.2	5.81×10^5	6.42×10^4
123	29	91	548	1.12	49.3	7.13×10^5	6.86×10^4
332	31	298	548	3.72	164	5.56×10^6	2.28×10^5

C2

TABLE A-3 Continued

Specimen R-20-1/4

P_{up} (psi)	P_{dn} (psi)	p (psi)	T (R)	m (lb/ft^2-sec.)	Re	fRe^2	Re/
375	31	341	548	4.72	208	7.11×10^6	2.89×10^5
371	31	337	549	3.76	166	6.95×10^6	2.3×10^5
525	32	489	549	5.64	249	1.4×10^7	3.47×10^5
925	33	884	546	10.6	466	4.35×10^7	6.48×10^5
532	32	496	546	5.68	251	1.44×10^7	3.49×10^5
226	33	192	523	2.24	96	2.8×10^6	1.33×10^5
395	56	342	526	4.36	196	8.56×10^6	2.73×10^5
485	68	416	531	4.96	222	1.25×10^7	3.08×10^5
712	102	612	535	7.5	334	2.66×10^7	4.64×10^5
1184	170	1012	546	13.1	574	6.99×10^7	7.98×10^5
927	132	794	546	9.92	436	4.29×10^7	6.06×10^5
813	116	696	546	8.55	376	3.3×10^7	5.22×10^5
696	99	596	541	7.2	318	2.47×10^7	4.43×10^5
419	60	360	542	4.28	189	8.94×10^6	2.63×10^5
253	38	216	539	2.42	107	3.3×10^6	1.49×10^5
150	25	124	525	1.42	64	1.2×10^6	8.89×10^4

TABLE A-3 Continued — Specimen R-20-1/4

p_{up} (psi)	p_{dn} (psi)	p (psi)	T (R)	m (lb/ft^2-sec.)	Re	fRe^2	Re/
225	35	190	526	2.25	101	2.74×10^6	1.4×10^5
396	58	340	531	4.38	196	8.45×10^6	2.72×10^5
1810	1054	753	527	17.0	767	1.19×10^8	1.06×10^6
1812	1054	755	526	17.2	777	1.2×10^8	1.08×10^6
1423	1024	392	523	10.5	475	5.39×10^7	6.61×10^5
1424	1025	390	523	10.5	475	5.37×10^7	6.61×10^5
1210	1002	202	523	7.18	324	2.51×10^7	4.51×10^5
1210	1003	200	523	7.18	324	2.49×10^7	4.51×10^5
1497	999	488	523	11.7	530	6.85×10^7	7.37×10^5
628	401	223	524	4.84	218	1.28×10^7	3.03×10^5
629	401	226	524	4.84	218	1.3×10^7	3.03×10^5
802	402	396	524	7.06	318	2.67×10^7	4.42×10^5
796	400	394	524	6.96	314	2.64×10^7	4.36×10^5
985	478	504	524	8.81	397	4.13×10^7	5.52×10^5
974	472	500	524	8.7	392	4.06×10^7	5.45×10^5
1148	557	589	524	10.5	474	5.62×10^7	6.59×10^5

TABLE A-3 Continued — Specimen R-20-1/4

P_{up} (psi)	P_{dn} (psi)	p (psi)	T (R)	m (lb/ft^2-sec.)	Re	fRe^2	Re/
1135	552	579	524	10.3	465	5.47×10^7	6.46×10^5
989	241	745	522	9.94	450	5.18×10^7	6.25×10^5
977	238	737	522	9.83	444	5.06×10^7	6.18×10^5
787	190	595	522	7.69	348	3.28×10^7	4.84×10^5
778	188	590	522	7.66	346	3.22×10^7	4.81×10^5
506	122	383	521	4.89	221	1.36×10^7	3.08×10^5
504	122	380	521	4.79	217	1.35×10^7	3.01×10^5
403	97	303	521	3.74	169	8.59×10^6	2.36×10^5
405	97	306	521	3.83	173	8.71×10^6	2.41×10^5

TABLE A-4 Low Temperature Isothermal Test Specimen R-20-1/2

ξ = .187 L = .515 A = 2.73×10^{-3} ft^2.

S = 2780 ft^{-1} d = 2.51×10^{-4} n = 3.9

P_{up} (psi)	P_{dn} (psi)	p (psi)	T (R)	m ($\frac{lb}{ft^2\text{-sec.}}$)	Re	fRe^2	Re/
203	29	184	500	1.2	52.4	1.19×10^6	8.12×10^4
411	54	373	500	2.66	116	4.83×10^6	1.8×10^6
602	79	546	500	3.96	173	1.04×10^7	2.68×10^5
812	108	741	500	5.72	251	1.9×10^7	3.89×10^5
807	108	734	500	5.23	228	1.87×10^7	3.54×10^5
1008	134	917	500	6.71	293	2.92×10^7	4.54×10^5
906	120	825	500	5.97	261	2.36×10^7	4.04×10^5
699	93	636	500	4.75	207	1.4×10^7	3.21×10^5
501	65	452	500	3.22	141	7.13×10^6	2.18×10^5
294	39	265	500	1.81	79	2.46×10^6	1.22×10^5
207	29	185	500	1.27	55.4	1.22×10^6	8.58×10^4
710	516	194	513	2.95	127	6.25×10^6	1.96×10^5
916	530	386	513	4.69	202	1.47×10^7	3.12×10^5
1091	550	538	514	6.00	258	2.32×10^7	3.99×10^5
962	491	470	513	5.24	225	1.8×10^7	3.49×10^5
814	504	308	513	3.96	170	1.07×10^7	2.64×10^5

TABLE A-4 Continued — Specimen R-20-1/2

P_{up} (psi)	P_{dn} (psi)	p (psi)	T (R)	m ($\frac{lb}{ft^2-sec.}$)	Re	fRe^2	Re/
718	495	222	513	3.17	136	7.08×10^6	2.1×10^5
376	32	345	543	2.26	93.2	3.22×10^6	1.44×10^5
481	32	454	554	2.94	122	5.23×10^6	1.88×10^5
652	33	628	553	4.03	166	9.66×10^6	2.57×10^5
783	34	760	553	4.91	202	1.39×10^7	3.14×10^5
653	31	632	553	4.06	168	9.7×10^6	2.6×10^5
373	30	347	553	2.22	91.5	3.14×10^6	1.42×10^5
198	26	174	500	4.54	100	3.92×10^6	1.55×10^5
405	54	367	500	9.93	220	1.65×10^7	3.41×10^5
406	53	367	500	10	221	1.66×10^7	3.43×10^5
608	80	551	500	15	333	3.72×10^7	5.16×10^5
806	107	732	500	21.1	467	6.54×10^7	7.24×10^5
1097	147	992	500	28	621	1.21×10^8	9.62×10^5
989	132	899	500	24.9	551	9.84×10^7	8.54×10^5
777	103	705	500	20.4	451	6.07×10^7	6.99×10^5
555	72	505	500	14	309	3.1×10^7	4.79×10^5

TABLE A-4 Continued Specimen R-20-1/2

p_{up} (psi)	p_{dn} (psi)	p (psi)	T (R)	m (lb/ft^2-sec.)	Re	fRe^2	RE/
327	42	293	500	7.8	173	1.07×10^7	2.68×10^5

TABLE A-5 Low Temperature Isothermal Test Specimen S-10-1/4

ξ = .1123 L = .25 A = 2.94×10^{-3} ft^2

S = 7860 ft^{-1} d = 5.71×10^{-5} n = 3.8

P_{up} (psi)	P_{dn} (psi)	p (psi)	T (R)	m (lb/ft^2-sec.)	Re	fRe^2	RE/
283	45	236	522	.190	1.84	7.39×10^4	1.18×10^4
572	114	458	526	.482	4.65	2.95×10^5	2.97×10^4
803	172	628	527	.730	7.01	5.72×10^5	4.48×10^4
1060	242	816	527	1.02	9.83	9.94×10^5	6.28×10^4
1413	337	1074	527	1.43	13.8	1.76×10^6	8.78×10^4
1148	266	880	523	1.13	10.9	1.18×10^6	6.96×10^4
1028	234	792	523	.992	9.59	9.5×10^4	6.12×10^4
760	165	594	522	.699	6.78	5.24×10^5	4.33×10^4
493	97	398	520	.411	3.99	2.26×10^5	2.54×10^4
406	75	330	520	.317	3.07	1.53×10^5	1.96×10^4
274	44	251	517	.189	1.84	7.13×10^4	1.18×10^4
563	114	495	522	.486	4.69	2.93×10^5	2.99×10^4
1057	239	897	526	1.02	9.85	9.99×10^5	6.29×10^4
350	92	258	520	.241	2.34	1.11×10^5	1.49×10^4
581	179	406	522	.462	4.48	2.97×10^5	2.86×10^4
888	298	594	526	.767	7.42	6.64×10^5	4.74×10^4

TABLE A-5 Continued

Specimen S-10-1/4

P_{up} (psi)	P_{dn} (psi)	p (psi)	T (R)	m ($\frac{lb}{ft^2-sec.}$)	Re	fRe^2	Re/
1241	439	806	528	1.13	10.9	1.27×10^6	6.96×10^4
1562	571	996	522	1.48	14.3	2.05×10^6	9.13×10^4
1232	439	796	517	1.13	11.1	1.31×10^6	7.09×10^4
888	300	592	516	.774	7.57	6.95×10^5	4.83×10^4
581	180	404	515	.465	4.56	3.05×10^5	2.91×10^4
273	67	206	513	.173	1.7	7.04×10^4	1.08×10^4

TABLE A-6 Low Temperature Isothermal Test Specimen S-20-1/4

ξ = .206 L = .248" A = 2.94×10^{-3} FT^2

S = 7136 ft^{-1} d = 1.15×10^{-4} n = 3.8

P_{up} (psi)	P_{dn} (psi)	p (psi)	T (R)	m (lb/ft^2-sec.)	Re	fRe^2	Re/
245	21	224	528	1.08	21	2.5×10^5	2.05×10^4
451	40	414	530	2.28	44.2	8.46×10^5	4.32×10^4
658	59	602	531	3.72	71.8	1.79×10^6	7.03×10^4
913	83	832	533	5.12	98.5	3.41×10^6	9.64×10^4
1093	102	998	535	6.49	125	4.85×10^6	1.22×10^5
858	78	786	533	4.8	92.4	3.03×10^6	9.04×10^4
687	62	628	533	3.49	67.2	1.94×10^6	6.58×10^4
456	41	420	533	2.38	46	8.6×10^5	4.5×10^4
233	19	214	531	1.04	20.2	2.24×10^5	1.98×10^4
163	17	146	530	.612	11.8	1.09×10^5	1.16×10^4
440	39	404	527	2.07	40.2	8.18×10^5	3.93×10^4
672	60	614	527	3.53	68.6	1.9×10^6	6.72×10^4
944	86	860	530	4.95	95.6	3.68×10^6	9.36×10^4
1117	103	1016	527	6.18	120	5.24×10^6	1.17×10^5
933	85	850	526	4.88	94.8	3.68×10^6	9.28×10^4
728	66	666	524	3.59	70	2.26×10^6	6.85×10^4

TABLE A-6 Continued — Specimen S-20-1/4

p_{up} (psi)	p_{dn} (psi)	p (psi)	T (R)	m ($\frac{lb}{ft^2}$-sec.)	Re	fRe^2	Re/
264	107	160	523	1.05	20.4	2.56×10^5	1.99×10^4
441	194	250	526	1.91	37.1	6.72×10^5	3.63×10^4
766	357	412	529	3.47	67.2	1.93×10^6	6.58×10^4
1134	545	594	533	5.41	104	4.11×10^6	1.02×10^5
1299	630	674	534	6.26	120	5.31×10^6	1.18×10^5
1085	519	570	533	5.17	99.7	3.75×10^6	9.76×10^4
856	402	458	533	3.98	76.7	2.37×10^6	7.5×10^4
577	262	318	531	2.58	49.8	1.11×10^6	4.88×10^4
351	150	206	529	1.47	28.5	4.32×10^5	2.78×10^4
191	74	120	527	.711	13.8	1.34×10^5	1.35×10^4

TABLE A-7 Low Temperature Isothermal Test Specimen S-20-1/2

ξ = .22 L = .495" A = 2.91×10^{-3} ft^2

S = 7060 ft^{-1} d = 1.25×10^{-4} n = 3.8

P_{up} (psi)	P_{dn} (psi)	p (psi)	T (R)	m (lb/ft^2-sec.)	Re	fRe^2	Re/
739	518	222	523	2.30	48.6	7.11×10^5	3.94×10^4
918	505	414	523	3.55	75	1.5×10^6	6.08×10^4
1104	506	602	525	4.70	98.8	2.45×10^6	8.01×10^4
1320	569	752	526	5.82	122	3.57×10^6	9.92×10^4
1610	706	904	526	7.21	151	5.28×10^6	1.23×10^5
1468	641	830	524	6.53	137	4.44×10^6	1.11×10^5
1195	515	682	524	5.23	110	2.96×10^6	8.92×10^4
741	342	398	517	3.00	63.7	1.13×10^6	5.16×10^4
510	202	308	517	2.05	43.5	5.73×10^5	3.53×10^4
324	120	206	515	1.20	25.6	2.41×10^5	2.08×10^4
380	131	248	562	1.34	27	2.74×10^5	2.19×10^4
514	186	328	562	1.90	38.4	4.96×10^5	3.12×10^4
731	277	452	562	2.86	57.5	9.85×10^5	4.66×10^4
984	388	594	557	4.0	81	1.8×10^6	6.56×10^4
1287	523	762	553	5.22	110	3.1×10^6	8.91×10^4
1449	600	846	549	6.18	126	3.96×10^6	1.02×10^5

TABLE A-7 Continued

Specimen S-20-1/2

P_{up} (psi)	P_{dn} (psi)	p (psi)	T (R)	m (lb/ft^2-sec.)	Re	fRe^2	Re/
1574	659	912	544	6.79	140	4.73×10^6	1.13×10^5
1370	570	796	540	5.86	121	3.67×10^6	9.82×10^4
1104	451	652	535	4.65	96.5	2.45×10^6	7.82×10^4
769	304	462	533	3.13	65.2	1.21×10^6	5.29×10^4
206	64	140	531	.662	13.8	9.3×10^4	1.12×10^4
196	63	134	524	.615	13	8.82×10^4	1.05×10^4
389	145	246	527	1.42	29.7	3.28×10^5	2.41×10^4
671	268	404	532	2.67	55.7	9.3×10^5	4.52×10^4
1048	438	612	537	4.4	91.3	2.18×10^6	7.4×10^4
1218	516	706	537	5.19	108	2.94×10^6	8.78×10^4
1410	604	810	539	6.08	126	3.86×10^6	1.02×10^5
1626	704	926	539	7.08	146	5.12×10^6	1.19×10^5
1402	600	806	532	6.05	126	3.96×10^6	1.02×10^5
1027	428	600	530	4.3	89.7	2.16×10^6	7.27×10^4
709	286	428	528	2.84	59.2	1.06×10^6	4.8×10^4
308	110	200	526	1.08	22.7	2.1×10^5	1.84×10^4

TABLE A-8 Low Temperature Isothermal Test Specimen C-10-1/4

ξ = .110 L = .247" A = 3.06×10^{-3} ft^2

S = 11500 ft^{-1} d = 3.83×10^{-5} ft n = 2.8

P_{up} (psi)	P_{dn} (psi)	p (psi)	T (R)	m ($\frac{lb}{ft^2-sec.}$)	Re	fRe^2	Re/
770	496	274	527	.728	4.7	1.01×10^5	3.14×10^3
960	524	436	527	1.04	6.73	1.88×10^5	4.49×10^3
1080	527	552	526	1.26	8.1	2.58×10^5	5.41×10^3
1295	467	828	528	1.66	10.7	4.22×10^5	7.15×10^3
1498	523	974	528	1.96	12.6	5.67×10^5	8.45×10^3
1322	471	850	526	1.70	11	4.43×10^5	7.35×10^3
1071	423	646	525	1.31	8.45	2.83×10^5	5.64×10^3
891	445	444	522	1.01	6.56	1.76×10^5	4.38×10^3
674	432	242	518	.644	4.19	8.05×10^4	2.8×10^3
764	519	238	570	.506	3.18	7.4×10^4	2.12×10^3
956	520	432	562	.778	4.82	1.6×10^5	3.22×10^3
1116	495	616	557	1.01	6.32	2.54×10^5	4.22×10^3
1325	531	790	553	1.26	7.86	3.81×10^5	5.25×10^3
1596	641	954	553	1.55	9.68	5.55×10^5	6.47×10^3
1248	490	756	549	1.19	7.46	3.47×10^5	4.98×10^3
1016	445	566	544	.925	5.83	2.23×10^5	3.9×10^3

TABLE A-8 Continued Specimen C-10-1/4

P_{up} (psi)	P_{dn} (psi)	p (psi)	T (R)	m (lb/ft^2-sec.)	Re	fRe^2	Re/
899	497	396	542	.740	4.68	1.5×10^5	3.13×10^3
777	499	272	542	.561	3.54	9.46×10^4	2.37×10^3
282	62	220	526	.248	1.6	2.21×10^4	1.07×10^3
525	130	396	531	.523	3.36	7.4×10^4	2.25×10^3
839	223	616	532	.892	5.71	1.85×10^5	3.82×10^3
994	269	726	531	1.08	6.92	2.62×10^5	4.63×10^3
1252	346	906	532	1.40	8.93	4.1×10^5	5.97×10^3
1045	286	760	526	1.16	7.46	2.94×10^5	4.98×10^3
880	239	644	524	.958	6.2	2.12×10^5	4.14×10^3
615	160	458	522	.637	4.13	1.05×10^5	2.76×10^3
314	73	240	516	.297	1.94	2.82×10^4	1.3×10^3

TABLE A-9 Low Temperature Isothermal Test Specimen C-10-1/2

ξ = .104 L = .484 A = 3.07×10^{-3} FT^2

S = 11600 ft^{-1} d = 3.58×10^{-5} ft n = 2.8

P_{up} (psi)	P_{dn} (psi)	p (psi)	T (R)	m (lb/ft^2-sec.)	Re	fRe^2	Re/
730	477	258	527	.355	2.13	4×10^4	1.64×10^3
946	519	434	531	.534	3.19	7.99×10^4	2.46×10^2
1139	526	620	531	.705	4.22	1.3×10^5	3.26×10^3
1275	503	780	531	.839	5.02	1.74×10^5	3.88×10^3
1498	504	1002	532	1.028	6.16	2.51×10^5	4.76×10^3
1387	485	906	529	.946	5.68	2.15×10^5	4.39×10^3
1191	485	710	523	.780	4.72	1.55×10^5	3.65×10^3
1004	500	512	522	.608	3.68	1×10^5	2.84×10^3
922	490	440	522	.534	3.23	8.11×10^4	2.5×10^3
721	539	192	522	.296	1.79	3.16×10^4	1.38×10^3
775	511	268	595	.301	1.67	3.34×10^4	1.29×10^3
948	506	444	593	.442	2.47	6.32×10^4	1.91×10^3
1125	506	624	591	.576	3.23	1×10^5	2.5×10^3
1342	500	846	588	.745	4.18	1.55×10^5	3.23×10^3
1551	518	1032	584	.894	5.04	2.16×10^5	3.89×10^3
1398	491	910	579	.797	4.52	1.78×10^5	3.49×10^3

TABLE A-9 Continued Specimen C-10-1/2

P_{up} (psi)	P_{dn} (psi)	p (psi)	T (R)	m (lb/ft^2-sec.)	Re	fRe^2	Re/
1164	483	684	573	.633	3.60	1.19×10^5	2.78×10^3
1002	488	520	571	.509	2.91	8.26×10^4	2.25×10^3
781	495	288	570	.328	1.88	3.92×10^4	1.45×10^3

TABLE A-10 Low Temperature Isothermal Test Specimen C-20-1/2

ϵ = .199 L = .501 A = 2.99×10^{-3} FT²

S = 10500 d = 7.6×10^{-5} n = 2.8

P_{up} (psi)	P_{dn} (psi)	p (psi)	T (R)	m (lb/ft²-sec.)	Re	fRe^2	Re/
209	18	192	526	.578	7.4	2.68×10^4	1.27×10^3
314	23	292	527	1.06	13.5	6.06×10^4	2.32×10^3
210	18	192	527	.581	7.44	2.69×10^4	1.27×10^3
323	23	300	527	1.09	13.9	6.37×10^4	2.38×10^3
412	28	386	530	1.42	18.2	1.04×10^5	3.11×10^3
646	43	606	532	2.45	31.1	2.54×10^5	5.33×10^3
864	58	808	533	3.53	44.9	4.51×10^5	7.7×10^3
942	64	882	533	3.96	50.3	5.38×10^5	8.62×10^3
1051	71	984	535	4.16	52.7	6.65×10^5	9.04×10^3
877	58	822	535	3.61	45.7	4.63×10^5	7.83×10^3
639	43	600	533	2.42	30.7	2.48×10^4	5.27×10^3
423	29	396	532	1.48	18.9	1.09×10^5	3.24×10^3
214	18	198	531	.602	7.66	2.79×10^4	1.31×10^3
309	98	210	522	.933	12	5.18×10^4	2.06×10^3
472	163	308	524	1.55	19.9	1.22×10^5	3.41×10^3
628	226	402	526	2.16	27.7	2.12×10^5	4.75×10^3

TABLE A-10 Continued — Specimen C-20-1/2

p_{up} (psi)	p_{dn} (psi)	p (psi)	T (R)	m (lb/ft^2-sec.)	Re	fRe^2	Re/
901	337	560	531	3.24	41.3	4.24×10^5	7.08×10^3
1117	428	686	531	4.11	52.3	6.49×10^5	8.96×10^3
1318	513	802	531	4.95	63	8.98×10^5	1.08×10^4
1506	594	910	531	5.72	72.8	1.17×10^6	1.25×10^4
1428	562	864	531	5.38	68.6	1.05×10^6	1.18×10^4
1184	458	724	529	4.38	55.9	7.28×10^5	9.38×10^3
894	337	556	526	3.22	41.3	4.24×10^5	7.08×10^3
429	147	280	522	1.39	17.9	1.01×10^5	3.07×10^3
206	61	142	518	.578	7.48	2.39×10^4	1.28×10^3

TABLE A-11 Elevated Temperature Isothermal Test Specimen R-10-1/4

ξ = .093 L = .216 in. A = 2.54×10^{-3} FT^2 S = 4160 ft^{-1} D = 7.77×10^{-5} ft. n = 3.9

P_{up} (psi)	P_{du} (psi)	p (psi)	T_1* (R)	T_2 (R)	T_3 (R)	T_4 (R)	T (lb/ft^2-sec.)	m	Re	fRe^2	Re/
1507	475	1024	1565	1528	1532	1532	1539	.504	3.2	6.18×10^5	4.92×10^4
1331	495	828	1676	1596	1612	1608	1623	.415	2.54	4.07×10^5	3.91×10^4
1095	491	594	1661	1630	1632	1637	1640	.315	1.92	2.47×10^5	2.95×10^4
916	507	400	1640	1598	1603	1620	1615	.238	1.46	1.55×10^5	2.25×10^4
717	498	210	1587	1544	1561	1566	1564	.152	.957	7.49×10^4	1.47×10^4
1453	476	970	1182	1197	1192	1189	1190	.576	4.36	1.05×10^5	6.72×10^4
1280	487	786	1204	1159	1155	1148	1166	.495	3.8	8.16×10^5	5.85×10^4
1096	519	570	1176	1155	1153	1147	1158	.392	3.02	5.5×10^5	4.66×10^4
924	505	410	1151	1139	1140	1141	1143	.311	2.42	3.62×10^5	3.72×10^4
704	506	190	1126	1126	1126	1139	1129	.181	1.42	1.46×10^5	2.19×10^4

*See Figure 6 for thermocouple locations

TABLE A-12 Elevated Temperature Isothermal Test Specimen R-20-1/4

$\mathcal{F}$ = .194 L = .267 A = 2.48×10^{-3} ft^2 S = 2720 ft^{-1} d = 2.67×10^{-4} n = 3.9

p_{up} (psi)	p_{du} (psi)	p (psi)	T_1* (R)	T_2 (R)	T_3 (R)	T_4 (R)	T (R)	m (lb/ft^2-sec.)	Re	fRe^2	Re/	
267	29	238	2023	1832	1817	1716	1848	1.29	24.9	2.05×10^5	3.47×10^4	
438	48	392	2004	1900	1895	1790	1900	2.24	42.6	5.21×10^5	5.92×10^4	
631	71	562	2107	1996	1996	1882	1994	3.33	61.2	9.66×10^5	8.51×10^4	
801	94	714	2092	2018	1996	1904	2001	4.48	82.2	1.55×10^6	1.14×10^5	
1097	134	964	2032	1992	1957	1882	1965	6.01	112	3.0×10^6	1.55×10^5	
888	105	784	2067	2018	1987	1900	1993	4.62	85.2	1.91×10^6	1.18×10^5	
769	90	680	2005	1965	1921	1848	1935	4.35	81.6	1.53×10^6	1.13×10^5	
539	61	478	2001	1935	1904	1817	1913	2.83	53.4	7.72×10^5	7.43×10^4	
330	36	292	2067	1921	1900	1800	1861	1.62	31.2	3.06×10^5	4.34×10^4	

*See Figure 6 for thermocouple locations

TABLE A-13 Elevated Temperature Isothermal Test Specimen R-20-1/2

ϵ = .187 L = .515 in. A = 2.73×10^{-3} S = 2780 ft^{-1} d = 2.51×10^{-4} n = 3.9

p_{up} (psi)	p_{du} (psi)	p (psi)	T_1* (R)	T_2 (R)	T_3 (R)	T_4 (R)	T (R)	m (lb/ft^2-sec.)	Re	fRe^2	Re/
242	20	222	1783	1533	1557	1568	1610	.656	13	1.04×10^5	2.02×10^4
371	25	346	1875	1635	1667	1587	1691	1.12	21.6	2.19×10^5	3.34×10^4
433	29	406	2041	1710	1740	1657	1830	1.24	22.6	2.5×10^5	3.51×10^4
658	42	614	2042	1858	1882	1796	1895	1.93	34.5	5.3×10^5	5.35×10^4
856	56	798	2104	1972	1984	1946	2002	2.57	44.3	7.91×10^5	6.87×10^4
1049	72	976	2060	1988	1996	2011	2014	3.3	56.7	1.17×10^6	8.79×10^4
935	63	868	2040	1950	1962	1991	1986	2.87	49.8	9.59×10^5	7.71×10^4
745	49	694	2076	1952	1962	1961	1988	2.2	38.1	6.09×10^5	5.91×10^4
521	34	486	2056	1884	1905	1864	1927	1.48	26.1	3.2×10^5	4.05×10^4
336	22	312	1977	1783	1800	1861	1855	.916	16.6	1.44×10^5	2.57×10^4
270	20	248	1888	1651	1676	1703	1729	2.93	13.8	1.09×10^5	2.14×10^4

*See Figure 6 for thermocouple locations

TABLE A-14 Elevated Temperature Isothermal Test Specimen S-10-1/4

ξ = .1123 L - .25 in. A = 2.94×10^{-3} ft^2 S = 7860 ft^{-1} D = 5.71×10^{-5} n = 3.8

p_{up} (psi)	p_{du} (psi)	p (psi)	T_1* (R)	T_2 (R)	T_3 (R)	T_4 (R)	T (R)	m (lb/ft^2-sec.)	Re	fRe^2	Re/
519	49	513	1995	1745	1742	1740	1806	.125	.524	1.38×10^4	3.35×10^3
712	81	689	2004	1771	1755	1740	1818	.208	.872	2.56×10^4	5.57×10^3
963	128	913	2027	1782	1772	1761	1836	.327	1.36	4.53×10^4	8.67×10^3
1075	150	1009	2016	1796	1785	1774	1843	.384	1.59	5.63×10^4	1.02×10^4
921	120	871	1987	1768	1760	1753	1817	.309	1.29	4.25×10^4	8.25×10^3
848	104	809	2040	1808	1792	1778	1855	.268	1.1	3.44×10^4	7.05×10^3
655	70	637	1996	1751	1753	1754	1814	.180	.755	2.17×10^4	4.82×10^3
533	49	523	1966	1693	1685	1678	1756	.131	.563	1.54×10^4	3.59×10^3

*See Figure 6 for thermocouple locations

TABLE A-15 Elevated Temperature Isothermal Test Specimen S-20-1/4

ξ = .206 L = .248 in. A = 2.94x10^{-3} ft^2 S = 7.36 ft^{-1} d = 1.15x10^{-4} ft. n = 3.8

P_{up} (psi)	P_{du} (psi)	p (psi)	T_1* (R)	T_2 (R)	T_3 (R)	T_4 (R)	T (R)	m (lb/ft^2-sec.)	Re	fRe^2	Re/
295	18	278	1886	1704	1693	1650	1733	.456	3.96	2.24x10^4	3.88x10^3
672	39	638	2038	1851	1817	1738	1861	1.46	12.1	9.91x10^4	1.18x10^4
887	55	836	1967	1858	1817	1769	1853	2.08	17.4	1.74x10^5	1.7x10^4
1061	69	994	1977	1900	1853	1803	1883	2.64	21.8	2.39x10^5	2.13x10^4
842	51	794	1957	1864	1818	1755	1849	1.94	16.2	1.58x10^5	1.58x10^4
647	37	610	1916	1810	1751	1691	1792	1.38	11.7	9.95x10^4	1.14x10^4
458	25	434	1923	1759	1716	1633	1758	.901	7.77	5.24x10^4	7.6x10^3
273	17	256	1903	1708	1691	1649	1738	.394	3.43	1.9x10^4	3.36x10^3

*See Figure 6 for thermocouple locations

TABLE A-16 Elevated Temperature Isothermal Test Specimen S-20-1/2

ξ = .22 L = .495 in. A = 2.91x10^{-3} ft^2 S = 7060 ft^{-1} d = 1.25x10^{-4}ft n = 3.8

p_{up} (psi)	p_{du} (psi)	p (psi)	T_1* (R)	T_2 (R)	T_3 (R)	T_4 (R)	T (R)	m (lb/ft^2-sec.)	Re	fRe^2	Re/	
738	489	252	2076	1848	1835	1822	1895	.891	7.9	3.86x10^4	6.4x10^3	
941	496	448	1992	1848	1848	1852	1885	1.47	13.1	8.11x10^4	1.06x10^4	
1142	501	642	2076	1904	1904	1902	1947	2.0	17.4	1.24x10^5	1.41x10^4	
1315	508	806	2058	1926	1935	1948	1967	2.43	21.2	1.68x10^4	1.72x10^4	
1500	508	992	1974	1904	1904	1905	1922	3.0	26.4	2.4x10^5	2.14x10^4	
1340	489	854	2027	1908	1908	1908	1938	2.58	22.5	1.85x10^5	1.82x10^4	
1097	499	598	2081	1921	1926	1930	1965	1.88	16.3	1.09x10^5	1.32x10^4	
916	502	414	2054	1891	1986	1882	1928	1.36	11.9	7.05x10^4	9.65x10^3	
703	494	208	1948	1807	1796	1783	1834	.78	7.07	3.35x10^4	5.73x10^3	

*See Figure 6 for thermocouple locations

TABLE A-17 Elevated Temperature Isothermal Test Specimen C-10-1/4

ξ = .110 L = .247 in. A = 3.06x10^{-3} ft^2 S = 11500 ft^{-1} d = 3.83 x 10^{-5} ft. n = 2.8

P_{up} (psi)	P_{du} (psi)	p (psi)	T_1* (R)	T_2 (R)	T_3 (R)	T_4 (R)	T (R)	m (lb/ft^2-sec.)	Re	fRe^2	Re/	
744	525	216	1689	1431	1426	1422	1492	.270	.863	6.88x10^3	5.77x10^2	
904	472	432	1663	1435	1430	1425	1488	.447	1.43	1.5x10^4	9.56x10^2	
1102	497	606	1721	1470	1462	1455	1527	.594	1.87	2.3x10^4	1.25x10^3	
1319	496	822	1652	1470	1467	1463	1513	.761	2.41	3.63x10^4	1.61x10^3	
1492	494	998	1682	1511	1505	1498	1549	.854	2.65	4.55x10^4	1.77x10^3	
1305	511	792	1640	1502	1498	1494	1534	.687	2.15	3.39x10^4	1.43x10^3	
1086	504	580	1659	1486	1483	1479	1527	.522	1.64	2.2x10^4	1.1x10^3	
907	503	400	1680	1482	1461	1443	1516	.380	1.20	1.36x10^4	8.03x10^2	
697	481	214	1642	1439	1440	1440	1490	.227	.725	6.36x10^3	4.84x10^2	

*See Figure 6 for thermocouple locations

TABLE A-18 Elevated Temperature Isothermal Test Specimen C-10-1/2

$\mathcal{F}$ = .104 L = .484 in. A = ~~3.07x10^{-3} ft^2~~ S = 11600 ft^{-1} d = 3.58 x 10^{-5} ft n = 2.8

p_{up} (psi)	p_{du} (psi)	p (psi)	T_1* (R)	T_2 (R)	T_3 (R)	T_4 (R)	T (R)	m (lb/ft^2-sec.)	Re	fRe^2	Re/
729	503	230	1647	1480	1479	1478	1521	.122	.358	3.0x10^3	2.77x10^2
924	518	414	1659	1490	1490	1490	1533	.200	.386	6.2x10^3	4.52x10^2
1101	477	630	1661	1518	1518	1518	1534	.279	.815	1.03x10^4	6.3x10^2
1303	503	806	1684	1520	1521	1521	1562	.369	1.07	1.45x10^4	8.26x10^2
1487	516	978	1659	1525	1525	1525	1559	.447	1.29	1.96x10^4	9.96x10^2
1117	487	636	1727	1531	1529	1528	1579	.279	.799	9.89x10^3	6.17x10^2
896	518	382	1693	1536	1535	1535	1575	.181	.52	5.28x10^3	4.02x10^2
735	504	236	1633	1504	1504	1504	1536	.120	.35	3.03x10^3	2.7x10^2

*See Figure 6 for thermocouple locations

TABLE A-19 Elevated Temperature Isothermal Test Specimen C-20-1/2

ξ = .199 L = .501 in. A = 2.99×10^{-3} ft^2 S = 10500 ft^{-1} d = 7.6×10^{-5} ft n = 2.8

P_{up} (psi)	P_{du} (psi)	p (psi)	T_1* (R)	T_2 (R)	T_3 (R)	T_4 (R)	T (R)	m (lb/ft^2-sec.)	Re	fRe^2	Re/
276	17	260	1667	1414	1418	1422	1479	.326	2.08	4.2×10^3	3.56×10^2
427	20	408	1667	1367	1376	1380	1447	.664	4.29	1.05×10^4	7.35×10^2
599	26	572	1809	1469	1477	1485	1560	1.04	6.42	1.73×10^4	1.1×10^3
800	37	764	1766	1544	1553	1561	1605	1.46	8.8	2.89×10^4	1.51×10^3
1036	49	988	1787	1587	1595	1603	1643	1.99	11.8	4.59×10^4	2.02×10^3
849	39	810	1774	1582	1592	1597	1640	1.54	9.16	3.1×10^4	1.57×10^3
537	23	512	1753	1519	1523	1532	1581	.922	5.61	1.34×10^4	9.61×10^2
435	20	414	1697	1469	1477	1481	1531	.656	4.09	9.5×10^3	7.01×10^2
261	16	244	1625	1414	1418	1422	1470	.30	1.92	3.76×10^3	3.29×10^2

*See Figure 6 for thermocouple locations

APPENDIX B

TABLE B-1 Heat Transfer Test Specimen R-10-3/8

ξ = .095 L = .377 in. A = 3.10×10^{-3} ft^2 S = 4110 ft^{-1} d = 8.05×10^{-5} n = 3.9

q (BTU/in²-sec)	p_{up} (psi)	p_{dn} (psi)	Δp (psi)	$T_{f\infty}$ * (R)	T_{mo} (R)	T_{mw} (R)	T_{fw} (R)	T_{LM} (R)	$\dot{m}$ (lb/ft²-sec.)	Re	fRe^2	$Re/[f(1-f)]^n$
0	786	37	746	520					.465	6.35	1.48×10^6	9.1×10^4
0	703	36	665	518					.41	5.61	1.2×10^6	8.03×10^4
0	633	36	595	517					.361	4.95	9.72×10^5	7.09×10^4
0	550	35	513	517					.308	4.23	7.34×10^5	6.05×10^4
0	459	33	424	517					.247	3.39	5.1×10^5	4.85×10^4
0	387	32	353	518					.201	2.75	3.58×10^5	3.94×10^4
0	319	31	286	519					.161	2.2	2.42×10^5	3.15×10^4
0	233	30	202	520					.109	1.5	1.28×10^5	2.13×10^4
0	212	29	181	520					.0974	1.33	1.04×10^5	1.9×10^4
7.5	830	39	789	517	530	731	649	580	.477	6.08	1.3×10^6	8.7×10^4
7.5	538	35	501	517	531	806	683	596	.279	3.48	5.08×10^5	4.99×10^4

*See Figure 6 for thermocouple locations

TABLE B-1 Heat Transfer Test Specimen R-10-3/8

ε = .095 L = .377 in. A = 3.10×10^{-3} ft^2 S = 4110 ft^{-1} d = 8.05×10^{-5} n = 3.9

q (BTU/in²-sec)	p_{up} (psi)	p_{dn} (psi)	Δp (psi)	$T_{f\infty}$ * (R)	T_{mo} (R)	T_{mw} (R)	T_{fw} (R)	T_{LM} (R)	$\dot{m}$ (lb/ft²-sec.)	Re	fRe^2	$Re/[\varepsilon(1-\varepsilon)]^n$
7.5	538	35	501	517	531	808	690	599	.279	3.47	5.01×10^5	4.97×10^4
7.5	539	35	502	520	531	810	691	601	.279	3.46	4.99×10^5	4.96×10^4
7.5	540	35	503	518	532	812	694	602	.281	3.48	5.01×10^5	4.99×10^4
7.5	360	32	326	520	532	935	740	624	.161	1.95	2.03×10^5	2.79×10^4
7.5	295	31	262	521	532	1050	741	624	.117	1.42	1.36×10^5	2.03×10^4
7.5	266	30	234	522	533	1153	754	631	.0964	1.11	9.88×10^4	1.59×10^4
7.5	336	32	302	522	533	997	761	634	.144	1.73	1.72×10^5	2.48×10^4
7.5	432	34	396	520	533	893	716	613	.206	2.53	3.06×10^5	3.62×10^4
7.5	460	34	423	520	533	873	709	610	.224	2.76	3.49×10^5	3.94×10^4
15	847	40	805	520	533	928	793	647	.471	5.58	1.04×10^6	7.99×10^4
15	622	36	583	520	533	1043	860	676	.313	3.6	5.1×10^5	5.15×10^4

*See Figure 6 for thermocouple locations

TABLE B-1 Heat Transfer Test Specimen R-10-3/8

ξ = .095 L = .377 in. A = 3.10×10^{-3} ft^2 S = 4110 ft^{-1} d = 8.05×10^{-5} n = 3.9

q (BTU/in^2-sec)	p_{up} (psi)	p_{dn} (psi)	Δp (psi)	$T_{f\infty}$ (R)	T_{mo} (R)	T_{mw} (R)	T_{fw} (R)	T_{LM} (R)	$\dot{m}$ (lb/ft^2-sec.)	Re	fRe^2	$Re/[f(1-\xi)]^n$
15	498	34	462	522	534	1193	902	695	.223	2.52	3.06×10^5	3.61×10^4
15	413	32	378	522	534	1448	1006	738	.163	1.77	1.83×10^5	2.54×10^4
15	360	31	326	524	534	1689	1077	768	.123	1.30	1.25×10^5	1.86×10^4
15	334	30	301	526	535	1840	1061	762	.101	1.07	1.1×10^5	1.53×10^4
15	365	32	331	526	535	1625	1077	769	.130	1.37	1.28×10^5	1.96×10^4
15	433	33	398	524	535	1368	996	735	.182	1.98	2.02×10^5	2.84×10^4
15	392	31	362	522	535	1674	1012	740	.15	1.63	1.64×10^5	2.33×10^4
15	350	29	321	524	535	1889	1116	783	.111	1.16	1.15×10^5	1.66×10^4
15	388	31	358	524	535	1661	1039	752	.146	1.56	1.54×10^5	2.24×10^4
15	444	32	412	524	535	1468	967	723	.190	2.09	2.22×10^5	3×10^4
15	490	32	458	523	536	1346	939	711	.224	2.49	2.82×10^5	3.56×10^4

*See Figure 6 for thermocouple locations

TABLE B-1 Heat Transfer Test Specimen R-10-3/8

ϕ = .095 L = .377 in. A = 3.10×10^{-3} ft^2 S = 4110 ft^{-1} d = 8.05×10^{-5} n = 3.9

q (BTU/in²-sec)	P_{up} (psi)	P_{dn} (psi)	Δp (psi)	$T_{f\infty}$* (R)	T_{mo} (R)	T_{mw} (R)	T_{fw} (R)	T_{LM} (R)	$\dot{m}$ (lb/ft²-sec.)	Re	fRe^2	$Re/[f(1-\phi)]^n$
0	292	32	259	520	535				.141	1.94	2.07×10^5	2.78×10^4
0	206	30	175	522	534				.0193	1.25	9.94×10^4	1.79×10^4
0	830	40	788	518	534				.487	6.7	1.7×10^6	9.59×10^4
0	710	38	670	517	533				.410	5.65	1.25×10^6	8.09×10^4
0	473	35	436	517	533				.253	3.48	5.5×10^5	4.99×10^4
0	532	33	500	520	530				.290	3.98	6.95×10^5	5.71×10^4

*See Figure 6 for thermocouple locations

TABLE B-2 Heat Transfer Test Specimen R-10-1/2

ϕ = .087 L = .455 in. A = 2.8×10^{-3} ft^2 S = 4330 ft^{-1} d = 6.94×10^{-5} ft n = 3.9

q (BTU/in²-sec)	p_{up} (psi)	p_{dn} (psi)	Δp (psi)	$T_{f\infty}$ (R)	T_{mo} (R)	T_{mw} (R)	T_{fw} (R)	T_{LM} (R)	$\dot{m}$ (lb/ft²-sec.)	Re	fRe^2	$Re/[f(1-\phi)]^{\frac{1}{n}}$
0	560	35	525	517					.204	2.42	4.45×10^5	4.71×10^4
0	788	37	750	516					.303	3.59	8.83×10^5	7×10^4
0	1001	38	964	516					.404	4.78	1.42×10^6	9.33×10^4
0	676	35	641	516					.249	2.95	6.5×10^5	5.76×10^4
5.8	962	36	924	521	522	982	657	586	.354	3.87	9.9×10^5	7.54×10^4
5.8	808	35	771	520	523	1029	672	593	.282	3.05	6.74×10^5	5.94×10^4
5.8	725	35	688	521	523	1049	677	596	.241	2.6	5.38×10^5	5.06×10^4
5.8	521	33	486	522	526	1166	715	613	.153	1.62	2.58×10^3	3.16×10^4
5.8	398	31	365	523	531	1333	706	610	.0984	1.04	1.51×10^5	2.03×10^4
5.8	519	33	484	523	529	1170	723	618	.152	1.6	2.51×10^5	3.11×10^4
5.8	694	36	656	522	526	1073	695	604	.227	2.42	4.75×10^5	4.73×10^4

*See Figure 6 for thermocouple locations

TABLE B-2 Heat Transfer Test Specimen R-10-1/2

ϕ = .087 L = .455 in. A = 2.8×10^{-3} ft^2 S = 4330 ft^{-1} d = 6.94×10^{-5} ft n = 3.9

q (BTU/in²-sec)	p_{up} (psi)	p_{dn} (psi)	Δp (psi)	$T_{f\infty}$ (R)	T_{mo} (R)	T_{mw} (R)	T_{fw} (R)	T_{LM} (R)	$\dot{m}$ (lb/ft²-sec.)	Re	fRe^2	$Re/[f(1-\phi)]^2$
7.8	778	29	748	522	524	1176	745	627	.256	2.67	5.5×10^5	5.2×10^4
7.8	544	27	515	523	529	1382	816	659	.151	1.52	2.38×10^5	2.96×10^4
7.8	462	26	434	525	533	1560	844	672	.113	1.12	1.65×10^5	2.19×10^4
7.8	774	30	742	523	529	1227	776	641	.249	2.56	5.16×10^5	4.98×10^4
11	804	30	772	523	529	1453	855	675	.248	2.46	4.95×10^5	4.81×10^4
11	604	28	574	526	533	1679	922	706	.159	1.53	2.53×10^5	2.99×10^4
11	512	27	483	529	540	1893	963	724	.115	1.09	1.7×10^5	2.13×10^4
11	687	29	655	528	535	1549	895	695	.196	1.91	3.37×10^5	3.72×10^4
11	773	30	741	526	533	1454	871	684	.233	2.29	4.43×10^5	4.47×10^4
0	655	31	623	523			-	-	.235	2.72	5.56×10^5	5.29×10^4
0	500	29	468	522					.163	1.92	3.39×10^5	3.74×10^4

*See Figure 6 for thermocouple locations

TABLE B-3 Heat Transfer Test Specimen R-20-1/4

ε = .194 L = .455 in. A = 2.48×10^{-3} ft^2 S = 2720 ft^{-1} d = 2.67×10^{-4} ft n = 3.9

q (BTU/in^2-sec)	P_{up} (psi)	P_{dn} (psi)	ΔP (psi)	$T_{f\infty}$ * (R)	T_{mo} (R)	T_{mw} (R)	T_{fw} (R)	T_{LM} (R)	$\dot{m}$ (lb/ft^2-sec.)	Re	fRe^2	$Re/[f(1-f)]^2$
0	395	36	358	535					4.13	184	8.21×10^6	2.56×10^5
0	412	36	375	539					4.28	190	8.77×10^6	2.64×10^5
0	238	29	208	542					2.37	97.8	2.5×10^6	1.36×10^5
7.5	417	37	381	535	535	853	579	557	4.31	187	8.35×10^6	2.6×10^5
7.5	417	38	381	539	538	858	582	560	4.31	186	8.28×10^6	2.59×10^5
7.5	232	30	204	540	539	907	610	574	2.27	96.4	2.4×10^6	1.34×10^5
7.5	232	30	204	539	539	906	610	573	2.27	96.4	2.42×10^6	1.34×10^5
7.5	85	29	59	531	531	1086	734	627	.710	28.6	2.47×10^5	1.34×10^5
7.5	85	29	59	531	531	1085	734	627	.705	32.3	2.47×10^5	4.49×10^4
7.5	57	28	32	527	529	1249	866	682	.401	19	8.18×10^4	2.64×10^4
7.5	46	26	23	527	530	1363	985	732	.279	10.1	8.22×10^4	1.4×10^4

*See Figure 6 for thermocouple locations

TABLE B-3 Heat Transfer Test Specimen R-20-1/4

ϕ = .194 L = .455 in. A = 2.48×10^{-3} ft^2 S = 2720 ft^{-1} d = 2.67×10^{-4} ft n = 3.9

q (BTU/in^2-sec)	p_{up} (psi)	p_{dn} (psi)	Δp (psi)	$T_{f\infty}$ * (R)	T_{mo} (R)	T_{mw} (R)	T_{fw} (R)	T_{LM} (R)	$\dot{m}$ (lb/ft^2-sec.)	Re	fRe^2	Re/[f(1-f)]
7.5	81	31	53	527	529	1099	740	627	.642	25.8	2.18×10^5	3.58×10^4
7.5	81	31	53	527	529	1098	743	629	.640	25.6	2.16×10^5	3.56×10^4
15	712	39	675	534	534	1067	598	565	.743	318	2.37×10^7	4.42×10^5
15	386	32	356	533	534	1159	649	589	3.92	164	6.29×10^6	2.28×10^5
15	149	32	119	530	531	1403	780	647	1.36	53.4	7.32×10^5	7.43×10^4
15	84	29	57	530	532	1595	975	730	.661	18.8	1.65×10^5	2.62×10^4
15	58	28	32	529	532	1763	1209	823	.376	12.6	5.34×10^4	1.74×10^4
15	51	28	25	529	533	1809	1274	848	.291	9.54	3.56×10^4	1.32×10^4
15	82	32	51	529	531	1463	924	708	.622	23	1.61×10^5	3.2×10^4
15	148	33	116	528	530	1257	737	627	1.35	54	7.69×10^5	7.5×10^4
15	632	37	597	529	529	968	601	564	6.59	283	1.86×10^7	3.94×10^5

*See Figure 6 for thermocouple locations

TABLE B-3 Heat Transfer Test Specimen R-20-1/4

ϕ = .194 L = .455 in. A = 2.48×10^{-3} ft^2 S = 2720 ft^{-1} d = 2.67×10^{-4} ft n = 3.9

q (BTU/in²-sec)	p_{up} (psi)	p_{dn} (psi)	Δp (psi)	$T_{f\infty}$ * (R)	T_{mo} (R)	T_{mw} (R)	T_{fw} (R)	T_{LM} (R)	$\dot{m}$ (lb/ft²-sec.)	Re	fRe^2	$Re/[\phi(1-\phi)]^n$
15	632	37	595	529	529	973	602	565	6.56	280	1.86×10^7	3.9×10^5
0	501	32	471	526					5.21	235	1.38×10^7	3.27×10^5
0	333	34	301	526					3.39	153	6.08×10^6	2.12×10^5

*See Figure 6 for thermocouple locations

TABLE B-4 Heat Transfer Test Specimen R-20-3/8

ϕ = .198 L = .383 in. A = 3.10×10^{-3} ft^2 S = 2690 ft^{-1} d = 2.76×10^{-4} n = 3.9

q (BTU/ft²-sec)	P_{up} (psi)	P_{dn} (psi)	Δp (psi)	$T_{f\infty}$ * (R)	T_{mo} (R)	T_{mw} (R)	T_{fw} (R)	T_{LM} (R)	$\dot{m}$ (lb/ft²-sec.)	Re	fRe^2	$Re/[\phi(1-\phi)]^3$
0	688	41	645	518					4.90	230	2×10^7	3.02×10^5
0	479	32	444	519					3.32	156	9.66×10^6	2.05×10^5
0	378	28	347	520					2.58	121	6.02×10^6	1.59×10^5
0	188	29	158	517					1.19	56	1.47×10^6	7.34×10^4
0	142	26	115	518					0.871	41.1	8.3×10^5	5.39×10^4
7.5	191	30	160	517	517	780	635	574	1.20	52.7	1.19×10^6	6.9×10^4
7.5	158	28	130	518	519	798	655	584	.974	42.2	7.81×10^5	5.53×10^4
7.5	103	24	78	518	519	843	719	613	.590	24.8	2.88×10^5	3.25×10^4
7.5	75	24	50	517	519	877	781	640	.394	16.1	1.30×10^5	2.11×10^4
7.5	60	24	35	517	520	948	854	671	.284	11.2	6.88×10^4	1.47×10^4
7.5	47	24	23	518	520	1049	983	726	.188	7.06	3.18×10^4	9.26×10^3

*See Figure 6 for thermocouple locations

TABLE B-4 Heat Transfer Test Specimen R-20-3/8

$\mathcal{F}$ = .198 L = .383 in. A = 3.10×10^{-3} ft^2 S = 2690 ft^{-1} d = 2.76×10^{-4} n = 3.9

q (BTU/in²-sec)	p_{up} (psi)	p_{dn} (psi)	Δp (psi)	$T_{f\infty}$ * (R)	T_{mo} (R)	T_{mw} (R)	T_{fw} (R)	T_{LM} (R)	$\dot{m}$ (lb/ft²-sec.)	Re	fRe^2	$Re/[f(1-\gamma)]^3$
7.5	40	24	16	519	522	1169	1149	793	.132	4.66	1.62×10^4	6.11×10^3
7.5	37	23	13	520	522	1279	1280	844	.106	3.59	1.06×10^4	4.7×10^3
7.5	92	47	45	500	503	865	691	590	.472	20.3	1.98×10^5	2.66×10^4
7.5	76	43	33	500	504	909	739	612	.354	14.9	1.14×10^5	1.95×10^4
7.5	62	40	23	502	505	967	815	646	.251	10.2	6.02×10^4	1.33×10^4
7.5	57	39	19	503	506	1003	882	675	.211	8.34	4.26×10^4	1.09×10^4
7.5	52	37	15	504	508	1056	966	710	.174	6.65	2.75×10^4	8.7×10^3
7.5	48	36	12	504	509	1124	1068	751	.139	5.13	1.82×10^4	6.72×10^3
7.5	44	34	10	507	513	1266	1239	819	.100	3.45	1.14×10^4	4.52×10^3
7.5	51	37	14	505	510	1086	999	724	.163	6.15	2.42×10^4	8.06×10^3
7.5	55	38	17	504	508	1044	1131	696	.191	7.4	3.42×10^4	9.69×10^3

*See Figure 6 for thermocouple locations

TABLE B-4 Heat Transfer Test Specimen R-20-3/8

ξ = .198 L = .383 in. A = 3.10×10^{-3} ft^2 S = 2690 ft^{-1} d = 2.76×10^{-4} n = 3.9

q (BTU/in^2-sec)	p_{up} (psi)	p_{dn} (psi)	Δp (psi)	$T_{f\infty}$ * (R)	T_{mo} (R)	T_{mw} (R)	T_{fw} (R)	T_{LM} (R)	$\dot{m}$ (lb/ft^2-sec.)	Re	fRe^2	$Re/[f(1-\xi)]^n$
7.5	60	40	21	504	507	999	851	662	.230	9.19	5.08×10^4	1.2×10^4
15	596	40	555	516	517	860	617	565	4.13	183	1.24×10^7	2.4×10^5
15	382	31	350	517	517	909	657	584	2.58	112	4.7×10^6	1.47×10^5
15	189	30	158	517	517	1011	761	631	1.18	48.6	9.32×10^5	6.36×10^4
15	161	29	132	517	518	1045	804	650	.984	39.7	6.32×10^5	5.21×10^4
15	115	26	88	518	520	1092	903	693	.658	25.5	2.71×10^5	3.34×10^4
15	73	25	47	518	521	1214	1101	773	.357	12.8	7.72×10^4	1.68×10^4
15	56	27	28	520	522	1469	1304	853	.218	7.34	3.08×10^4	9.62×10^3
15	51	26	24	520	522	1576	1424	897	.183	5.96	2.2×10^4	7.8×10^3
15	49	26	22	520	523	1697	1517	931	.166	5.27	1.79×10^4	6.9×10^3
15	296	35	260	516	517	524	521	518	1.96	92.7	3.71×10^6	1.21×10^5

*See Figure 6 for thermocouple locations

TABLE B-4 Heat Transfer Test Specimen R-20-3/8

ε = .198 L = .383 in. A = 3.10×10^{-3} ft^2 S = 2690 ft^{-1} d = 2.76×10^{-4} n = 3.9

q (BTU/in²-sec)	P_{up} (psi)	P_{dn} (psi)	Δp (psi)	$T_{f\infty}$* (R)	T_{mo} (R)	T_{mw} (R)	T_{fw} (R)	T_{LM} (R)	$\dot{m}$ (lb/ft²-sec.)	Re	fRe^2	$Re/(\varepsilon(1-\varepsilon))^3$
15	465	38	425	515	516	522	517	516	3.22	153	9.32×10^6	2×10^5
15	595	39	555	514	514	522	517	515	4.16	197	1.54×10^7	2.58×10^5
15	93	46	46	500	504	1215	873	669	.474	18.8	1.52×10^5	2.47×10^4
15	84	44	40	500	505	1278	924	690	.405	15.8	1.13×10^5	2.06×10^4
15	73	41	32	501	506	1358	1009	726	.321	12.1	7.12×10^4	1.58×10^4
15	61	38	23	503	508	1475	1215	805	.230	8.03	3.49×10^4	1.05×10^4
15	53	35	17	505	510	1661	1496	912	.162	5.19	1.7×10^4	6.8×10^3
15	47	34	14	508	515	1938	1831	1032	.113	3.34	9.72×10^3	4.37×10^3
15	48	33	14	508	516	1943	1837	1034	.113	3.34	9.67×10^3	4.37×10^3
15	55	36	19	506	512	1632	1394	876	.180	5.96	2.16×10^4	7.81×10^3
15	60	38	22	505	510	1566	1284	835	.216	7.4	3.04×10^4	9.69×10^3

*See Figure 6 for thermocouple locations

TABLE B-4 Heat Transfer Test Specimen R-20-3/8

$\mathcal{F}$ = .198 L = .383 in. A = 3.10×10^{-3} ft^2 S = 2690 ft^{-1} d = 2.76×10^{-4} n = 3.9

q (BTU/in^2-sec)	p_{up} (psi)	p_{dn} (psi)	Δp (psi)	$T_{f\infty}$* (R)	T_{mo} (R)	T_{mw} (R)	T_{fw} (R)	T_{LM} (R)	$\dot{m}$ (lb/ft^2-sec.)	Re	fRe^2	$Re/[f(1-f)]^n$
15	69	40	29	504	508	1454	1087	758	.284	10.4	5.59×10^4	1.36×10^4
15	88	45	43	501	506	1313	930	694	.43	16.7	1.25×10^5	2.18×10^4
0	75	47	29	504					.340	16.2	1.6×10^5	2.13×10^4
0	90	46	44	501					.470	22.3	2.75×10^5	2.92×10^4

*See Figure 6 for thermocouple locations

TABLE B-5 Heat Transfer Test Specimen R-20-1/2

ξ = .187 L = .515 in. A = 2.73×10^{-3} ft^2 S = 4330 ft^{-1} d = 2.51×10^{-4} ft n = 3.9

q (BTU/in²-sec)	P_{up} (psi)	P_{dn} (psi)	ΔP (psi)	$T_{f\infty}$ * (R)	T_{mo} (R)	T_{mw} (R)	T_{fw} (R)	T_{LM} (R)	$\dot{m}$ (lb/ft²-sec.)	Re	fRe^2	$Re/[f(1-\xi)]^2$
7.5	781	35	739	530	529	775	589	559	4.33	176	1.29×10^7	2.73×10^5
7.5	418	29	384	530	529	856	629	578	2.24	888	3.38×10^6	1.38×10^5
7.5	242	32	205	530	529	976	709	615	1.23	46.9	9.63×10^5	7.28×10^4
7.5	180	29	147	530	529	1038	756	638	.863	32.1	4.84×10^5	4.98×10^4
7.5	134	27	103	530	529	1124	814	662	.592	21.5	2.39×10^5	3.34×10^4
7.5	101	27	70	531	529	1187	899	699	.422	14.8	1.14×10^5	2.29×10^4
7.5	75	26	46	531	529	1327	1045	759	.276	9.16	4.89×10^4	1.42×10^4
7.5	65	27	34	531	531	1454	1204	822	.203	6.37	2.71×10^4	9.88×10^3
7.5	55	26	26	531	531	1599	1403	897	.147	4.37	1.49×10^4	6.77×10^3
7.5	52	25	24	529	531	1650	1544	948	.128	3.66	1.15×10^4	5.68×10^3
7.5	67	29	36	529	531	1438	1130	792	.222	7.15	3.27×10^4	1.11×10^4

*See Figure 6 for thermocouple locations

TABLE B-5 Heat Transfer Test Specimen R-20-1/2

ϕ = .187 L = .515 in. A = 2.73×10^{-3} ft^2 S = 4330 ft^{-1} d = 2.51×10^{-4} ft n = 3.9

q (BTU/in^2-sec)	p_{up} (psi)	p_{dn} (psi)	Δp (psi)	$T_{f\infty}$* (R)	T_{mo} (R)	T_{mw} (R)	T_{fw} (R)	T_{LM} (R)	$\dot{m}$ (lb/ft^2-sec.)	Re	fRe^2	Re/$[f(1-\phi)]^n$
7.5	95	33	61	529	531	1220	907	701	.385	13.5	9.91×10^4	2.09×10^4
7.5	123	36	87	530	531	1343	827	668	.537	19.4	1.96×10^5	3.01×10^4
7.5	204	36	167	533	531	989	723	623	.996	37.6	6.7×10^5	5.84×10^4
7.5	344	36	306	535	532	878	665	598	1.81	70.5	2.13×10^6	1.09×10^5
7.5	614	38	573	534	532	788	622	577	3.42	136	7.43×10^6	2.11×10^5
15	780	35	735	533	532	997	660	594	4.33	169	1.11×10^7	2.62×10^5
15	591	30	555	533	532	1072	692	609	3.26	125	6.06×10^6	1.94×10^5
15	430	29	396	533	532	1168	732	627	2.30	86.6	2.98×10^6	1.34×10^5
15	247	29	215	535	533	1376	849	680	1.22	42.7	7.76×10^5	6.62×10^4
15	189	29	158	535	533	1494	944	720	.885	30.4	4.1×10^5	4.71×10^4
15	146	28	115	535	533	1659	1074	773	.644	21	2.01×10^5	3.27×10^4

*See Figure 6 for thermocouple locations

TABLE B-5 Heat Transfer Test Specimen R-20-1/2

ξ = .187 L = .515 in. A = 2.73×10^{-3} ft^2 S = 4330 ft^{-1} d = 2.51×10^{-4} ft n = 3.9

q (BTU/ft²-sec)	p_{up} (psi)	p_{dn} (psi)	Δp (psi)	$T_{f\infty}$ * (R)	T_{mo} (R)	T_{mw} (R)	$T_{\xi w}$ (R)	T_{LM} (R)	$\dot{m}$ (lb/ft²-sec.)	Re	fRe^2	$Re/[f(1-\xi)]^n$
15	134	28	104	534	533	1702	1123	792	.578	18.6	1.6×10^5	2.89×10^4
15	181	30	149	534	533	1523	969	730	.837	28.6	3.62×10^5	4.44×10^4
15	209	32	175	534	533	1477	910	705	.966	34.6	5.28×10^5	5.37×10^4
15	433	33	397	535	534	1160	706	616	2.31	88.1	3.17×10^6	1.36×10^5
15	756	35	717	533	533	1012	643	586	4.15	163	1.08×10^7	2.53×10^5

TABLE B-6 Heat Transfer Test Specimen R-40-1/4

$\mathcal{F}$ = .401 L = .244 in. A = 2.57×10^{-3} ft^2 S = 1780 ft^{-1} d = 9.05×10^{-4} ft n = 3.9

q (BTU/in^2-sec)	p_{up} (psi)	p_{dn} (psi)	Δp (psi)	$T_{f\infty}$ * (R)	T_{mo} (R)	T_{mw} (R)	T_{fw} (R)	T_{LM} (R)	$\dot{m}$ (lb/ft^2-sec.)	Re	fRe^2	Re/$[f(1-\gamma)]^{\frac{1}{3}}$
0	51	30	21	522					2.24	343	1.82×10^6	8.72×10^4
0	63	35	28	524					2.93	448	2.92×10^6	1.16×10^5
0	76	39	37	526					3.69	563	4.5×10^6	1.46×10^5
0	84	39	44	527					4.18	640	5.77×10^6	1.66×10^5
0	40	29	10	524					1.42	217	7.34×10^5	5.65×10^4
7.5	75.2	30.2	44.4	495	497	722	520	507	3.94	624	5.65×10^6	1.62×10^5
7.5	46.5	21.7	24.6	496	497	773	535	515	2.24	354	2.02×10^6	9.2×10^4
7.5	32.7	20.8	11.7	496	498	817	551	523	1.30	206	7.55×10^5	5.36×10^4
7.5	29.0	20.7	8.1	496	498	844	564	529	1.02	161	4.85×10^5	4.19×10^4
7.5	30.6	26.8	3.8	496	499	897	688	587	.715	113	2.62×10^5	2.94×10^4
7.5	24.3	22.1	2.0	497	502	1004	653	571	.436	68.9	1.11×10^5	1.79×10^4

*See Figure 6 for thermocouple locations

TABLE B-6 Heat Transfer Test Specimen R-40-1/4

$\bar{F}$ = .401 L = .244 in. A = 2.57×10^{-3} ft^2 S = 1780 ft^{-1} d = 9.05×10^{-4} ft n = 3.9

q (BTU/ft²-sec)	p_{up} (psi)	p_{dn} (psi)	Δp (psi)	$T_{f\infty}$* (R)	T_{mo} (R)	T_{mw} (R)	T_{fw} (R)	T_{LM} (R)	$\dot{m}$ (lb/ft²-sec.)	Re	fRe^2	$Re/[f(1-\bar{F})]^2$
7.5	22.4	20.7	1.6	498	503	1073	694	590	.353	55.7	8.23×10^4	1.45×10^4
7.5	20.2	19.2	.9	498	505	1186	852	659	.231	36.5	4.23×10^4	9.48×10^3
7.5	20.0	19.4	.5	499	507	1367	1063	746	.148	23.3	2.35×10^4	6.07×10^3
7.5	22.8	21.8	.9	499	506	1175	844	656	.247	38.9	4.76×10^4	1.01×10^4
7.5	27.7	26.0	1.7	499	504	1037	672	581	.420	66.2	1.09×10^5	1.72×10^4
7.5	40.5	35.4	5.0	496	499	848	564	529	.994	157	4.56×10^5	4.09×10^4
7.5	48.8	40.8	7.9	495	498	804	544	519	1.42	225	8.58×10^5	5.86×10^4
15	73.2	33.6	39.3	494	496	903	537	515	3.7	572	4.65×10^6	1.49×10^5
15	49.3	24.4	24.6	495	497	972	558	526	2.32	354	1.92×10^6	9.2×10^4
15	32.7	21.5	11.0	495	498	1087	590	541	1.25	187	5.89×10^5	4.87×10^4
15	36.0	30.6	5.2	496	499	1155	605	549	.921	137	3.32×10^5	3.55×10^4

*See Figure 6 for thermocouple locations

TABLE B-6 Heat Transfer Test Specimen R-40-1/4

ε = .401 L = .244 in. A = 2.57×10^{-3} ft^2 S = 1780 ft^{-1} d = 9.05×10^{-4} ft n = 3.9

q (BTU/in^2-sec)	p_{up} (psi)	p_{dn} (psi)	Δp (psi)	$T_{f\infty}$ * (R)	T_{mo} (R)	T_{mw} (R)	T_{fw} (R)	T_{LM} (R)	$\dot{m}$ (lb/ft^2-sec.)	Re	fRe^2	$Re/[\varepsilon(1-\varepsilon)]^3$
15	31.2	27.5	3.5	496	500	1258	642	566	.681	99.6	1.85×10^5	2.59×10^4
15	26.4	23.9	2.3	498	504	1404	709	597	.470	66.1	9.15×10^4	1.72×10^4
15	22.9	21.2	1.5	499	506	1554	853	660	.331	43.6	4.14×10^4	1.13×10^4
15	21.4	20.1	1.1	500	508	1706	916	687	.247	31.7	2.6×10^4	8.24×10^3
15	23.5	22.7	.6	501	510	1882	1174	790	.188	22	1.14×10^4	5.72×10^3
15	26.1	25.0	.9	502	510	1667	943	699	.264	33.5	2.52×10^4	8.71×10^3
15	29.7	28.2	1.3	502	508	1502	763	624	.373	51	5.36×10^4	1.32×10^3
15	37.5	34.7	2.6	499	506	1272	648	570	.635	92.3	1.66×10^5	2.4×10^4
15	41.7	37.7	3.8	499	504	1170	508	552	.859	127	2.84×10^5	3.29×10^4
15	49.7	42.1	7.4	498	503	1064	571	534	1.37	206	6.93×10^5	5.36×10^4
0	51	30	21	522					2.24	343	1.82×10^6	8.72×10^4

*See Figure 6 for thermocouple locations

TABLE B-6 Heat Transfer Test Specimen R-40-1/4

$\mathcal{F}$ = .401 L = .244 in. A = 2.57×10^{-3} ft^2 S = 1780 ft^{-1} d = 9.05×10^{-4} ft n = 3.9

q (BTU/in^2-sec)	p_{up} (psi)	p_{dn} (psi)	Δp (psi)	$T_{f\infty}$ * (R)	T_{mo} (R)	T_{mw} (R)	T_{fw} (R)	T_{LM} (R)	$\dot{m}$ (lb/ft^2-sec.)	Re	fRe^2	$Re/[f(1-\mathcal{F})]^2$
0	38	28	9.52	524					1.25	191	6.69×10^5	4.96×10^4
0	36	27	8.57	524					1.19	182	5.95×10^5	4.73×10^4
0	32	26	6.85	523					.992	152	4.26×10^5	3.95×10^4
0	35	32	2.85	522					.632	96.8	2.04×10^5	2.52×10^4
0	31	29	2.00	522					.474	72.7	1.29×10^5	1.89×10^4
0	26	25	1.05	521					.268	41.1	5.74×10^4	1.07×10^4
0	25	24	.87	521					.218	33.5	4.62×10^4	8.71×10^3

*See Figure 6 for thermocouple locations

TABLE B-7 Heat Transfer Test Specimen R-40-3/8

$\mathcal{F}$ = .399 L = .407 in. A = 2.97×10^{-3} ft^2 S = 1790 ft^{-1} d = 8.97×10^{-4} n = 3.9

q (BTU/in²-sec)	P_{up} (psi)	P_{dn} (psi)	ΔP (psi)	$T_{f\infty}$ * (R)	T_{mo} (R)	T_{mw} (R)	T_{fw} (R)	T_{LM} (R)	$\dot{m}$ (lb/ft²-sec.)	Re	fRe^2	$Re/[f(1-f)]^n$
0	80	34	45	503					2.78	435	3.52×10^6	1.14×10^5
0	61	28	32	503					1.99	311	1.97×10^6	8.15×10^4
0	43	24	18	502					1.24	194	8.32×10^5	5.08×10^4
0	38	23	15	502					1.07	168	6.36×10^5	4.39×10^4
0	33.4	23	10.1	503					.808	126	3.93×10^5	3.31×10^4
0	30	22.8	7.0	503					.626	97.8	2.54×10^6	2.56×10^4
7.5	46	30	16	502	502	858	571	536	1.26	188	7.25×10^5	4.94×10^4
7.5	42	28	13	502	502	873	579	540	1.07	159	5.32×10^5	4.16×10^4
7.5	31	23.9	6.95	503	503	953	626	562	.623	89.7	1.99×10^5	2.35×10^4
7.5	28	22	5.2	503	503	989	653	575	.498	70.9	1.3×10^5	1.86×10^4
7.5	25	22	2.8	504	504	1067	730	610	.317	43.5	5.78×10^4	1.14×10^4

*See Figure 6 for thermocouple locations

TABLE B-7 Heat Transfer Test Specimen R-40-3/8

ξ = .399 L = .407 in. A = 2.97×10^{-3} ft^2 S = 1790 ft^{-1} d = 8.97×10^{-4} n = 3.9

q (BTU/in²-sec)	p_{up} (psi)	p_{dn} (psi)	Δp (psi)	$T_{f\infty}$ * (R)	T_{mo} (R)	T_{mw} (R)	T_{fw} (R)	T_{LM} (R)	$\dot{m}$ (lb/ft²-sec.)	Re	fRe^2	$Re/[\xi(1-\xi)]^2$
7.5	23	21	1.9	504	504	1153	813	646	.230	30.4	3.21×10^4	7.97×10^3
7.5	22	21	1.6	504	504	1189	862	667	.200	25.8	2.44×10^4	6.77×10^3
7.5	24	21	1.95	504	504	1143	707	600	.240	33.3	3.79×10^4	8.72×10^3
7.5	26	23	2.85	504	504	1051	724	607	.336	44	5.61×10^4	1.15×10^4
7.5	83	41	41.1	501	501	776	538	519	2.72	416	3.26×10^6	1.09×10^5
15	83	41	41	501	501	1008	571	535	2.72	408	3.03×10^6	1.07×10^5
15	67	36	30	501	501	1059	588	543	2.06	306	1.78×10^6	8.01×10^4
15	43	27	15.5	501	501	1167	644	570	1.14	1.63	5.58×10^5	4.28×10^4
15	32	24	8.4	502	502	1299	710	600	.697	96.9	2.15×10^5	2.54×10^4
15	30	23	6.1	503	503	1367	744	616	.552	75.2	1.39×10^5	1.97×10^4
15	27	23	3.45	504	504	1506	874	672	.367	47.2	6.07×10^4	1.24×10^4

*See Figure 6 for thermocouple locations

TABLE B-7 Heat Transfer Test Specimen R-40-3/8

F = .399 L = .407 in. A = 2.97×10^{-3} ft^2 S = 1790 ft^{-1} d = 8.97×10^{-4} n = 3.9

q (BTU/in²-sec)	P_{up} (psi)	P_{dn} (psi)	Δp (psi)	$T_{f\infty}$ * (R)	T_{mo} (R)	T_{mw} (R)	T_{fw} (R)	T_{LM} (R)	$\dot{m}$ (lb/ft²-sec.)	Re	fRe^2	$Re/[g(1-g)]^n$
15	32	30	1.5	505	505	1657	1056	747	.234	28.1	2.55×10^4	7.36×10^3
15	30	29	1.25	506	506	1766	1212	810	.193	21.9	1.66×10^4	5.73×10^3
15	42	37	4.2	504	504	1369	745	617	.549	71.4	1.29×10^5	1.87×10^4
15	53	39	12.9	502	502	1168	638	567	1.18	170	6.16×10^5	4.44×10^4
15	87	40	45	501	501	1029	567	533	2.90	435	3.44×10^6	1.14×10^5
0	87	40	45	499					2.90	456	4.02×10^6	1.19×10^5
0	64	33	30	499					1.99	312	2.04×10^6	8.18×10^4
0	45	26	18	499					1.24	196	8.99×10^5	5.12×10^4
0	39	25	14.5	499					1.04	163	6.47×10^5	8.28×10^4
0	36	30	6.6	501					0.67	105	3×10^5	2.75×10^4

*See Figure 6 for thermocouple locations

TABLE B-8 Heat Transfer Test Specimen R-40-1/2

ε = .408 L = .492 in. A = 2.45×10^{-3} ft^2 S = 1770 ft^{-1} d = 9.31×10^{-4} ft n = 3.9

q (BTU/in²-sec)	P_{up} (psi)	P_{dn} (psi)	ΔP (psi)	$T_{f\infty}$ * (R)	T_{mo} (R)	T_{mw} (R)	T_{fw} (R)	T_{LM} (R)	$\dot{m}$ (lb/ft²-sec.)	Re	fRe^2	$Re/(f(1-f))^3$
0	91	42	46	504					3.57	578	3.78×10^6	1.47×10^5
0	79	39	40	505					3.02	488	2.91×10^6	1.24×10^5
0	69	37	33	506					2.56	414	2.14×10^6	1.06×10^5
0	47	29	18	504					1.54	248	8.47×10^5	6.34×10^4
0	44	29	16	504					1.39	225	7.28×10^5	5.74×10^4
0	42	28	14	504					1.26	205	6.08×10^5	5.22×10^4
7.5	38.9	33.6	5.7	500	501	906	616	556	.715	108	2.02×10^5	2.75×10^4
7.5	36.5	32.3	4.6	501	504	937	639	567	.604	90.3	1.49×10^5	2.3×10^4
7.5	32.8	29.7	3.4	502	506	994	683	587	.461	67.2	9.1×10^4	1.71×10^4
7.5	28.2	26.4	2.2	505	508	1113	779	632	.293	40.8	4.38×10^4	1.04×10^4
7.5	26.9	25.4	1.9	505	508	1165	842	659	.248	33.5	3.28×10^4	8.55×10^3

*See Figure 6 for thermocouple locations

TABLE B-8 Heat Transfer Test Specimen R-40-1/2

ξ = .408 L = .492 in. A = 2.45×10^{-3} ft^2 S = 1770 ft^{-1} d = 9.31×10^{-4} ft n = 3.9

q (BTU/in^2-sec)	p_{up} (psi)	p_{dn} (psi)	Δp (psi)	$T_{f\infty}$ * (R)	T_{mo} (R)	T_{mw} (R)	T_{fw} (R)	T_{LM} (R)	$\dot{m}$ (lb/ft^2-sec.)	Re	fRe^2	$Re/[f(1-\xi)]^n$
7.5	25.3	24.1	1.6	506	509	1247	927	695	.195	25.4	2.3×10^4	6.48×10^3
7.5	27.1	25.4	1.9	506	509	1166	839	658	.249	33.7	3.31×10^4	8.59×10^3
7.5	28.4	26.2	2.1	505	508	1118	783	634	.289	40	4.13×10^4	1.02×10^4
7.5	31.4	28.5	2.8	504	507	1041	718	605	.406	58.2	6.77×10^4	1.48×10^4
7.5	38	33.3	4.6	501	504	943	638	567	.618	92.2	1.53×10^5	2.35×10^4
15	86	39	45	517	518	936	588	552	3.32	505	2.81×10^6	1.29×10^5
15	66	34	32	518	518	995	608	562	2.40	361	1.52×10^6	9.21×10^4
15	46	28	18	516	517	1090	653	582	1.46	214	5.86×10^5	5.46×10^4
15	40	26	14	517	518	1154	677	593	1.16	168	3.91×10^5	4.3×10^4
15	34	25	8.8	517	519	1253	732	614	.829	117	2.02×10^5	2.99×10^4
15	38	33.6	4.8	517	520	1352	790	644	.616	84.5	1.2×10^5	2.16×10^4

*See Figure 16 for thermocouple locations

TABLE B-8 Heat Transfer Test Specimen R-40-1/2

ε = .408 L = .492 in. A = 2.45×10^{-3} ft^2 S = 1770 ft^{-1} d = 9.31×10^{-4} ft n = 3.9

q (BTU/in²-sec)	p_{up} (psi)	p_{dn} (psi)	Δp (psi)	$T_{f\infty}$ (R)	T_{mo} (R)	T_{mw} (R)	T_{fw} (R)	T_{LM} (R)	$\dot{m}$ (lb/ft²-sec.)	Re	fRe^2	$Re/[f(1-p)^3]$
15	34	30.8	3.2	517	520	1459	863	675	.466	62.1	6.46×10^4	1.58×10^4
15	30.8	28.4	2.6	517	522	1591	964	717	.347	44.4	4.19×10^4	1.13×10^4
15	28.8	26.9	2.1	517	522	1706	1060	756	.272	33.6	2.81×10^4	8.57×10^3
15	26	24.8	1.5	519	526	1932	1311	855	.175	19.8	1.36×10^4	5.06×10^3
15	29.3	27.3	2.2	518	523	1627	1041	749	.290	36	3.05×10^4	9.19×10^3
15	31.8	29.1	2.8	517	522	1497	930	703	.383	49.7	4.85×10^4	1.27×10^4
15	40.1	34.7	5.5	514	517	1283	753	626	.698	97.8	1.53×10^5	2.49×10^4
15	44	36.5	7.6	514	517	1203	701	603	.900	129	2.49×10^5	3.3×10^4
15	49	31.0	17	514	515	1069	642	576	1.52	225	6.17×10^5	5.74×10^4
0	38	27	11	505					1.09	177	4.41×10^5	4.51×10^4
0	33	25	8	505					.851	138	2.86×10^5	3.51×10^4

*See Figure 6 for thermocouple locations

TABLE B-8 Heat Transfer Test Specimen R-40-1/2

$\mathcal{F}$ = 4.08 L = .492 in. A = 2.45×10^{-3} ft^2 S = 1770 ft^{-1} d = 9.31×10^{-4} ft n = 3.9

q (BTU/in²-sec)	p_{up} (psi)	p_{dn} (psi)	Δp (psi)	$T_{f\infty}$ * (R)	T_{mo} (R)	T_{mw} (R)	T_{fw} (R)	T_{LM} (R)	$\dot{m}$ (lb/ft²-sec.)	Re	fRe^2	$Re/[f(1-p)]^{\frac{1}{2}}$
0	31	25	6	503					.718	116	2.08×10^5	2.97×10^4
0	30.7	25.4	5.3	504					.666	108	1.84×10^5	2.75×10^4
0	27	23.5	3.5	504					.499	80.9	1.1×10^5	2.06×10^4
0	23.8	21.8	2.0	504					.351	56.9	5.64×10^4	1.45×10^4

*See Figure 6 for thermocouple locations

TABLE B-9 Heat Transfer Test Specimen S-20-3/8

ξ = .2118 L = .369 in. A = 2.91×10^{-3} ft^2 S = 7102 ft^{-1} d = 1.19×10^{-4} ft n = 3.8

q (BTU/in²-sec)	p_{up} (psi)	p_{dn} (psi)	Δp (psi)	$T_{f\infty}$* (R)	T_{mo} (R)	T_{mw} (R)	T_{fw} (R)	T_{LM} (R)	$\dot{m}$ (lb/ft²-sec)	Re	fRe^2	$Re/[f(1-f)]^n$
0	835	38	798	538					4.22	83.6	2.01×10^6	7.52×10^4
0	679	33	647	540					3.34	66.1	1.36×10^6	5.95×10^4
0	460	29	431	539					2.11	41.7	6.06×10^5	3.75×10^4
0	297	35	263	535					1.25	24.8	2.54×10^5	2.23×10^4
0	268	33	234	535					1.09	21.6	2.06×10^5	1.94×10^4
0	211	31	180	534					.805	16	1.27×10^5	1.44×10^4
0	173	29	145	533					.618	12.3	8.62×10^4	1.11×10^4
0	165	29	137	532					.578	11.5	7.87×10^4	1.04×10^4
0	146	28	119	531					.493	9.85	6.16×10^4	8.86×10^3
0	121	32	90	530					.371	7.43	4.09×10^4	6.69×10^3
0	99	30	69	530					.270	5.4	2.66×10^4	4.86×10^3

*See Figure 6 for thermocouple locations

TABLE B-9 Heat Transfer Test Specimen S-20-3/8

ξ = .2118 L = .369 in. A = 2.91×10^{-3} ft^2 S = 7102 ft^{-1} d = 1.19×10^{-4} ft n = 3.8

q (BTU/in²-sec)	p_{up} (psi)	p_{dn} (psi)	Δp (psi)	$T_{f\infty}$* (R)	T_{mo} (R)	T_{mw} (R)	T_{fw} (R)	T_{LM} (R)	$\dot{m}$ (lb/ft²-sec.)	Re	fRe^2	$Re/(f(1-f))^n$
0	91	30	62	530					.236	4.72	2.24×10^4	4.25×10^3
0	84	29	56	529					.206	4.13	1.9×10^4	3.72×10^3
0	68	28	41	528					.141	2.82	1.18×10^4	2.54×10^3
0	62	30	33	527					.112	2.24	9.13×10^3	2.02×10^3
7.5	830	37	795	540	537	677	583	561	4.18	80.6	1.81×10^6	7.25×10^4
7.5	566	31	536	540	537	693	594	566	2.69	51.6	8.22×10^5	4.65×10^4
7.5	300	31	269	538	533	730	633	584	1.25	23.6	2.14×10^5	2.12×10^4
7.5	259	29	231	538	533	740	649	592	1.04	19.5	1.55×10^5	1.75×10^4
7.5	202	29	174	537	533	771	682	607	.754	13.8	8.83×10^4	1.24×10^4
7.5	166	31	137	535	531	799	717	622	.573	10.3	5.62×10^4	9.30×10^3
7.5	133	29	105	534	530	849	777	648	.410	7.21	3.2×10^4	6.49×10^3

*See Figure 6 for thermocouple locations

TABLE B-9 Heat Transfer Test Specimen S-20-3/8

ϵ = .2118 L = .369 in. A = 2.91×10^{-3} ft^2 S = 7102 ft^{-1} d = 1.19×10^{-4} ft n = 3.8

q (BTU/in²-sec)	P_{up} (psi)	P_{dn} (psi)	Δp (psi)	$T_{f\infty}$* (R)	T_{mo} (R)	T_{mw} (R)	T_{fw} (R)	T_{LM} (R)	$\dot{m}$ (lb/ft²-sec.)	Re	fRe^2	$Re/[f(1-f)]^{\frac{1}{2}}$
7.5	107	31	77	533	530	920	871	688	.274	4.62	1.75×10^4	4.16×10^3
7.5	97	30	68	533	529	970	929	713	.221	3.64	1.31×10^4	3.28×10^3
7.5	84	28	57	531	529	1170	1144	799	.136	2.07	7.4×10^3	1.87×10^3
7.5	100	30	70	529	526	951	907	701	.234	3.90	1.43×10^4	3.51×10^3
7.5	174	32	144	529	526	793	701	611	.584	10.7	6.42×10^4	9.61×10^3
7.5	297	30	268	533	530	727	629	580	1.26	23.8	2.14×10^5	2.14×10^4
15	820	37	785	538	535	796	619	578	4.12	78	1.65×10^6	7.02×10^4
15	612	31	582	538	535	833	644	589	2.92	54.7	8.8×10^5	4.92×10^4
15	440	30	411	537	534	871	678	605	1.96	36.1	4.26×10^5	3.25×10^4
15	302	30	272	535	533	928	734	629	1.26	22.6	1.82×10^5	2.03×10^4
15	265	30	236	535	533	960	762	642	1.06	18.8	1.34×10^5	1.69×10^4

*See Figure 6 for thermocouple locations

TABLE B-9 Heat Transfer Test Specimen S-20-3/8

ε = .2118 L = .369 in. A = 2.91×10^{-3} ft^2 S = 7102 ft^{-1} d = 1.19×10^{-4} ft n = 3.8

q (BTU/in^2-sec)	p_{up} (psi)	p_{dn} (psi)	Δp (psi)	$T_{f\infty}$ * (R)	T_{mo} (R)	T_{mw} (R)	$T_{\ell w}$ (R)	T_{LM} (R)	$\dot{m}$ (lb/ft^2-sec.)	Re	fRe^2	$Re/[f(\varepsilon-p)]^n$
15	224	32	193	535	533	1012	797	657	.845	14.7	9.03×10^4	1.32×10^4
15	163	30	134	534	532	1128	917	708	.538	8.92	3.96×10^4	8.03×10^3
15	137	30	108	533	531	1217	997	741	.400	6.43	2.49×10^4	5.79×10^3
15	119	32	88	533	531	1370	1088	770	.282	4.41	1.68×10^4	3.97×10^3
15	110	30	81	533	531	1512	1138	798	.223	3.41	1.32×10^4	3.07×10^3
15	96	30	66	533	533	1820	1692	1003	.114	1.49	5.62×10^3	1.34×10^3
15	108	30	79	531	531	1414	1150	801	.237	3.62	1.25×10^4	3.26×10^3
15	204	30	175	530	529	1041	821	665	.736	12.7	7.29×10^4	1.14×10^4
15	286	34	253	531	529	942	735	627	1.16	20.9	1.65×10^5	1.88×10^4
0	302	35	268	533					1.26	25.2	2.72×10^5	2.27×10^4
0	271	33	239	533					1.10	21.9	2.15×10^5	1.97×10^4

*See Figure 6 for thermocouple locations

TABLE B-9 Heat Transfer Test Specimen S-20-3/8

ξ = .2118 L = .369 in. A = 2.91×10^{-3} ft^2 S = 7102 ft^{-1} d = 1.19×10^{-4} ft n = 3.8

q (BTU/in^2-sec)	p_{up} (psi)	p_{dn} (psi)	Δp (psi)	$T_{f\infty}$* (R)	T_{mo} (R)	T_{mw} (R)	$T_{\ell\omega}$ (R)	T_{LM} (R)	$\dot{m}$ (lb/ft^2-sec.)	Re	fRe^2	$Re/[f(1-f)]^2$
0	198	30	169	533					.729	14.5	1.14×10^5	1.31×10^4

*See Figure 6 for thermocouple locations

TABLE B-10 Heat Transfer Test Specimen S-30-3/8

ξ = .319 L = .375 in. A = 2.92×10^{-3} ft^2 S = 6650 ft^{-1} d = 1.92×10^{-4} ft n = 3.8

q (BTU/in²-sec)	p_{up} (psi)	p_{dn} (psi)	Δp (psi)	$T_{f\infty}$* (R)	T_{mo} (R)	T_{mw} (R)	T_{fw} (R)	T_{LM} (R)	$\dot{m}$ (lb/ft²-sec.)	Re	fRe^2	$Re/[f(1-f)]^3$
0	86.2	43.0	42.6	513					.733	24.1	4.83×10^4	7.99×10^3
0	71.3	39.3	31.8	512					.538	17.7	3.1×10^4	5.87×10^3
0	65.3	37.2	27.9	512					.466	15.4	2.53×10^4	5.11×10^3
0	58.7	34.8	23.6	513					.387	12.8	1.94×10^4	4.24×10^3
0	50.	31.5	18.1	513					.286	9.43	1.3×10^4	3.13×10^3
0	45.7	30.0	15.4	513					.235	7.74	1.02×10^4	2.57×10^3
0	43.4	29.1	14.0	513					.212	6.99	8.96×10^3	2.32×10^3
0	41.0	28.2	12.5	513					.187	6.16	7.64×10^3	2.04×10^3
0	37.4	26.6	10.4	513					.151	4.98	5.86×10^3	1.65×10^3
0	31.7	24.3	7.1	513					.0966	3.18	3.49×10^3	1.05×10^3
0	42.0	28.8	12.8	513					.195	6.43	8.0×10^3	2.13×10^3

*See Figure 6 for thermocouple locations

TABLE B-10 Heat Transfer Test Specimen S-30-3/8

$\mathcal{F}$ = .319 L = .375 in. A = 2.92×10^{-5} ft^2 S = 6650 ft^{-1} d = 1.92×10^{-4} ft n = 3.8

q (BTU/in^2-sec)	P_{up} (psi)	P_{dn} (psi)	Δp (psi)	$T_{f\infty}$* (R)	T_{mo} (R)	T_{mw} (R)	T_{fw} (R)	T_{LM} (R)	$\dot{m}$ (lb/ft^2-sec.)	Re	fRe^2	Re/[f(1-f)]$^{1/3}$
0	46.5	30.6	15.5	512					.240	7.90	1.05×10^4	2.62×10^3
7.5	87.5	43.8	43.0	512	512	928	649	578	.733	22.3	3.76×10^4	7.39×10^3
7.5	68.9	38.8	29.7	513	513	997	704	603	.490	14.5	1.93×10^4	4.81×10^3
7.5	58.8	35.1	23.4	513	513	1056	758	628	.363	10.5	1.21×10^4	3.47×10^3
7.5	50.7	31.8	18.5	513	514	1130	840	663	.265	7.38	7.4×10^3	2.45×10^3
7.5	46.2	30.0	15.9	513	515	1183	920	697	.212	5.71	5.24×10^3	1.9×10^3
7.5	42.4	28.1	13.9	514	516	1279	1012	735	.168	4.36	3.73×10^3	1.44×10^3
7.5	40.6	27.1	13.1	514	517	1342	1112	775	.145	3.64	2.99×10^3	1.21×10^3
7.5	38.8	26.1	12.3	515	517	1405	1257	832	.121	2.89	2.27×10^3	9.58×10^2
7.5	47.8	30.7	16.7	514	516	1175	900	689	.226	6.12	5.82×10^3	2.03×10^3
7.5	54.1	33.5	20.2	514	515	1099	813	652	.300	8.44	8.88×10^3	2.8×10^3

*See Figure 6 for thermocouple locations

TABLE B-10 Heat Transfer Test Specimen S-30-3/8

ϕ = .319 L = .375 in. A = 2.92×10^{-5} ft^2 S = 6650 ft^{-1} d = 1.92×10^{-4} ft n = 3.8

q (BTU/in²-sec)	P_{up} (psi)	P_{dn} (psi)	Δp (psi)	$T_{f\infty}$ * (R)	T_{mo} (R)	T_{mw} (R)	$T_{\ell w}$ (R)	T_{LM} (R)	$\dot{m}$ (lb/ft²-sec.)	Re	fRe^2	$Re/[\phi(1-\phi)]^2$
7.5	72.5	40.7	31.5	513	514	987	693	598	.524	15.6	2.19×10^4	5.17×10^3
15	88.6	44.5	43.5	513	514	1296	757	627	.729	21.0	3.19×10^4	6.98×10^3
15	75.0	41.1	33.5	514	515	1443	865	674	.538	14.8	1.82×10^4	4.91×10^3
15	70.2	39.5	30.4	514	515	1519	999	730	.476	12.4	1.29×10^4	4.12×10^3
15	61.2	35.8	25.0	515	517	1625	1064	756	.363	9.25	8.68×10^4	3.07×10^3
15	55.1	33.1	21.6	515	517	1731	1312	852	.286	6.72	5.13×10^3	2.23×10^3
15	47.8	29.6	17.7	516	521	1826	1792	1025	.193	4.	2.38×10^3	1.33×10^3
15	51	31.5	19.1	517	520	1689	1304	851	.234	5.5	4.26×10^3	1.82×10^3
15	57.6	34.7	22.6	516	520	1519	1059	755	.319	8.14	7.49×10^3	2.70×10^3
15	74.7	41.7	32.7	515	517	1294	826	658	.531	14.8	1.88×10^4	4.92×10^3
0	82.7	38.4	43.7	513					.705	23.1	4.59×10^4	7.67×10^3

*See Figure 6 for thermocouple locations

TABLE B-10 Heat Transfer Test Specimen S-30-3/8

ϵ = .319 L = .375 in. A = 2.92×10^{-5} ft^2 S = 6650 ft^{-1} d = 1.92×10^{-4} n = 3.8

q (BTU/in²-sec)	p_{up} (psi)	p_{dn} (psi)	Δp (psi)	$T_{f\infty}$* (R)	T_{mo} (R)	T_{mw} (R)	$T_{\ell w}$ (R)	T_{LM} (R)	$\dot{m}$ (lb/ft²-sec.)	Re	fRe^2	$Re/[f(1-\gamma)]^{\frac{1}{2}}$
0	71.5	36.3	34.8	513					.555	18.2	3.25×10^4	6.03×10^3
0	59.3	32.3	26.6	513					.411	13.5	2.12×10^4	4.47×10^3
0	43.6	26.8	16.4	513					.231	7.56	9.99×10^3	2.51×10^3

*See Figure 6 for thermocouple locations

TABLE B-11 Heat Transfer Test Specimen C-10-1/4

ε = .110 L = .247 in. A = 3.06×10^{-3} ft^2 S = 11500 ft^{-1} d = 3.83×10^{-5} ft n = 2.8

q (BTU/ft^2-sec)	P_{up} (psi)	P_{dn} (psi)	ΔP (psi)	$T_{f\infty}$ * (R)	T_{mo} (R)	T_{mw} (R)	T_{fw} (R)	T_{LM} (R)	$\dot{m}$ (lb/ft^2-sec.)	Re	fRe^2	Re/[f(1-f)]^n
0	837	38	802	515					.922	6.02	2.08×10^5	4.02×10^3
0	607	35	574	515					.642	4.21	1.11×10^5	2.81×10^3
0	547	34	514	515					.563	3.69	8.93×10^4	2.46×10^3
0	463	33	431	515					.468	3.06	6.4×10^4	2.04×10^3
0	362	31	331	515					.349	2.29	3.9×10^4	1.53×10^3
7.5	824	31	795	515	513	732	630	570	.846	5.19	1.62×10^5	3.47×10^3
7.5	615	29	588	515	513	758	668	588	.579	3.48	8.4×10^4	2.32×10^3
7.5	540	28	514	515	514	781	693	600	.490	2.91	6.19×10^4	1.95×10^3
7.5	445	26	420	515	514	814	734	618	.372	2.17	3.91×10^4	1.45×10^3
7.5	355	31	324	515	514	871	793	644	.258	1.46	2.25×10^4	9.76×10^2
7.5	311	30	282	515	516	922	854	670	.203	1.12	1.58×10^4	7.51×10^2

*See Figure 6 for thermocouple locations

TABLE B-11 Heat Transfer Test Specimen C-10-1/4

ξ = .110 L = .247 in. A = 3.06×10^{-3} ft^2 S = 11500 ft^{-1} d = 3.83×10^{-5} ft n = 2.8

q (BTU/in^2-sec)	p_{up} (psi)	p_{dn} (psi)	Δp (psi)	$T_{f\infty}$ * (R)	T_{mo} (R)	T_{mw} (R)	T_{fw} (R)	T_{LM} (R)	$\dot{m}$ (lb/ft^2-sec.)	Re	fRe^2	$Re/[f(1-f)]^n$
7.5	238	27	211	515	517	1069	997	730	.116	.603	7.52×10^3	4.03×10^2
7.5	325	31	295	515	517	911	829	660	.225	1.26	1.78×10^4	8.4×10^2
7.5	510	35	476	515	516	790	702	604	.459	2.72	5.41×10^4	1.82×10^3
7.5	598	28	571	515	516	772	677	592	.565	3.38	7.80×10^4	2.26×10^3
15	828	31	800	515	516	914	732	617	.808	4.71	1.36×10^5	3.15×10^3
15	664	29	636	515	515	966	794	644	.597	3.39	7.91×10^4	2.26×10^3
15	587	28	560	516	516	1010	846	667	.498	2.76	5.7×10^4	1.84×10^3
15	474	26	448	516	516	1095	942	709	.350	1.87	3.24×10^4	1.25×10^3
15	402	32	370	516	517	1189	1032	744	.255	1.31	2.06×10^4	8.77×10^2
15	345	30	315	516	519	1257	1128	782	.194	.967	1.35×10^4	6.46×10^2
15	308	29	280	518	521	1327	1208	815	.157	.760	9.78×10^3	5.08×10^2

*See Figure 6 for thermocouple locations

TABLE B-11 Heat Transfer Test Specimen C-10-1/4

ε = .110 L = .247 in. A = 3.06×10^{-3} ft^2 S = 11500 ft^{-1} d = 3.83×10^{-5} ft n = 2.8

q (BTU/in^2-sec)	p_{up} (psi)	p_{dn} (psi)	Δp (psi)	$T_{f\infty}$ * (R)	T_{mo} (R)	T_{mw} (R)	T_{fw} (R)	T_{LM} (R)	$\dot{m}$ (lb/ft^2-sec.)	Re	fRe^2	$Re/[\varepsilon(1-\varepsilon)]^3$
15	268	28	241	518	519	1479	1333	862	.107	.501	6.48×10^3	3.34×10^2
15	354	32	324	518	522	1189	1045	751	.230	1.18	1.57×10^4	7.86×10^2
15	649	30	621	519	520	960	788	644	.628	3.56	7.58×10^4	2.38×10^3
15	830	33	800	519	518	951	731	619	.877	5.11	1.36×10^5	3.41×10^3
0	281	30	253	515					.255	1.67	2.37×10^4	1.16×10^3
0	259	29	230	515					.228	1.49	1.98×10^4	9.95×10^2
0	229	29	201	515					.196	1.28	1.56×10^4	8.55×10^2
0	181	27	155	515					.144	.942	9.7×10^3	6.29×10^2
0	147	26	121	515					.107	.7	6.28×10^3	4.68×10^2

See Figure 6 for thermocouple locations

TABLE B-12 Heat Transfer Test Specimen C-20-1/2

ξ = .199 L = .501 in. A = 2.99×10^{-3} ft^2 S = 10500 ft^{-1} d = 7.6×10^{-5} ft n = 2.8

q (BTU/in^2-sec)	p_{up} (psi)	p_{dn} (psi)	Δp (psi)	$T_{f\infty}$* (R)	T_{mo} (R)	T_{mw} (R)	T_{fw} (R)	T_{LM} (R)	$\dot{m}$ (lb/ft^2-sec.)	Re	fRe^2	$Re/[f(1-\beta)]^n$
0	829	38	792	523					2.55	32.7	4.27×10^5	5.6×10^3
0	434	37	396	522					1.22	15.7	1.18×10^5	2.69×10^3
0	382	35	346	522					1.04	13.4	9.06×10^4	2.3×10^3
0	304	32	271	522					.789	10.2	5.74×10^4	1.75×10^3
0	236	29	206	522					.575	7.4	3.43×10^4	1.27×10^3
0	232	30	203	522					.562	7.24	3.34×10^4	1.24×10^3
0	192	28	164	522					.445	5.73	2.26×10^4	9.82×10^2
0	132	33	99	522					.262	3.37	1.03×10^4	5.78×10^2
0	112	31	81	522					.208	2.67	7.24×10^3	4.58×10^2
0	95	30	65	522					.161	2.06	5.1×10^3	3.53×10^2
0	75	28	47	522					.107	1.38	3.03×10^3	2.36×10^2

*See Figure 6 for thermocouple locations

TABLE B-12 Heat Transfer Test Specimen C-20-1/2

ϕ = .199 L = .501 in. A = 2.99×10^{-3} ft^2 S = 10500 ft^{-1} d = 7.6×10^{-5} ft d = 2.8

q (BTU/in^2-sec)	p_{up} (psi)	p_{dn} (psi)	Δp (psi)	$T_{f\infty}$ * (R)	T_{mo} (R)	T_{mw} (R)	T_{fw} (R)	T_{LM} (R)	$\dot{m}$ (lb/ft^2-sec)	Re	fRe^2	$Re/[f(1-\phi)]^{1/3}$
7.5	800	37	763	523	522	725	615	568	2.44	29.7	3.32×10^5	5.1×10^3
7.5	666	33	627	524	522	740	630	575	1.93	23.4	2.19×10^5	4.01×10^3
7.5	431	26	405	522	522	774	670	593	1.17	13.9	8.67×10^4	2.38×10^3
7.5	303	26	278	522	523	803	712	612	.741	8.59	3.99×10^4	1.47×10^3
7.5	258	35	223	522	526	836	712	612	.590	6.86	2.85×10^4	1.17×10^3
7.5	229	33	196	522	529	865	738	624	.494	5.67	2.15×10^4	9.71×10^2
7.5	178	29	150	522	546	940	813	657	.327	3.63	1.15×10^4	6.21×10^2
7.5	151	27	125	522	577	1020	894	691	.232	2.49	7.30×10^3	4.26×10^2
7.5	135	26	109	522	606	1085	956	717	.180	1.89	5.41×10^3	3.23×10^2
7.5	111	30	81	522	890	1200	1060	760	.107	1.08	3.01×10^3	1.85×10^2
7.5	141	33	108	522	584	1022	882	686	.216	2.32	6.30×10^3	3.99×10^2

*See Figure 6 for thermocouple locations

TABLE B-12 Heat Transfer Test Specimen C-20-1/2

ϵ = .199 L = .501 in. A = 2.99×10^{-3} ft^2 S = 10500 ft^{-1} d = 7.6×10^{-5} ft d = 2.8

q (BTU/in²-sec)	p_{up} (psi)	p_{dn} (psi)	Δp (psi)	$T_{f\infty}$ * (R)	T_{mo} (R)	T_{mw} (R)	$T_{\ell w}$ (R)	T_{LM} (R)	$\dot{m}$ (lb/ft²-sec.)	Re	fRe^2	$Re/[\epsilon(1-\epsilon)]^3$
7.5	225	33	193	521	529	862	690	602	.517	6.08	2.26×10^4	1.04×10^3
7.5	403	28	376	522	520	785	660	588	1.146	13.6	7.76×10^4	2.34×10^3
15	838	29	810	522	522	921	688	601	2.68	31.5	3.2×10^5	5.4×10^3
15	430	27	403	522	522	1013	774	640	1.19	13.4	7.26×10^4	2.3×10^3
15	327	28	300	522	524	1056	833	665	.812	8.95	3.83×10^4	1.53×10^3
15	251	32	220	522	534	1144	889	689	.537	5.77	2.06×10^4	9.89×10^2
15	199	27	172	522	573	1285	1034	749	.341	3.47	1.06×10^4	5.94×10^2
15	178	25	152	522	610	1407	1166	801	.249	2.42	7.21×10^3	4.15×10^2
15	157	32	124	522	707	1564	1314	858	.164	1.52	4.65×10^3	2.60×10^2
15	127	29	98	523	720	1596	1338	868	.108	.991	2.95×10^3	1.7×10^2
15	142	33	109	523	648	1259	1060	760	.218	2.19	5.04×10^3	3.75×10^2

*See Figure 6 for thermocouple locations

TABLE B-12 Heat Transfer Test Specimen C-20-1/2

ε = .199 L = .501 in. A = 2.99×10^{-3} ft^2 S = 10500 ft^{-1} d = 7.6×10^{-5} ft d = 2.8

q (BTU/in²-sec)	P_{up} (psi)	P_{dn} (psi)	Δp (psi)	$T_{f\infty}$ (R)	T_{mo} (R)	T_{mw} (R)	$T_{\varepsilon w}$ (R)	T_{LM} (R)	$\dot{m}$ (lb/ft²-sec)	Re	fRe^2	$Re/[f(1-p)]^{.5}$
15	214	30	184	522	542	1042	840	668	.527	5.79	1.60×10^4	9.92×10^2
15	317	35	282	522	524	960	739	624	.955	11.	4.14×10^4	1.88×10^3
15	378	29	349	522	522	916	727	619	1.208	13.9	6.05×10^4	2.39×10^3
0	358	29	330	522					1.208	15.5	8.01×10^4	2.66×10^3
0	313	27	286	522					1.027	13.2	6.11×10^4	2.26×10^3
0	202	33	169	522					.59	7.6	2.5×10^4	1.3×10^3

*See Figure 6 for thermocouple locations

TABLE B-13 Heat Transfer Test Specimen C-30-1/2

ε = .300 L = .494 in. A = 2.70×10^{-3} ft^2 S = 9790 ft^{-1} d = 1.23×10^{-4} ft n = 2.8

q (BTU/in²-sec)	p_{up} (psi)	p_{dn} (psi)	Δp (psi)	$T_{f\infty}$* (R)	T_{mo} (R)	T_{mw} (R)	T_{fw} (R)	T_{LM} (R)	$\dot{m}$ (lb/ft²-sec.)	Re	fRe^2	$Re/[f(1-f)]^3$
0	622	38	585	525					4.64	96.2	6.76×10^5	7.59×10^3
0	527	33	495	531					3.90	80.1	4.72×10^5	6.32×10^3
0	400	30	371	530					2.83	58.3	2.74×10^5	4.6×10^3
0	323	29	295	530					2.21	45.4	1.78×10^5	3.58×10^3
0	215	33	182	525					1.35	29.9	9×10^4	2.36×10^3
0	189	31	159	524					1.15	23.9	6.16×10^4	1.88×10^3
0	151	28	123	523					.868	18.1	3.88×10^4	1.43×10^3
0	119	30	90	523					.635	13.1	2.34×10^4	1.03×10^3
0	106	29	79	522					.539	11.2	1.89×10^4	8.83×10^2
0	86	33	55	522					.388	8.04	1.16×10^4	6.34×10^2
0	73	30	44	522					.303	6.31	8.04×10^3	4.98×10^2

*See Figure 6 for thermocouple locations

TABLE B-13 Heat Transfer Test Specimen C-30-1/2

ϕ = .300 L = .494 in. A = 2.70×10^{-3} ft^2 S = 9790 ft^{-1} d = 1.23×10^{-4} ft n = 2.8

q (BTU/in^2-sec)	p_{up} (psi)	p_{dn} (psi)	Δp (psi)	$T_{f\infty}$ * (R)	T_{mo} (R)	T_{mw} (R)	T_{fw} (R)	T_{LM} (R)	$\dot{m}$ (lb/ft^2-sec.)	Re	fRe^2	$Re/[\phi(1-\phi)]^2$
0	63	29	36	521					.235	4.88	5.88×10^3	3.85×10^2
0	51	29	23	520					.149	3.09	3.26×10^3	2.44×10^2
7.5	644	39	607	539	535	865	577	558	4.75	94.6	6.32×10^5	7.46×10^3
7.5	584	37	550	541	538	872	582	561	4.30	85.3	5.13×10^5	6.73×10^3
7.5	498	33	467	540	538	892	586	563	3.59	71.1	3.72×10^5	5.61×10^3
7.5	356	33	325	540	537	918	597	568	2.43	47.8	1.85×10^5	3.77×10^3
7.5	218	29	191	537	533	962	630	582	1.32	25.6	6.53×10^4	2.02×10^3
7.5	196	28	170	533	531	972	643	586	1.16	22.3	5.2×10^4	1.76×10^3
7.5	134	34	102	532	533	1032	718	620	.659	12.3	2.05×10^4	9.68×10^2
7.5	121	32	91	531	535	1062	754	636	.554	10.2	1.57×10^4	8.00×10^2
7.5	100	29	74	530	547	1138	834	670	.391	6.92	9.55×10^3	5.46×10^2

*See Figure 6 for thermocouple locations

TABLE B-13 Heat Transfer Test Specimen C-30-1/2

ξ = .300 L = .494 in. A = 2.70×10^{-3} ft^2 S = 9790 ft^{-1} d = 1.23×10^{-4} ft n = 2.8

q (BTU/in^2-sec)	p_{up} (psi)	p_{dn} (psi)	Δp (psi)	$T_{f\infty}$ * (R)	T_{mo} (R)	T_{mw} (R)	T_{fw} (R)	T_{LM} (R)	$\dot{m}$ (lb/ft^2-sec.)	Re	fRe^2	$Re/[f(1-\bar{f})]^2$
7.5	87	27	63	530	571	1219	926	710	.283	4.82	6.28×10^3	3.80×10^2
7.5	81	25	58	529	594	1270	999	739	.229	3.79	4.89×10^3	2.99×10^2
7.5	76	30	48	528	670	1414	1172	808	.156	2.43	3.28×10^3	1.92×10^2
7.5	72	29	45	528	749	1534	1311	861	.119	1.78	2.52×10^3	1.40×10^2
7.5	85	32	55	526	601	1284	1011	742	.229	3.79	5.08×10^3	2.98×10^2
7.5	130	30	102	525	530	1046	723	619	.637	11.9	1.96×10^4	9.36×10^2
7.5	202	35	169	528	522	973	632	578	1.19	23.2	5.64×10^4	1.83×10^3
7.5	224	37	189	529	522	965	620	573	1.36	26.6	7.06×10^4	2.10×10^3
15	645	39	609	534	532	1120	602	567	4.74	93.4	6.11×10^5	7.36×10^3
15	531	33	500	535	533	1166	614	574	3.85	75.4	4.03×10^5	5.94×10^3
15	431	29	404	535	533	1219	632	582	2.03	58.7	2.57×10^5	4.63×10^3

*See Figure 6 for thermocouple locations

TABLE B-13 Heat Transfer Test Specimen C-30-1/2

ϕ = .300 L = .494 in. A = 2.70×10^{-3} ft^2 S = 9790 ft^{-1} d = 1.23×10^{-4} ft n = 2.8

q (BTU/in²-sec)	p_{up} (psi)	p_{dn} (psi)	Δp (psi)	$T_{f\infty}$ * (R)	T_{mo} (R)	T_{mw} (R)	T_{fw} (R)	T_{LM} (R)	$\dot{m}$ (lb/ft²-sec.)	Re	fRe^2	$Re/[f(1-\phi)]^3$
15	318	28	292	535	532	1279	662	596	2.11	40.2	1.32×10^5	3.17×10^3
15	200	28	174	533	531	1369	749	635	1.15	21.0	4.50×10^4	1.66×10^3
15	162	31	133	532	532	1434	829	670	.831	14.7	2.57×10^4	1.16×10^3
15	139	28	113	531	537	1490	914	705	.642	11.	1.68×10^4	8.66×10^2
15	111	28	85	531	530	1704	1174	810	.370	5.77	7.58×10^3	4.55×10^2
15	225	33	195	529	527	1382	715	617	1.34	25.1	6.1×10^4	1.98×10^3
15	495	36	461	530	527	1210	615	571	3.55	69.8	3.55×10^5	5.5×10^3
15	831	39	795	531	529	1104	609	569	6.35	125	1.01×10^6	9.85×10^3
0	624	36	588	523					4.67	97.	6.86×10^5	7.65×10^3
0	565	33	533	523					4.23	87.7	5.64×10^5	6.92×10^3
0	459	32	427	523					3.34	69.2	3.71×10^5	5.46×10^3

*See Figure 6 for thermocouple locations

TABLE B-13 Heat Transfer Test Specimen C-30-1/2

$\mathcal{F}$ = .300 L = .494 in. A = 2.70×10^{-3} ft^2 S = 9790 ft^{-1} d = 1.23×10^{-4} in n = 2.8

q (BTU/ft²-sec)	p_{up} (psi)	p_{dn} (psi)	Δp (psi)	$T_{f\infty}$ * (R)	T_{mo} (R)	T_{mw} (R)	T_{fw} (R)	T_{LM} (R)	$\dot{m}$ (lb/ft²-sec.)	Re	fRe^2	$Re/[f(1-\beta)]^3$
0	318	30	289	523					2.16	44.9	1.78×10^5	3.54×10^3

*See Figure 6 for thermocouple locations

THE FOLLOWING PAGES ARE DUPLICATES OF ILLUSTRATIONS APPEARING ELSEWHERE IN THIS REPORT. THEY HAVE BEEN REPRODUCED HERE BY A DIFFERENT METHOD TO PROVIDE BETTER DETAIL